Tolerance Analysis of Compliant Assemblies

Thesis · April 1998

CITATIONS
51

READS
929

1 author:

Karl G. Merkley
Brigham Young University - Provo Main Campus
16 PUBLICATIONS **289** CITATIONS

SEE PROFILE

TOLERANCE ANALYSIS OF COMPLIANT ASSEMBLIES

by

Karl G. Merkley

A dissertation submitted to the faculty of

Brigham Young University

in partial fulfillment of the requirements for the degree of

Doctor of Philosophy

Department of Mechanical Engineering

Brigham Young University

April 1998

BRIGHAM YOUNG UNIVERSITY

GRADUATE COMMITTEE APPROVAL

of a dissertation submitted by

Karl G. Merkley

This dissertation has been read by each member of the following graduate committee and by majority vote has been found to be satisfactory.

Date	Kenneth W. Chase, Chair
Date	Thomas W. Sederberg
Date	Larry Howell
Date	Greg Jensen
Date	Jordan J. Cox

BRIGHAM YOUNG UNIVERSITY

FINAL READING APPROVAL

I have read the dissertation of Karl G. Merkley in its final form and have found that (1) its format, citations, and bibliographical style are consistent and acceptable and fulfill university and department requirements; (2) its illustrative materials including figures, tables, and charts are in place; and (3) the final manuscript is satisfactory to the graduate committee and is ready for submission to the university library.

Date

Kenneth W. Chase
Chair, Graduate Committee

Approved for the the Department

Alan R. Parkinson
Chair, Department of Mechanical Engineering

Accepted for the the College

Douglas M. Chabries
Dean, College of Engineering and Technology

ABSTRACT

TOLERANCE ANALYSIS OF COMPLIANT ASSEMBLIES

Karl G. Merkley

Department of Mechanical Engineering

Doctor of Philosophy

This dissertation presents methods for combining tolerance analysis of assemblies and finite element analysis to predict assembly force, stress, and deformation in assemblies of compliant parts, such as airframes and automotive bodies. Assemblies of flexible parts are frequently subject to misalignment due to dimensional variation, gravity loads, and residual stress induced distortion. A steady-state contact solution is derived for closure of misaligned surfaces at known contact points, such as bolts or weld locations. This contact solution is expanded to include statistical variation in the contact point locations. An important finding is the covariance that arises from this statistical solution due to both material and geometric effects.

Material covariance is caused by elastic coupling between contact points and

can be calculated from the stiffness matrix for the component parts. Geometric covariance arises form constraints on random variation of the mating surfaces due to surface continuity conditions. As part of the geometric covariance solution, the theory of random Bézier curves is developed. Random Bézier curves provide a method of mapping a profile tolerance on a curve to tolerance bands about the Bézier control points. Random Bézier curves may be subtracted to define the mean gap and covariance between two mating surfaces. This random quantity is used as input into the steady-state contact solution. Several example problems are given demonstrating the method and the results are validated by comparison with Monte Carlo simulations.

ACKNOWLEDGMENTS

This work was sponsored by the Office of Naval Research, contract #N00014-92-J-4064, Boeing Commercial Aircraft Company, and the Association for the Development of Computer Aided Tolerancing Software (ADCATS).

I would like to thank my advisor, Dr. Kenneth W. Chase, for giving me the opportunity and the motivation to complete this work. I would also like to acknowledge the support of my wife and family in completing this Ph.D. program.

Contents

List of Figures

List of Tables

Chapter 1

Introduction

This dissertation develops the theory and general methods for performing tolerance analysis on assemblies of compliant parts, where the tolerances must account for allowable assembly stress and fit. The compliance of a part is determined by the material properties and the geometry. Methods are developed for describing the fit between splined curves in terms of random Bézier curves. Random polynomials are used to describe the covariance in the compliant tolerance analysis.

This dissertation provides a method for statistically predicting the residual stresses induced by assembly forces that occur due to assembly tolerance stack-up. The final result is the displacement at the mating surfaces of parts due to the assembly process and the compliance of the parts. The mating surface displacements can then be used to determine the residual stresses in each part of the

assembly.

The term *compliant tolerance analysis* was adopted during the 1996 ADCATS conference. During the discussion, there was some concern voiced about the term *flexible tolerance analysis*, used prior to the conference. It was felt that there could be confusion with other manufacturing terms: flexible work cells and flexible assembly processes. There was also concern with the term *deformable tolerance analysis*, because of possible negative connotations of the word deform. In structural analysis, compliance is defined as the ability of an object to elastically deform under load. As this method was developed, it was apparent that it relied upon the compliance matrix, the inverse stiffness matrix. The term compliant is used in this dissertation to describe assembly processes involving components that exhibit compliance.

1.1 Motivation

Traditional tolerance analysis techniques rely upon rigid body motions, translations or rotations, to account for small kinematic variations that occur in an assembly of parts. Figure 1.1 shows a simple stacked block problem with one vector loop superimposed on this model. The vector loop can be used to solve dimensional variations in the assembly that occur due to variation in length, form, or kinematic

shift. However, in some applications there is measurable deformation in addition to kinematic shift. For example, the block is subject to measurable deformation if it is manufactured from a material that is orders of magnitude less stiff than the cylinder and the base. There is still a kinematic shift that can occur, but the characteristic lengths of the vector loops are changed due to the compliance of the parts in the assembly. A classical example of this type of problem is press fit cylinders. Tolerances of the mating parts must be specified to assure an adequate interference fit without exceeding the strength of the material. A more general example of this problem occurs in assemblies that include thin shells, such as the skin of an airplane, the front quarter panel of an automobile, or the interior panels of a passenger railway car as shown in figure 1.2. The fiberglass panels in this example are quite flexible taken individually but are very stiff in the assembled form. The inherent compliance of the parts is necessary to obtain the proper fit. Thin shell parts tend to exhibit both complex geometry and a considerable flexibility.

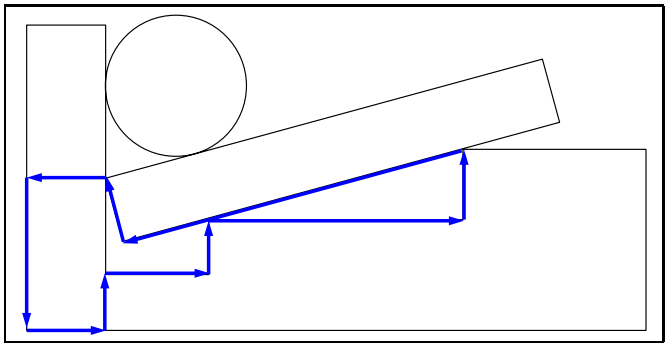

Figure 1.1: One loop of a rigid body tolerance Analysis.

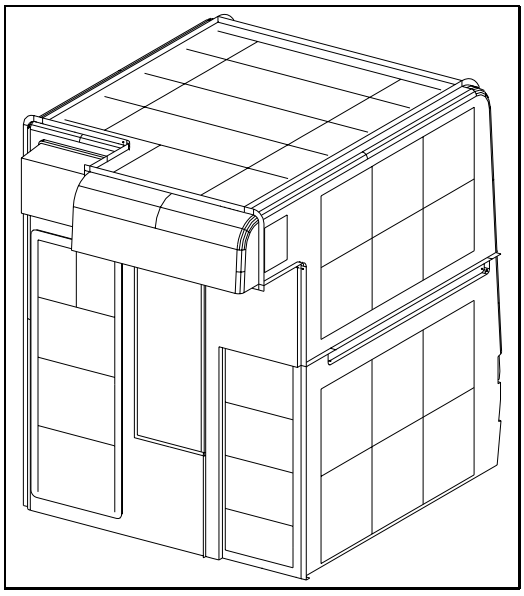

Figure 1.2: Steel reinforced fiberglass railway passenger car.

Specific mathematical tools are required to properly model both the flexibility and the complex geometry. Random Bézier curves are introduced in this dissertation as a method for modeling flexible, complex assembly. Random Bézier curves can model complex shapes and the continuous variation with these shapes. By using random Bézier curves, the gap or interference of mating parts may be defined as input into the compliant tolerance analysis algorithms.

Tolerance stack-up of mating thin-shell parts is responsible for misalignment in the assembly. However, these misalignments may be absorbed by the compliance of the components. Excessive variation due to warpage, shrinkage, etc. may lead to tolerance stack-ups that result in increased assembly stresses. Assembly stresses may lead to part failure, premature failure of the assembly, over design of

the assembly, or undesirable aesthetics.

The procedure for applying tolerance analysis of compliant assemblies can be demonstrated using the flanged plates shown in figure 1.3. The components are

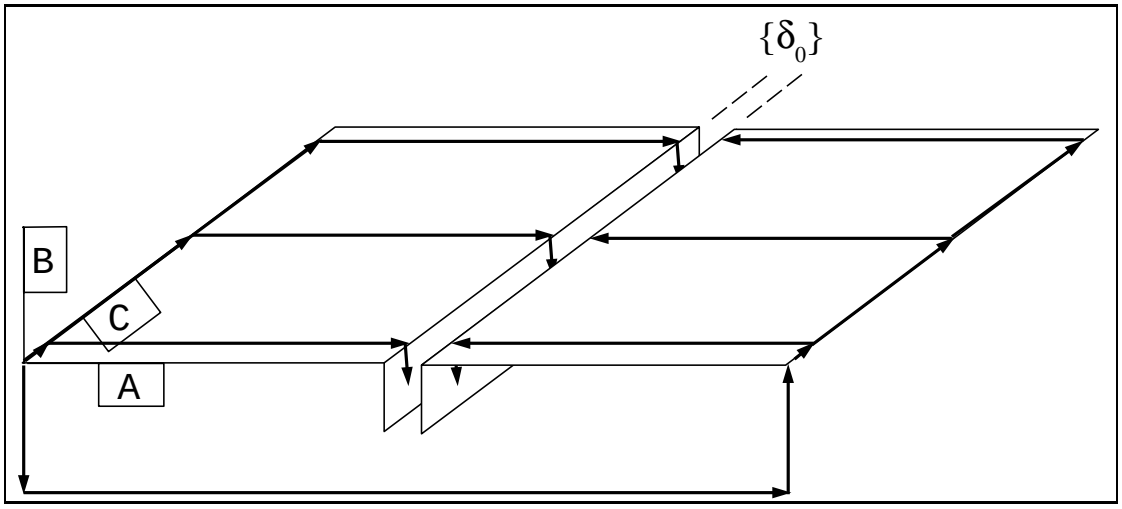

Figure 1.3: Flanged plates with vector loops defining the gap $\{\delta_o\}$

placed in the nominal positions, and vector loops are constructed to the assembly points. The vector loops are used in a tolerance analysis to describe the rigid body variation in the assembly. If a population of assemblies is considered, this variation is typically defined as a statistical quantity defining the gap or interference between two mating parts by characterizing the mean and variance of the mating surfaces.

The statistical gap can be used as input to a stochastic finite element analysis (SFEA) that can define the statistical assembly displacements, forces and stresses. A gap, such as $\{\delta_o\}$ in 1.4, may be treated as a displacement boundary applied to

the the FEA model to force closure of the gaps. The corresponding closure forces and stresses required to close the gap are critical analytical results. By developing a statistical solution, the range of assembly force and stress may be estimated from a single solution, rather than analyzing randomly generated assemblies and computing the statistical parameters point-by-point by summing the results of numerous FEA analyses.

The method of constructing multiple vector loops to describe each contact point has two disadvantages. First, it can be tedious. Consider a a large panel with rivets every two inches. Requiring vector loops to every assembly point would be so time consuming as to prohibit practical application. In addition, separate vector loops would imply independent variation at each rivet point. In real applications, the variations tend to be related due to the surface continuity of the panel. This related

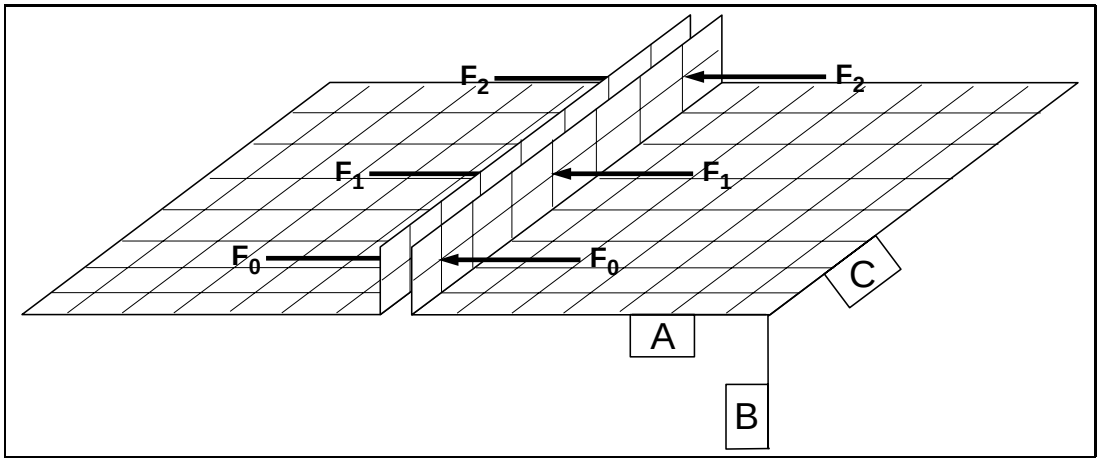

Figure 1.4: Finite element model of flanged plates with closure forces.

variation is defined as *geometric covariance* in this dissertation.

Random Bézier curves may be used to define a single continuous gap due to surface variation and the geometric covariance between two mating parts. Figure 1.5 shows how the control points of a random Bézier curve vary for a given gap variation as determined by the vector loop tolerance analysis. A family of Bézier curves is defined by clouds of control points. Multiple vector loops are not required because the variation may be determined at any parametric value of the random Bézier curve. The number of loops required is sufficient to locate and orient the mating surfaces. In practice, the order of the random Bézier curve must be determined by the manufacturing process and experience. The random Bézier curve defines a statistical (covariant) gap that can be input to the stochastic finite element

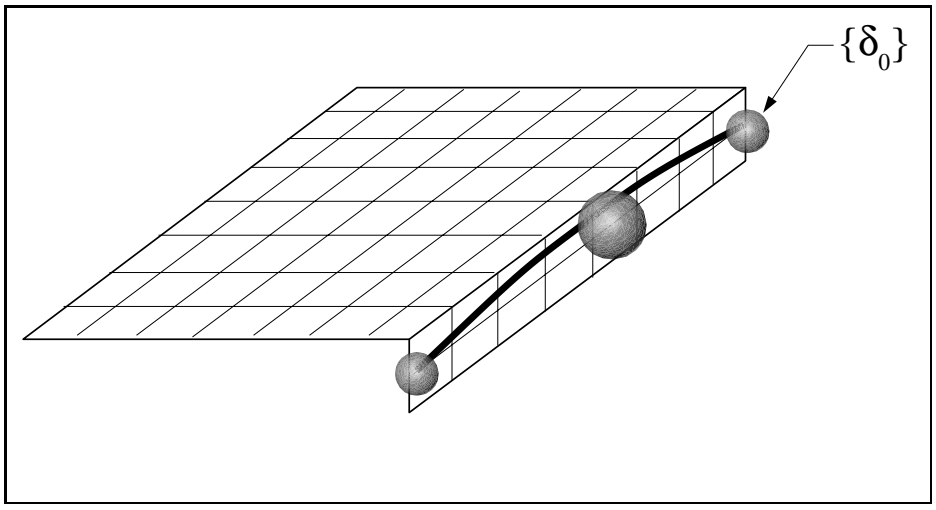

Figure 1.5: Flanged plate finite element model with the gap $\{\delta_0\}$ defined by a random Bézier curves.

analysis.

1.2 Objective

The objective of this research is to develop a general approach for including part compliance with tolerance analysis. It merges existing technologies in finite element analysis and tolerance analysis. It develops the necessary theory for assembling compliant structures that contain complex shapes.

1.3 Procedure

This dissertation accomplishes the following tasks:

1. Verify linear assumptions for tolerance analysis.
2. Develop the theory of assembly of compliant parts.
3. Verify linear assumptions for the assembly of compliant parts.
4. Develop the theory of random Bézier curves.
5. Develop methods describing statistical covariance in compliant tolerance stack-ups.
6. Apply these new theories to sample problems.

7. Indicate future directions on developing this research.

1.4 Scope

This research develops and verify the basic mathematics of tolerance analysis of compliant assemblies. The theory developed in this dissertation is subject to the assumptions of linear material behavior and small displacements. Since the inputs to the analysis are based on tolerance values, which are typically small as compared to part size, these assumptions should be valid. Material plasticity, buckling, or process nonlinearities, such as welding, are not addressed in this dissertation. However, it does indicate a method of inferring information about parts where the material extends into the plastic range.

1.5 Overview

The remainder of this dissertation presents the theory and methods for performing tolerance analysis of compliant assemblies.

Chapter 2 gives a comprehensive literature review of the necessary fields. Chapter 3 gives background and verification of linear tolerance analysis methods. Chapter 4 develops the theory for adding part compliance to these tolerance analysis methods. Chapter 5 develops the theory describing random Bézier curves.

Chapter 6 discusses the effects of covariance in compliant tolerance analysis and use random Bézier curves as a tool to describe geometric covariance. Chapter 7 gives verification of these methods and sample problems. Chapter 8 provides conclusions and a comprehensive discussion of future directions for research.

Chapter 2

Review of Previous Research

This research covers a wide number of fields. This literature survey overviews the most important areas that are required to understand this subject. It begins with a general review of the necessary subjects and continues with a history of tolerance analysis research performed at Brigham Young University.

2.1 General Literature Review

Related research includes the areas of 1) Tolerance Analysis, 2) Finite Element Analysis, 3) Statistics, and 4) Computer-aided Geometric Design. The following literature review addresses each of these areas.

2.1.1 Tolerance Analysis

Tolerance analysis is the process of estimating the accumulation of the design tolerances on component dimensions and features to ensure that parts will assemble during production. Tolerance synthesis or allocation is the reverse process of tolerance analysis by which rational assignment of tolerances to parts may be made during the design phase. During the tolerance analysis/synthesis process, systems of non-linear equations must be solved. Because manufacturing variations involve small changes about the nominal dimensions, the non-linear assembly equations are amenable to linearization techniques as demonstrated by Gao (1993).

A comprehensive review of dimensioning, tolerancing, and analysis processes may be found in Roy *et al.* (1991) and Chase and Parkinson (1991). This work will provide an overview of prior research.

Guilford (1992) reviewed tolerance representations and divided tolerance mathematizations into three approaches: *offset solids, feasibility space*, and *parameter space*.

Offset solids were defined by Requicha (1984, 1986) and Rossignac (1986). In this method, offset surfaces are calculated from the initial solid model and tolerances. This method supports the same concept of a tolerance zone as the ANSI standard; however, it does not support variations in surface orientation. This

makes it impossible to model non-linear effects such as surface angularity (Robinson 1989).

Srinivasan and Jayaraman (1989, 1989) augmented the offset solid approach by defining Virtual Boundary Requirements (VBRs). VBRs can accurately model the constraints imposed on a model due to the tolerances. Wilhelm (1992) implemented VBRs in an expert system to perform both tolerance analysis and tolerance synthesis. He notes that VBRs are difficult to define for complex assemblies.

Turner and Wozny (1990) developed the theory of *feasibility space*. In this approach the variational model is derived from the boundary of the nominal part. The variational model represents the set of all feasible parts. The tolerances are then applied to the set of feasible parts and are used as an assembly constraint, which allows this method to encompass geometric feature variations as well as variations of size. It also allows for statistical and worst case analyses of tolerances. This method has been implemented in the GEOS package at Rensseleaer Polytechnic Institute (Turner 1989).

The theory of *parameter spaces* was one of the first concepts proposed to evaluate tolerances on geometric models. Hillyard and Braid (1978) discussed the possibility of using variable dimensions or parameters in a solid modeler to represent dimensional variation. Light and Gossard also evaluated a parametric geometric modeler (1982). A kinematic formulation using transformation matrices,

as in robotics, is presented by Rivest *et al.* (1993). It is interesting to note that this is similar to the approach evaluated by Robinson at BYU (1989). However, Rivest only considered open loop assemblies.

Vector tolerancing must be considered to be a subset of the parameter space method. Fortini (1967) first introduced the concept of vector tolerancing. A comprehensive study of vector tolerancing applied to 2-D assemblies was advanced by Bjorke (1978). This method did not include a complete set of kinematic constraints on the vector model. Vector models have been utilized extensively at BYU for both 2-D (Marler 1988) and 3-D (Robinson 1989) assemblies. A similar method for building the vector loops was developed independently and is presented by Ogot (1994). However, in this case it is only used to define the 2-D assembly equations for a Monte Carlo analysis. This parallels the work done by Gao (1993). Martinsen (1993) showed that vector tolerancing methods can be applied to define individual parts composed of different surfaces, although the exact implementation for spline surfaces is vague.

There are various concerns that have been raised concerning vector methods. Vector models may not model the ANSI (ASME 1995) definition of a tolerance zone correctly. Voelcker (1993) also claims that vector tolerancing can not deal with imperfect form and “ambiguous datum references”. Goodrich (1991) and Ward (1993) have demonstrated that form variation can be treated in vector assembly

models. Also, it is questionable if any system can deal with ambiguous datum references. It seems reasonable to require that datum references be correctly specified for both tolerance analysis and later manufacturing processes.

Wirtz (1993) makes the argument that vector tolerancing of parts should be included in the ISO/STEP tolerancing standard. However, Voelcker (1993) claims that the arguments for vector tolerancing may violate the “process independence dictum” that has been implicit in tolerancing applications.

It is unclear what Voelcker means by “process independence.” When parts are made, features are located from datums, which makes subsequent processes subject to accumulated error. Choice of datums and dimensioning schemes can produce different variational and accumulation effects. Good dimensioning practices and production setups attempt to minimize dimensional interdependence, but there will always be some dependency present. It is precisely this accumulation of variation that statistical tolerance analysis attempts to capture. The processes may be random and independent, but the dimensions are not.

For example, consider a piece of rough bar stock that has been mounted in a lathe, turned, faced on one end, and then cut off to length. The axes of the tool carriage are not perfectly aligned with the spindle axis. The first end facing process will produce a non-perpendicular surface relative to the cylinder axis. How is the length of the cylinder measured? The final length depends on two facing processes

plus set-up errors.

It is unfortunate that Vector Assembly Modeling is associated with some of these problems. In the case of assemblies, the vectors represent the base dimensions and the variations critical to the assembly. Dimensional variations within the assembly are treated as independent variations; therefore, process independence is not violated.

2.1.2 Finite Element Analysis

Finite Element analysis (FEA) reduces the solution of the partial differential equations of solid mechanics to a set of linear equations solvable by matrix algebra. Linear solutions are accomplished by setting up a stiffness matrix for small deformations about the undeformed state. This is similar to the DLM, where a set of vector assembly models are simplified to perform tolerance analysis. These two linearized systems are well suited for combination into a general system for modeling assemblies with small size variations and deformations.

Finite element analysis has been utilized as an engineering tool for decades. Standard texts (Cook 1989; Reddy 1993; Zienkiewicz and Taylor 1988) in this field provide the basis of understanding that is sufficient for this dissertation.

In addition, Crisfield (1986) and Armenakas (1991) provide derivations for the

technique of substructuring the stiffness matrix to create a “super-element.” This method reduces the degrees of freedom in the stiffness matrix to only those degrees of freedom that exist at a defined boundary. Super-elements can be used with a vector loop model to describe the stiffness-driven behavior of individual parts in a compliant assembly. Each super-element represents a single part. The super-element representation reduces the finite element model to include just the mating surfaces, making the problem more tractable for design.

The problem of bringing two bodies into contact and examining the stresses at the contact surface has been studied at length (Zhong and Mackerle 1994; Mottershead 1993). The contact analysis method that is typically available in commercial FEA codes uses generalized interface elements that can include frictional effects and large deformations. This method requires a non-linear solution. Non-linear contact solutions can have convergence problems (Rizzo 1991) and are computationally expensive. These characteristics make this solution method unacceptable for linear tolerance analysis.

The DLM tolerance analysis procedure uses a linear Taylor’s series approximation to model tolerance variance. It would be desirable to use a linear finite element method to calculate the contact forces. Francavilla (1975) developed a method for calculating linear contact solutions using compliance matrices. This method requires small deformations, nodes existing at all contact locations, and negligible

friction. The method has been demonstrated to give accurate results for simple press-fit cylinder problems. The method has lain largely fallow because of the restrictions placed on it. However, it is ideal for dealing with assembly tolerances. Typically, tolerance stack-up accumulations are relatively small compared to the geometry. Also, if the deformations are examined at fastener locations, contact is guaranteed. In many assembly problems, friction can be ignored for a first order solution.

2.1.3 Computer Aided Geometric Design

Computer Aided Geometric Design (CAGD) has blossomed rapidly with the development of computers and CAD systems. Texts by Farin (1988a) and Bartels *et al.* (1987) provide the basis that is needed to understand the field. The book by Choi (1991) is a useful reference on the fundamentals of surface modeling.

Free-form surfaces must be modeled correctly to analyze many flexible assemblies. Mathematical tools are needed to model surface tolerance zones on individual surfaces and to define the gaps or interferences between mating surfaces. We have chosen Bézier curves and surfaces to model these objects in an assembly for compliant tolerance analysis.

As noted before, one of the primary for tolerance models uses the concept of offset surfaces. The subject of offset curves and surfaces has been widely studied

because of its utility in many applications, such as numerically controlled milling for toolpath generation. Offset curves cannot be generally defined as rational polynomial curves, because the offset is defined by the length of the normal vector, thereby introducing a square root into the denominator of the offset polynomial (Farouki and Neff 1990).

Farouki (1990) has demonstrated that a certain class of polynomials do exist that have rational polynomials for offsets. However, it is not generally applicable to all curves. Klass (1983) developed an offset approximation for planar cubic splines, but did not provide an error bounds for these offsets. Sederberg (1992) derived an error bound to the Hermite approximation of the offset curve.

An alternate method for defining an offset curve is to use the concept of a medial axis transform (Blum 1967). A medial axis transform defines a shape by a medial curve and a radius at each point along the curve. The medial curve and the radius can both be defined as functions of the same parameter allowing arbitrary symmetric shapes to be defined in terms of two functional expressions. Gelston (1992) demonstrated methods of recovering the original geometry from these functional definitions. Medial axis transforms could be expanded to include statistical variation of curves and surfaces for use in tolerance analysis.

This dissertation builds on these previously defined methods and develops the concept of a statistically defined offset. There is no single curve that is used to

define the offset. Instead, a family of curves is defined that have a given probability of lying within a defined plus or minus offset of a curve.

2.1.4 Statistics

Statistics provides mathematical tools for describing random variations in systems.

Spotts (1959, 1960) pointed out that to correctly allocate tolerances within an assembly, statistical methods should be used. However, even with the latest release of ANSI Y14.5.1M, Walker (1993) acknowledges that little effort has been placed on statistical tolerancing.

In this dissertation, statistics is used to describe the covariance between points in a compliant tolerance analysis. Covariance occurs when statistical variables are not randomly independent. The correlation between the variables is measured by the covariance. Appendix A of this dissertation provides some definitions and examples demonstrating the mathematics of covariance.

Statistics is also be used to define the multivariate distribution of Bézier control points based on the tolerance band defined on the curve and vice-versa. It is also needed to understand how the distributions of the control points can be combined with other curves/surfaces in an assembly. The text by Johnson and Wichern (1988) provides a basis for dealing with multivariate statistics, including

covariance matrices. The concept of random Bernstein polynomials is mentioned by Onicescu (1975) where it is considered as a subset of random polynomials (Bharucha-Reid and Sambandham 1986). Sederberg (1992) developed the concept of interval Bézier curves. This method defines the control points over a given interval to approximate curves and surfaces. Combining the interval definition with a statistical distribution lead to the use of random Bézier curves in this research.

2.1.5 Tolerancing Compliant Assemblies

Gordis and Flannelly (1994) examined stresses arising from bolt hole tolerances. They showed how the variation in a simple assembly may be mapped into the frequency domain and solved as transient dynamic finite element problem. Also Fang and Liou (1994) applied system dynamics to assembly variation by analyzing a low velocity dynamic assembly of components. This was accomplished by adding springs at the contact points and updating the stiffness matrix at each point in a dynamic solution.

Liu and Hu have pioneered the area of tolerancing compliant assemblies. They show that in assemblies of sheet metal on a rigid frame the final tolerances correspond more closely to the tolerance of the rigid frame (1995). This is clearly a function of part compliance. Part deformation must be considered to accurately predict the assembly tolerances. They introduce the concept of *mechanistic vari-*

ation simulation to analyze the assembly stack-up of deformable parts. In this concept, Monte Carlo analysis is used to randomly displace nodes in a finite element model and then determine the mean and standard deviation of the assembly. They expand the concept of *mechanistic variation simulation* and show how order of assembly (parallel *vs.* serial) affect assembly tolerances (Liu, Hu, and Woo 1995). Finally, they develop the *Method of Influence Coefficients* (Liu and Hu 1995) as a more efficient method of calculating variations due to compliant assemblies. This method uses a sensitivity matrix obtained from the influence coefficients of the unassembled and assembled parts. These sensitivities are combined statistically using a root sum square to determine the mean and standard deviation. Hu *et al.* deal only with spot-welded sheet metal assemblies. They do not describe how to combine tolerance stack-ups with compliant assemblies, and they apply their methods only to simple geometry.

2.2 A Chronology of Tolerance Analysis at BYU

Computer-aided Tolerance Analysis has been an area of research at Brigham Young University (BYU) since 1984. In that year, Dr. Kenneth W. Chase formed the Association for the Development of Computer Aided Tolerancing Software (ADCATS), a consortium which grew to 12 member companies interested in tolerance analysis. There has been a great deal of research in tolerance analysis at BYU

during the last decade; unfortunately, much of this research is not generally accessible. However work is significant because it forms the basis for a commercial, CAD-based tool (Texas Instruments 1994).

2.2.1 Foundations of Tolerance Analysis

The initial fundamental research in tolerance analysis at BYU was performed by Greenwood (1987). He performed an in depth literature survey and evaluated non-linear methods – the Method of System Moments, Monte Carlo Simulation, and Hasofer-Lind Reliability Index – versus linear methods.

2.2.2 Tolerance Design

Tolerance Design is the assignment of tolerances based on process capabilities, cost, performance requirements, *etc.* This process is also known as tolerance synthesis or tolerance allocation. This is a difficult problem because there is only one assembly tolerance condition and many unknown component tolerances that must be determined.

The initial work in this area was also performed by Greenwood. He developed the Uncertain Mean Model which extends linearized methods to allow for a mean shift or bias in the statistical tolerance data (Chase and Greenwood 1988; Green-

wood and Chase 1987; Greenwood and Chase 1988; Greenwood and Chase 1990).

Haugland (1987) and Loosli (1987) also performed research in this area. They applied the method of Lagrange multipliers and cost versus tolerance functions to allocate the specified assembly tolerance among the component dimensions to achieve the least cost. Their algorithm could also select the most economical process for the task (Chase et al. 1990).

Larsen (Larsen 1989) developed a hybrid Monte Carlo method that included the Method of System Moments. This method used parametrically defined statistical assembly distributions to rapidly reallocate component tolerances without repeating the Monte Carlo simulation.

Andersen (1990) generalized the Lagrange multiplier method to include multiple loop problems and mixed exponent cost functions. An efficient and robust iteration scheme was devised to find the set of tolerances yielding minimum cost.

2.2.3 Vector Assembly Modeling

Vector Assembly Models have been the principle tool used to describe assembly constraints. A number of researchers have made significant contributions in this area.

Marler (1988) developed the Direct Linearization Method (DLM) for 2-D tolerance analysis of assemblies. This method allowed an assembly to be described in terms of vector chains added tip-to-tail, with kinematic joints inserted to represent the the degrees of freedom between mating parts. Small dimensional variations were applied to the vectors, and tolerance accumulation was estimated statistically by root mean squares. This method allowed the tolerance model to include the closed-loop kinematic constraints to describe small adjustments between mating parts which occur as a result of dimensional variations. It reduced complex nonlinear assembly equations to a simplified linear system that could be solved by matrix algebra.

Robinson (1989) implemented a 3-D graphical tolerance modeler in Alpha_1 (University of Utah 1988), an experimental solid modeler developed at the University of Utah. He represented the transformation matrices commonly used in robotics and kinematics as 3-D vector loops.

Simmons (1990) used network graph theory to develop an algorithm for automatically generating the vector loops needed in the DLM in two dimensions. The user was required to locate the joints and datums on the model, then the automatic loop generator was able to complete the vector model.

Carr (1993) defined open loop tolerance specifications that apply to assemblies. He defined a comprehensive set of assembly tolerance specifications patterned

after the ANSI Y14.5M-1982 standards. ANSI Y14.5M-1982 defines component tolerances such as parallelism and perpendicularity that relate two surfaces on the *same* part. In contrast, assembly feature tolerances relate two surfaces on two *different* components in an assembly. For example, a machined slot which is specified to be parallel to an edge is controlled by a *component* tolerance, but the parallelism between the edge of a car door and the door post is an *assembly* feature tolerance. As an addition to standard ANSI Y14.5M-1982 dimensional and feature tolerance specifications, Carr proposed a new set of symbols for assembly tolerance specifications and developed the open vector loops required to analyze each type.

One of the continuing concerns with the DLM is the assumption of linearity. Gao (1993) developed a Monte Carlo simulation that included the non-linear effects of kinematic constraints on an assembly as well as dimensional and geometric feature variation. The results of Monte Carlo analyses were compared with the linearized solutions. The results of this comparison showed that the linearized method is accurate to within 0.1% in predicting the variance of critical assembly features.

2.2.4 CAD-Based Tolerancing

Tolerance analysis tools need to be accessible to to designers and engineers. To accomplish this goal, research efforts have been directed at integrating tolerance

analysis with Computer-aided Design (CAD) systems.

Rime (1988) provided the first proof that vector tolerance models could be integrated with existing CAD systems. He created a 1-D tolerance modeler that was linked to CADAM^{TM}. The tolerance model was created graphically, with geometric data extracted directly from CADAM. The resulting 1-D stack-up was analyzed statistically.

Chun (1988) implemented a 2-D graphical tolerance modeler within Hewlett Packard's ME10^{TM} CAD package. A modeling procedure for 2-D assemblies was developed. The models implemented Marler's DLM using vector tolerances. The system of equations describing assembly variation could be derived directly from the graphical vector model.

Larsen (1991) refined the automatic closed loop generation algorithm to make it robust. He developed a new modeler in AutoCAD^{TM} to graphically create 2-D tolerance models for analysis by the DLM. He introduced the concept of datum paths as a tool to help the user construct a tolerance model using datum referenced dimensions.

Jackson (1992) developed the Application Interface Specification (AIS). The AIS provided a consistent interface for applications to access geometric information from large Computer-aided Engineering (CAE) codes. The AIS was used to integrate the Parasolids^{TM} modeler with the Computer-aided Tolerancing Software

(CATS).

Trego (1993) implemented Carr's tolerance specifications in the tolerance modeler AutoCATS, based on AutoCAD^{TM}. This included extending automatic loop generation to include "open loops", which describe gaps or other assembly tolerances.

Cheney (1994) developed a parallel to the AIS for user-interfaces. The User-Interface Specification (UIS) developed the set of interactions required to interface user commands between large CAE codes and other applications. The UIS was implemented between CATS and CADDS5^{TM}.

Stoddard (1995) developed a method to automate the creation of joints based on geometric assembly constraints.

2.2.5 GD&T

Geometric Dimensioning and Tolerancing (GD&T) has reference to the application of the ANSI-Y14.M standards (ASME 1995). This standard specifies tolerances for form, such as cylindricity or runout, as well as tolerances on size.

Goodrich (1991) defined methods for including geometric feature tolerances as specified by ANSI Y14.5M-1982 into the DLM. He showed that feature variations accumulate statistically and propagate kinematically, just like size variations. He

also characterized each variation by the way it propagates through each of the 12 types of 3-D kinematic joints. He included methods for describing both worst case and statistical tolerancing with feature tolerances. He also developed a 3-D graphical modeler for CATIA^{TM} which included three sources of assembly variation: dimensional, geometric, and kinematic.

Ward (1993) simplified Goodrich's feature tolerance model from 132 cases to eight basic cases. A system of feature tolerances were implemented in a 3-D tolerance modeler built on CATIA^{TM}.

Robinson (1989) implemented feature tolerances in a 3-D graphical modeler.

Gao (1993) developed methods of including form tolerances in a 2-D Monte Carlo simulation.

2.2.6 Advanced Tolerance Design

Research that includes tolerance analysis of specific topics or non-linear approaches is considered in this section on advanced design.

Nielsen (1989) evaluated statistical methods for tolerance allocation of mating hole patterns. He developed a new method based on Fourier convolution integrals that was faster and more accurate than Monte Carlo simulations.

Peterson (1990) developed a Monte Carlo simulation for assembling random

hole patterns. This simulation used constrained non-linear optimization techniques which improved the algorithm's speed and robustness.

Brown (1995) expanded the application of feature tolerances for assemblies by developing a statistical characterization of position tolerances for both components and assemblies. This work included the effects of covariance by Gaussian integration of the volume of the probability density function inside a circular tolerance zone.

Glancy (1994) developed methods for including non-linear, non-normal component distributions in second-order tolerance analysis model. This method was as computationally fast as the linearized method and as accurate as the Monte Carlo method with 100,000 samples.

Huo (1995) developed new methods of evaluating tolerances in mechanical assemblies based on the concept of a variation polygon. The variation polygon provides a graphical representation of the tolerance sensitivities that can be rapidly interpreted in different configurations of a mechanism.

Law (1996) developed methods for anticipating and calculating the effects of statistical covariance on multiple functional specifications in an assembly of parts based on Gaussian integration in n-dimensional variate space. The functional specifications are typically the engineering requirements that must be met by an assembly. Law demonstrated that covariant relationships between assembly vari-

ables can significantly affect the allowable tolerances on the individual components.

Anderson (Anderson 1997) examined the effects of surface variation on the rotational error in mating surfaces. He found that the magnitude of rotational variation was dependent on the spatial frequency of the surface. The analysis showed that both high and low frequency surface variation had small effects on the rotational error of a mating surface. However, an intermediate frequency band had strong effects on the rotation. He developed a set of non-dimensional design curves based on the variation frequency relative to the contact length to describe the rotational error.

2.2.7 Compliant Tolerance Analysis

Including part compliance with tolerance analysis is a area of research that is pioneered in this dissertation. Previous presentations of this work have begun to spawn more interest in this field of research (Merkley et al. 1996).

2.2.8 Robust Optimization

Parallel research has also been conducted at BYU in the area of robust optimization. This research has examined the effects of placing tolerances on the design

parameters and constraints in a non-linear optimization process.

Billings (1986) used optimization tools to evaluate the effect of tolerances on the performance of an engineering model.

Emch (1992, 1993, 1994) used worst case tolerance bands on design and constraint variables in a non-linear optimization.

Lewis (1993, 1993, 1994)(Parkinson and Lewis 1993) applied second order Taylor series expansions to account for non-linearities in an optimization function.

Webb (1994, 1995) applied non-linear optimization techniques to minimize the variance function.

2.2.9 Conclusion

Research at BYU has steadily proceeded towards the development of a comprehensive system for 2-D and 3-D tolerance analysis of assemblies which is adaptable to integration with commercial CAD systems.

2.3 Summary

This literature survey gives an overview of research that has been performed in the area of tolerance analysis. It also shows that the underlying research exists to de-

velop a comprehensive system for analyzing the effects of manufacturing variation in compliant assemblies.

Chapter 3

Background

This chapter presents a mathematical basis for representing tolerances in terms of Vector Assembly Models. A theory of tolerance representations is introduced and compared with Vector Assembly Models. A solution method for vector assembly models is developed using linearization techniques. These results are compared with closed form solution validating this technique.

There are well defined standards for describing tolerances assigned to the parts defined on an engineering drawing. However, the application of these standards to three dimensional solid models is difficult. Since solid models have a mathematically complete definition, Requicha (Requicha and Chan 1986) points out that there also should be a mathematically complete method of specifying the variations in a solid model. This has been the focus of the ASME Y14.5.1M (Walker and Srinivasan 1993) committee on the mathematization of tolerances.

3.1 Tolerancing Theory

Srinivasan (1989) and Jayaraman (1989) have presented a method called Virtual Boundary Requirements (VBRs) that has a sound mathematical basis for representing tolerances on solid models. The papers describing this method have been widely cited and have been implemented in a tolerance synthesis tool (Wilhelm 1992). The concept of VBRs focuses on the need to represent tolerances as a set of functional requirements.

Functional tolerances must be defined in the context of an assembly. Even the simplest parts have functional tolerances that are valid only when viewed as part of an assembly. By examining only individual parts, it is impossible to determine whether they will meet the function specified by the engineering requirements on that part.

The most obvious example of the functional requirement is the simple go/no-go gauge for inspecting hole diameters, as shown in figure 3.1. The gauge consists of two cylinders of different outside diameters. The inside diameter of the ring must be large enough to fit over the small cylinder yet small enough not to pass over the larger cylinder. The act of placing the ring on the gauge is an assembly operation.

Srinivasan and Jayaraman describe the mathematics necessary to create a *virtual* functional gauge. The VBRs are converted into a mathematical statement

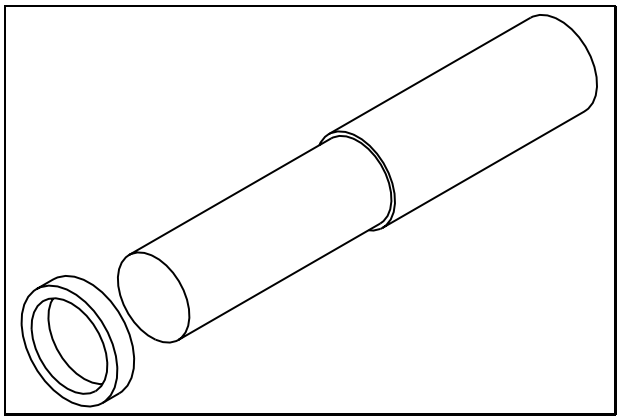

Figure 3.1: Simple go-no go gauge.

called a *conditional tolerance*. The conditional tolerance defines the parameters in an assembly and the limits on these parameters. These can be used to define a virtual gauge or boundary for each part in an assembly. Although this mathematical definition is useful, Srinivasan and Jayaraman do not develop an algorithmic approach for defining the conditional tolerances. This chapter will show that conditional tolerances on an assembly can be developed in an algorithmic manner using the vector loop approach and that these equations can be accurately solved using linear approximations.

Srinivasan and Jayaraman state seven requirements that are essential to a working theory of tolerances.

1. It must be invariant under rigid body transformations

2. It must relate the solid to its underlying surfaces and half-spaces.

3. It must define a containment condition, how one part constrains the motion of an other; a material side condition, which side is material and impenetrable; and a closeness condition, a distance measure for any two parts.

4. It must define datum references, either between parts in an assembly or fixed datum planes in space.

5. It must define the nominal surfaces without any tolerance values associated with it.

6. It must define tolerance specifications for both geometric form and size as well as spatial relationships to a datum or another object.

7. It must relate scalar tolerance specification values and rigid body transformations.

Item number 7 is crucial. It implies that with every tolerance defined on a part there is motion, a rigid body transformation, that is associated with that part and its mating parts. When parts are assembled, there are small relative rotations and translations that occur due to part variation. This motion can only be defined within an assembly of parts. The solution to this problem requires the application of kinematics. An algorithmic method may be derived to define the conditional tolerance on an assembly by using the basic elements of kinematics: vectors, joints, and datums.

A kinematic Vector Assembly Model is based on a vector loop or chain. Each vector describes a nominal part dimension. The vectors form a chain or path from the part datum to a mating surface. When a vector loop traverses part boundaries in an assembly, it must pass through a joint that describes the allowable motion along the boundary.

Vector Assembly Models address all seven requirements that Srinivasan and Jayaraman state as essential for defining a theory of tolerances.

1. Vectors are invariant under rigid body transformations.

2. Vectors must lie within a part or along its boundaries; they may not leave a part without traversing a joint. This defines the half-space of the solid.

3. Joints along part boundaries define the containment condition. The vector locations specify the material side. Vectors must start and end within a part. At a joint a vector must end and a new vector must begin. Vectors never extend outside a part. A distance measure is provided by the difference of any two vectors.

4. Vectors are defined from part or assembly datums.

5. Vectors define the nominal geometry.

6. Variations in the vectors may be caused by either variation in size or geomet-

ric form.

7. Vector loops are based on kinematic principles.

It should be noted that vector loops are distinct from the vector tolerancing models proposed by Wirtz (1993). Wirtz's vector models are used to define single parts. A Vector Assembly Model is only applicable in an assembly.

3.2 Conditional Tolerances

This section will demonstrate the techniques for deriving the conditional tolerances for two simple problems, a tab in a slot and a pin in a hole. These conditional tolerances will be compared to the solution derived by Srinivasan where feasible.

Other researchers (Ogot and Gillmore 1994; Rivest, Fortin, and Morel 1993) have previously recognized that the tolerance analysis problem is related to kinematics and posed the assembly problem in terms of general transformation matrices. Using this approach, assembly variation may be obtained by concatenating the matrices containing the variation. However, these transformation matrices are not intuitive; they do not give additional insight into the engineering problem. They also do not lead to a direct statement of the conditional tolerances on an assembly. This section will demonstrate how to represent assemblies by vector loops and how to derive the conditional tolerance statement from the vector loops.

Tolerance analysis assumes that the preliminary design is complete. The preliminary design determines the nominal form and function of a part. The requirements for form and function are stated as engineering requirements on the design. From these, the nominal sizes are specified to match the desired form and achieve the required function. The tolerance synthesis/analysis problem is typically solved after this stage. Assembly tolerance limits on key features are determined from performance limits. Assembly tolerances must then be translated into component tolerance by selecting tolerances based on process capabilities and performing tolerance analysis.

3.2.1 Conditional Tolerances on a Tab in a Slot

The assembly constraint problem for any two-body, two contact-point problem has a closed form solution. These problems are analogous to a kinematic four-bar linkage. There are four vectors and two contact points in the assembly. One simple assembly that exhibits these characteristics is a tab that slides in a slot. This commonly occurring design feature is shown in figure 3.2.

This section will evaluate the two dimensional problem of a tab skewed in a slot. A vector loop diagram must be created to solve this problem. This requires that datums and contact points be located for the parts in the assembly. The contact points must be classified by the type of motion allowed at the contact point.

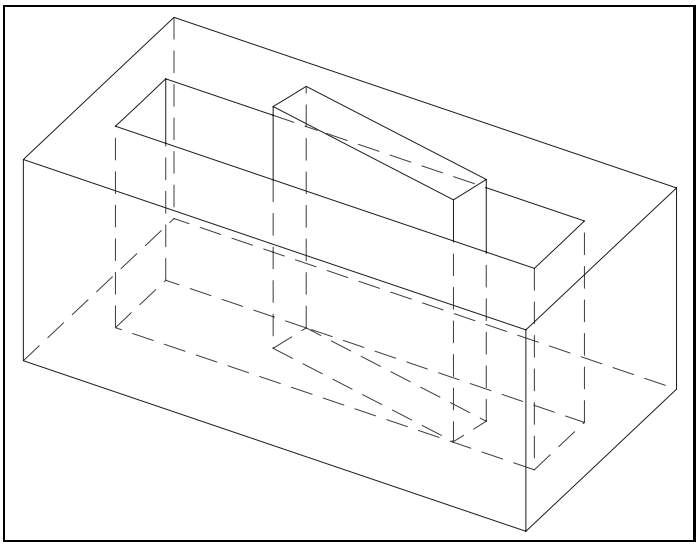

Figure 3.2: Tab in a slot interaction.

The contact points become kinematic joints in the vector loop model. Vectors can then be drawn from the datums to the kinematic joints along the independent dimensions of the parts. The vector loop may not be unique. However, different vector loops represent a common solution.

Figure 3.3 shows the tab skewed in the slot along with its associated vector loop.

The application of vector loop methods provides an algorithmic method to define the conditional tolerances for the assembly. As noted earlier, it is assumed that this step is performed after dimensions for form and function have been determined. Each engineering dimension becomes an *independent variable*. It is defined on the drawing as an engineering requirement and is independent of any

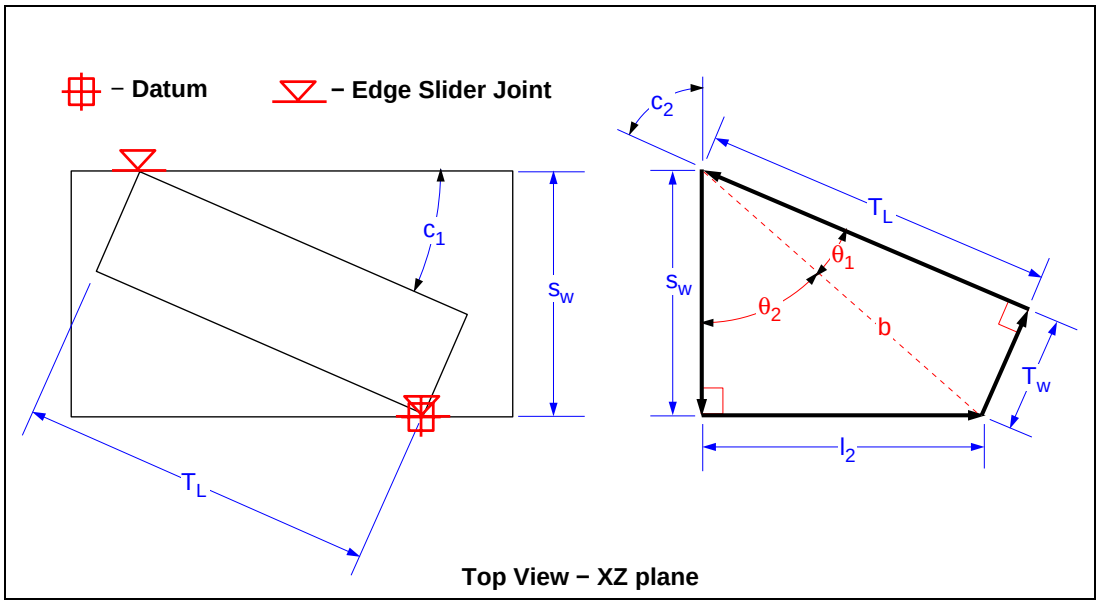

Figure 3.3: Skewed tab in a slot.

other value. Assembly parameters that change as the engineering dimensions are modified are *dependent variables*. The parameter space of the problem is

$$\mathbf{z} = \{s_w, T_w, T_L \,|\, l_2, c_2\}, \tag{3.1}$$

where s_w is the slot width, T_w is the tab width, T_L is the tab length, l_2 and c_2 are dependent variables in the system. The angle c_1 is the complement of c_2.

The vector loop equations for this system are

$$x = T_w \cos(c_2) - T_L \sin(c_2) + l_2 \leq 0 \tag{3.2}$$

$$z = T_w \sin(c_2) + T_L \cos(c_2) - s_w \leq 0 \tag{3.3}$$

This system of equations can be solved directly for the dependent variables, l_2 and

c_2. However, a simpler solution can be derived using the geometry of the vector loop. A diagonal b can be constructed across the quadrilateral of the vector loop. The length of this diagonal element is

$$b = \sqrt{T_L^2 + T_w^2}. \tag{3.4}$$

The length of the dependent variable l_2 is then

$$l_2 = \sqrt{b^2 - s_w^2} = \sqrt{T_L^2 + T_w^2 - s_w^2}. \tag{3.5}$$

From this solution, it is apparent that

$$\sqrt{T_L^2 + T_w^2} \geq s_w \tag{3.6}$$

must hold for l_2 to be real.

Equation 3.3 provides the final constraint when the z component has its maximum value as zero

$$T_w \sin(c_2) + T_L \cos(c_2) \leq s_w. \tag{3.7}$$

Together these two constraints assure that the tab will fit in the slot and prevent rotation. The conditional tolerances Z over the parameter space $\mathbf{z}$ can be written as

$$Z = \left\{ \begin{array}{c} (s_w > 0) \wedge (T_L > 0) \wedge (T_w > 0) \wedge (\sqrt{T_L^2 + T_w^2} \geq s_w) \\ T_L \cos(c_2) + T_w \sin(c_2) \leq s_w \end{array} \right\} \tag{3.8}$$

for the skewed tab/slot problem in the XZ plane.

The term *constraint tolerance* for this set of equations presents some difficulty. These equations represent assembly conditions or kinematic constraints on the system. They make no reference to allowable manufacturing variation in the system. However, this terminology is still currently used.

3.2.2 Conditional Tolerances on the Pin in a Hole

The pin in a hole problem is another simple two body, two contact-point problem. Srinivasan shows that this problem also has a closed form solution. An example of the pin-hole assembly is shown in figure 3.4. This problems allows both the conditional tolerances and the vector loop expressions to be written in closed form. It also provides a point of comparison for the two assembly expressions.

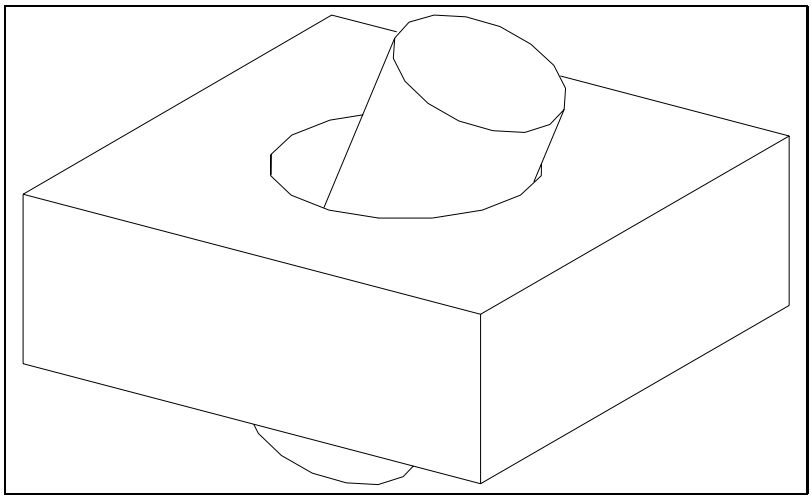

Figure 3.4: Pin/hole interaction.

The set of all dimensions in the problem is shown in figure 3.5. The pin diameter s_1, the hole diameter S_n, and the hole height l_1, are the engineering dimensions defined in this problem. The tilt angle c_3, the contact length l_2, the offset distance x_d, and the offset angle c_4, are all dependent assembly parameters. These seven dimensions form the parameter space $\mathbf{z}$ that must be constrained by the conditional tolerances. The total parameter space is

$$\mathbf{z} = \{s_1, S_n, l_1 \,|\, c_3, l_2, x_d, c_4\}. \tag{3.9}$$

The vector loop for this assembly including datums and joints is shown in figure 3.6. For this problem, the datum location is chosen to simplify the analysis and visualization of the vector loops. In a real part, the datum would be located at a

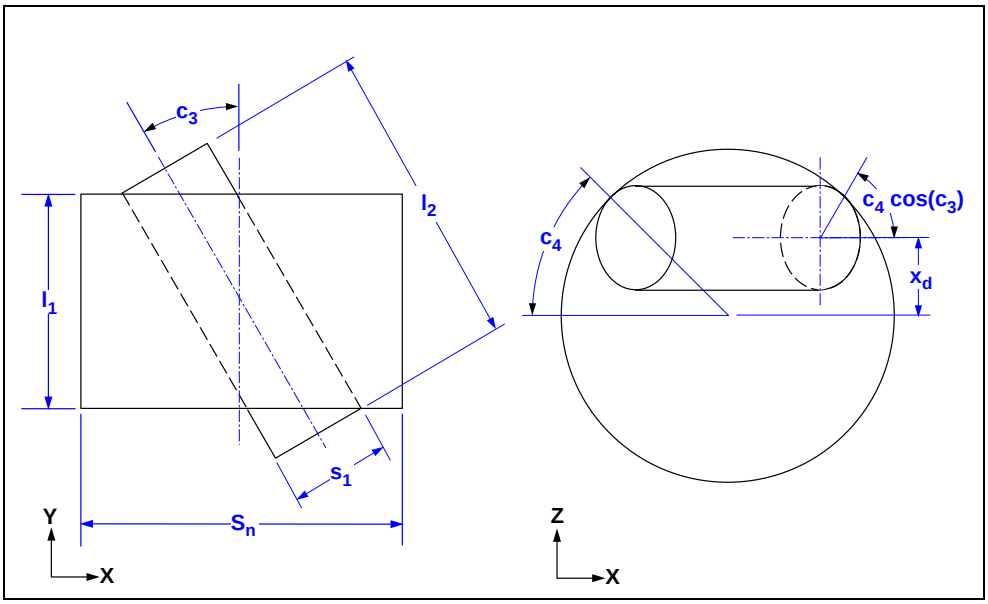

Figure 3.5: Dimensions on the pin-hole assembly.

measurable location.

This vector loop can be converted into a set of equations by traversing the vectors and summing vector components in the x, y, and z directions.

$$x = x_d \cos(90^o) - \frac{l_2}{2}\sin(c_3) - \frac{s_1}{2}\sin(c_4)\cos(c_3) \tag{3.10}$$

$$+\frac{S_n}{2}\sin(c_4) + \frac{l_1}{2}\cos(90^o) \leq 0, \tag{3.11}$$

$$y = x_d \sin(90^o) + \frac{l_2}{2}\cos(c_3) - \frac{s_1}{2}\sin(c_4)\sin(c_3) \tag{3.12}$$

$$+\frac{S_n}{2}\sin(0)\sin(c_4) - \frac{l_1}{2}\cos(0) \leq 0, \tag{3.13}$$

$$z = x_d \cos(90^o) + \frac{l_2}{2}\sin(180^o) + \frac{s_1}{2}\cos(c_4)\cos(c_3) \tag{3.14}$$

$$-\frac{S_n}{2}\cos(c_4) + \frac{l_1}{2}\sin(0) \leq 0. \tag{3.15}$$

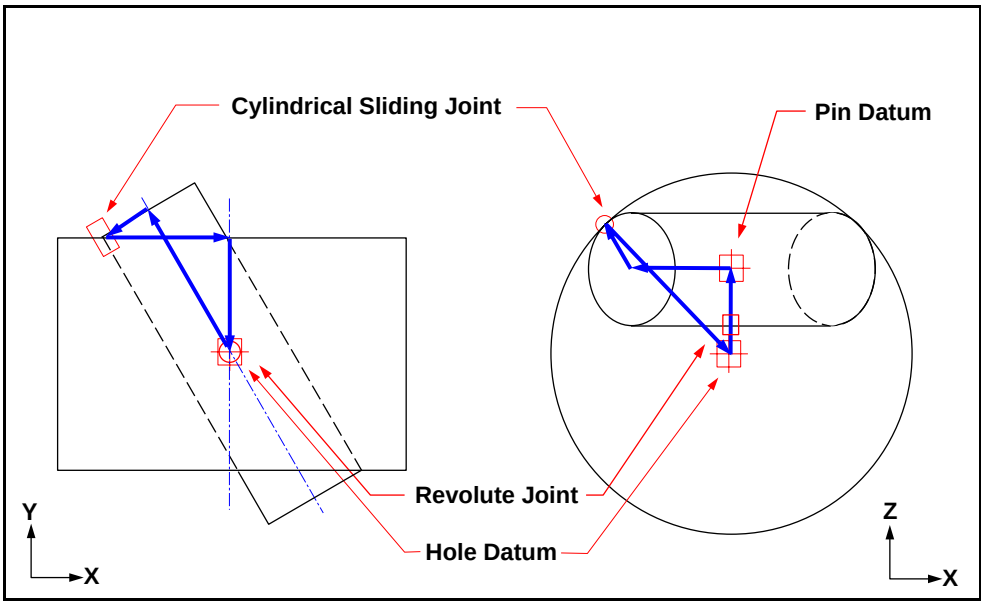

Figure 3.6: Datum and kinematic joints for the pin-hole problem.

The inequalities signify that the vector loops are constructed with the assembly at a maximum configuration. The vector are typically solved for the maximum value. Simplifying these expressions yields,

$$x = \frac{1}{2}\left(-l_2 \sin(c_3) - s_1 \sin(c_4)\cos(c_3) + S_n \sin(c_4)\right) \leq 0, \tag{3.16}$$

$$y = \frac{1}{2}\left(l_2 \cos(c_3) - s_1 \sin(c_4)\sin(c_3) - l_1\right) \leq 0, \tag{3.17}$$

$$z = x_d + \frac{1}{2}\left(s_1 \cos(c_4)\cos(c_3) - S_n \cos(c_4)\right) \leq 0. \tag{3.18}$$

Orientation of the Pin

The pin-hole problem may be divided into two separate problems, the orientation of the pin and the position of the pin. The orientation or tilt of the pin must be evaluated at the maximum material condition (MMC). The maximum tilt occurs when the pin is aligned with a plane through the center of the hole. This implies that the c_4 angle must be equal to zero. The XY plane may be used to contain this maximum position. Figure 3.7 shows an enlarged view of the loop defined in this plane. Equations 3.16 and 3.17 can thus be simplified

$$x = \frac{1}{2}(-l_2 \ \sin(c_3) - s_1 \ \cos c_3 - S_n) \leq 0, \tag{3.19}$$

$$y = \frac{1}{2}(l_2 \ \cos c_3 - s_1 \ \sin(c_3) - l_1) \leq 0. \tag{3.20}$$

The tilt angle, c_3, and the contact length, l_2, in figure 3.7 are the dependent

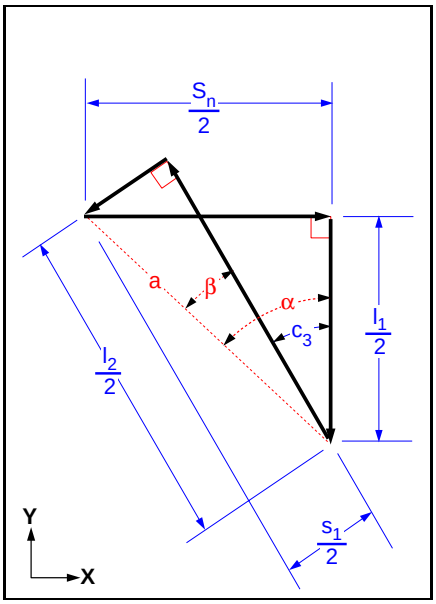

Figure 3.7: Dimensions and kinematic vector loop.

variables. They are not specified by any engineering requirement and result only as a consequence of the assembly process. These equations can be further simplified by eliminating the dependent variable l_2,

$$s_1 \sec c_3 + l_1 \tan c_3 - S_n \leq 0. \tag{3.21}$$

This constraint forces the hole to always be larger than the pin.

The other constraint on the system is imposed by the sliding joint. The contact length, marked a in figure 3.7, must be greater than the hole radius so the pin does not spin inside the hole. The length of a is easily seen from figure 3.7 to be $\sqrt{l_2^2 + s_1^2}$. The constraint applied by the sliding joint is then

$$\sqrt{l_2^2 + s_1^2} > S_n. \tag{3.22}$$

Also by definition, the independent variables must be non-zero. They have values on an engineering drawing.

Assembling all these constraints, the conditional tolerances Z over the parameter space $\mathbf{z}$ can be written as

$$Z = \left\{ \begin{array}{c} (s_1 > 0) \wedge (l_1 > 0) \wedge (\sqrt{l_2^2 + s_1^2} > S_n) \\ (s_1 \sec(c_3) + l_1 \tan(c_3) - S_n \leq 0) \end{array} \right\}. \tag{3.23}$$

The vector loop allows the conditional tolerances to be derived directly from the geometry with the knowledge of the independent variables.

This result is very similar to Srinivasan's result of

$$Z = \left\{ \begin{array}{l} (s_1 > 0) \wedge (l_1 > 0) \wedge (0 \leq c_3 < \frac{\pi}{2}) \\ \wedge (s_1 \sec(c_3) + l_1 \tan(c_3) - S_n \leq 0) \end{array} \right\}. \tag{3.24}$$

Equation 3.23 does not apply a constraint directly to a dependent variable. The constraint of $0 \leq c_3 < \frac{\pi}{2}$ in equation 3.24 is valid. It keeps the pin from spinning through the hole. However, because it is a dependent variable, its value is defined by other independent variables in the system. The angle can not be directly measured and should not be constrained. Equation 3.23 changes this constraint to reflect the sliding joint that exists between the two cylinders. This constraint also prohibits the pin from spinning in the hole and is derived directly from the vector loop.

Position of the Pin

Positional tolerance data can also be determined using Vector Assembly Models. Distances between any two points in an assembly or between a point and a datum are calculated using an open vector loop. Since these loops are not closed, the vectors do not sum to zero. An open loop adds no additional dependent variables to the problem, but there must be enough information from the closed loops to solve for the vector lengths and orientations. The pin-hole problem requires an open vector loop and an additional closed vector loop to solve the position problem.

For the open loop, the desired position is the location of the center of the pin relative to the datum at the center of the hole. Figure 3.8 shows a simple vector model that represents this position.

The new closed loop vector loop is composed of dimensions in the XZ plane as shown in figure 3.9. The c_4 angle is no longer assumed to be zero, so the pin can be placed at any distance x_d from the center of the hole. The positional constraint can be found directly from equation 3.18.

$$x_d + \frac{1}{2}(s_1 \cos(c_4) - S_n \cos(c_4)) \leq 0. \tag{3.25}$$

The values c_3, x_d, and c_4 are all unknown or dependent variables. The tilt angle, c_3, is defined by the vector loop describing orientation. This leaves two unknowns and only one equation. One of the two dependent variables, x_d or c_4, must be defined to

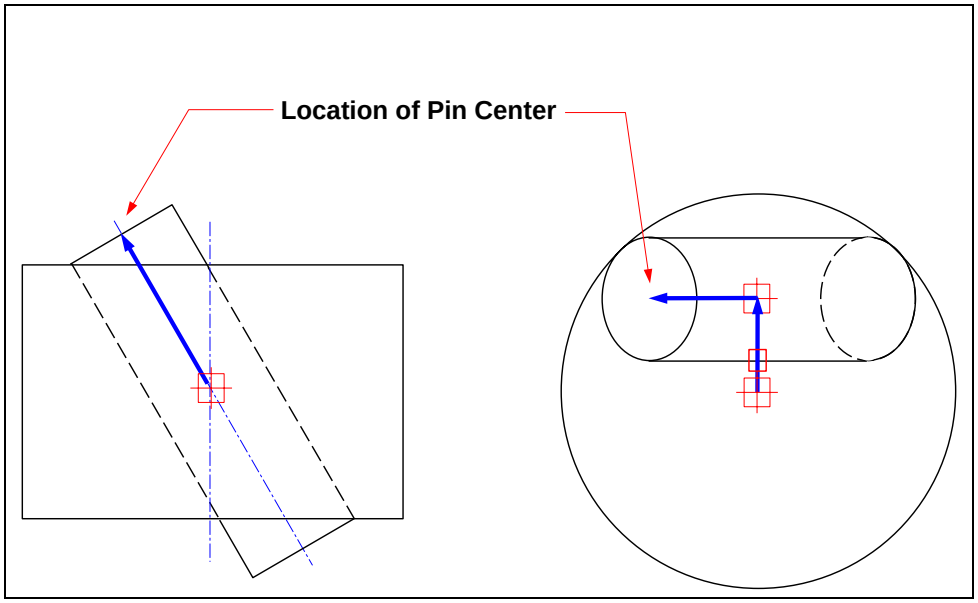

Figure 3.8: Open vector loop for determining pin position.

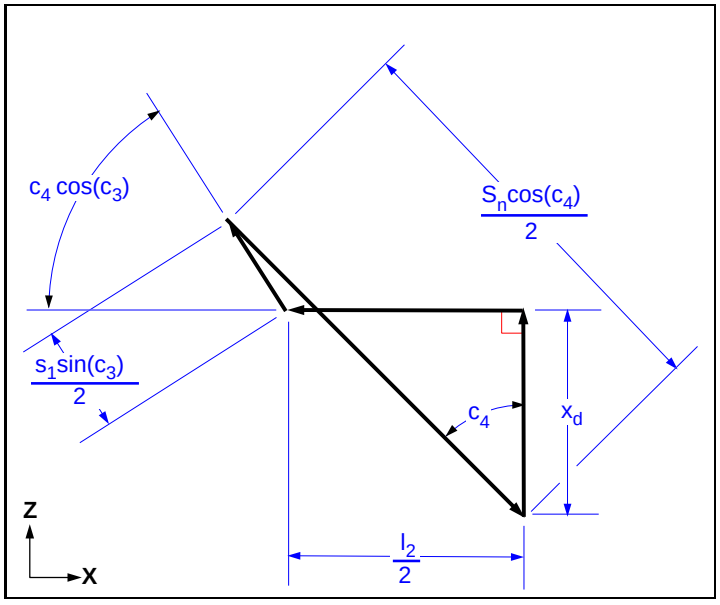

Figure 3.9: Kinematic vector loop for determining position.

solve the system of equations 3.16, 3.17 and 3.18. The system as posed is under-constrained. In terms of a kinematic solution, the c_4 angle can be considered as the input crank angle to a kinematic linkage problem. Treating the c_4 angle as an input or known variable creates a fully constrained system. Thus, the full set of conditional tolerances for the problem are

$$Z = \left\{ \begin{array}{c} (s_1 > 0) \wedge (l_1 > 0) \wedge (\sqrt{l_2^2 + s_1^2} > S_n) \wedge (0 \leq c_4 \leq 2\pi) \wedge \\ (s_1 \sec(c_3) + l_1 \tan(c_3) - S_n \leq 0) \wedge x_d + \frac{1}{2}(s_1 \cos(c_4) - S_n \, cos(c_4)) \leq 0 \end{array} \right\}. \tag{3.26}$$

This set of conditional tolerances fully constrains the assembly. The location of the center of the top of the pin may be obtained by traversing the vector loop to that point.

An animated graphical simulation of this assembly has been created. A sample view is shown in figure 3.10. The equations derived for the conditional tolerances are used to constrain the maximum position of the pin in the hole. The simulation allows the user to interactively modify the independent variables on either the pin or the hole and view the resulting configuration at any angle, c_4.

This simulation shows the utility of a kinematic approach to deriving conditional tolerances. The vector loop method provides a means of directly calculating the maximum values of the conditional tolerances of a system. It also provides methods for visualizing the effects of changes to the independent engineering parameters of the system based on kinematic principles. This allows engineers and

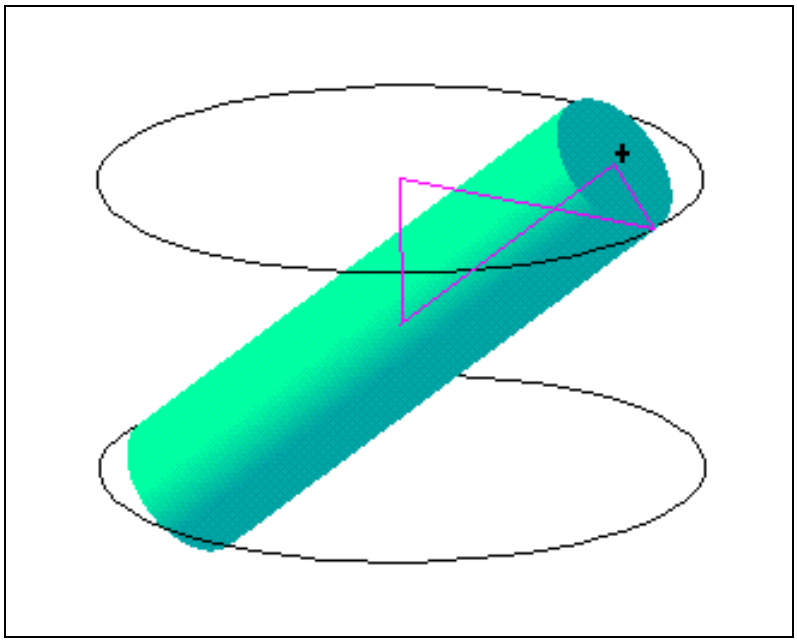

Figure 3.10: Pin/Hole graphical simulation.

designers to rapidly view the effects of different configurations in an assembly.

The choice of datums and the independence of the c_4 angle do not provide a good comparison with Srinivasan's conditional tolerance statement for the position of the pin. It should be noted, however, that the conditional tolerances derived from the vector loop statement given above are much less complex.

3.3 Linearized Constraint Based Solutions

Conditional tolerances can be used to analyze dimensional variation in an assembly. The equations contain non-linear expressions in terms of the dependent vari-

ables. The nonlinear terms are frequently analyzed using Monte Carlo simulation (Rubinstein 1981; Gao 1993). In Monte Carlo simulation, the independent engineering parameters in the assembly are modified and the dependent variables are calculated to determine the new position of the assembly. This process is performed thousands of times using random variations of the independent variables to determine a statistical result that includes all the nonlinear effects. This type of analysis can be very time consuming for complex problems or large standard deviations.

The non-linear constraint equations can also be solved by approximating them as linear equations. If the approximating assumptions are valid, complex systems may be rapidly solved and alternate configurations may be easily evaluated.

It is important to understand that the dependent variables determine the final location and orientation of parts in the assembly. These variables are frequently the kinematic variables that allow for small adjustments. Both solution techniques mentioned above solve for these dependent variables.

In the simple problems presented here, it is possible to find closed form solutions for the dependent variables. The following sections will compare the closed form solution with the Direct Linearization Method (DLM). They will show when linearized solutions are valid and when full nonlinear solutions must be used.

3.3.1 Closed-form Solution of the Pin Orientation

The orientation of the pin in a hole is determined by the angle c_3 in equation 3.23. This angle is embedded in a nonlinear equation. There are several ways to solve for this angle. One way is to use trigonometric identities to pose the problem as a quadratic equation in terms of $\tan(\frac{1}{2}\, c_3)$ so that

$$\frac{(S_n + s_1)}{l_1} \tan^2(\frac{1}{2}\, c_3) - 2\, \tan(\frac{1}{2}\, c_3) + \frac{-S_n + s_1}{l_1} = 0. \tag{3.27}$$

In many cases it is anticipated that the first and third terms of this quadratic equation will be small with respect to the second term. This will cause the solutions to be close to zero. To be more sensitive to these solutions, Srinivasan multiplies the traditional quadratic formula by the conjugate of the numerator to obtain

$$x = \frac{2\, c}{-b \pm \sqrt{b^2 - 4\, a\, c}}. \tag{3.28}$$

Thus, roots that would have been found near zero will now approach infinity.

Applying this equation and solving first for the quadratic and then for c_3, it can be shown that

$$c_3 = 2\, \tan^{-1} \left(\frac{S_n - s_1}{l_1 \left(1 + \sqrt{1 + \frac{(S_n - s_1)(S_n + s_1)}{{l_1}^2}}\right)} \right). \tag{3.29}$$

Even for an assembly as simple as a pin in a hole, the solution for the dependent variables leads to complex solutions. For most problems, it is impractical to solve explicitly for the dependent variables.

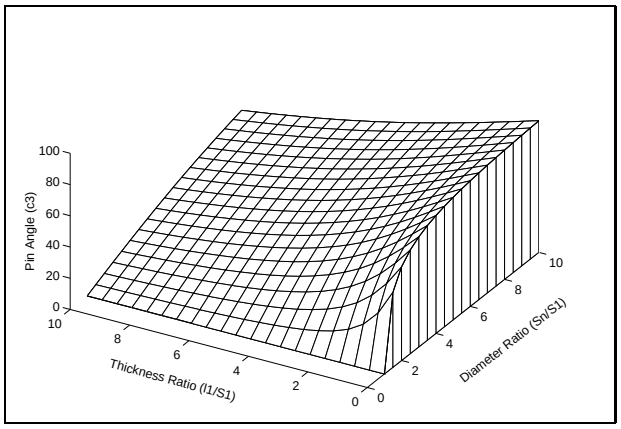

Figure 3.11: Design space for pin/hole problem.

Figure 3.11 shows a surface plot of the variable c_3 as the diameter ratio S_n/s_1 and the thickness ratio l_1/s_1 vary. Over a large range of the design space, the surface is quite linear. The greatest areas of non-linearity occur for thin plates where l_1/s_1 is small.

The vector loop can also give insight into the geometry of the problem. If a line is constructed, as shown in figure 3.7, and labeled a, the angle c_3 can be described as the difference between the angles α and β. Solving for α and β in terms of the arcsine gives

$$c_3 = \sin^{-1}\left(\frac{S_n}{\sqrt{S_n^2 + l_1^2}}\right) - \sin^{-1}\left(\frac{s_1}{\sqrt{S_n^2 + l_1^2}}\right). \tag{3.30}$$

Note that the arcsine will not fail until $s_1 > \sqrt{S_n^2 + l_1^2}$, which will occur after the physical limit of the interference fit forces the c_3 angle to be 0. Over this range, it provides the same results as equation 3.29 and is algorithmically easier to imple-

ment.

Taking derivatives of equation 3.29 with respect to each of the independent variables gives

$$\frac{\partial c_3}{\partial s_1} = -\frac{1}{\sqrt{{l_1}^2 + {S_n}^2 - {s_1}^2}}, \tag{3.31}$$

$$\frac{\partial c_3}{\partial S_n} = \frac{{l_1}^2 + S_n\, s_1 - {s_1}^2 + l_1\sqrt{{l_1}^2 + {S_n}^2 - {s_1}^2}}{\sqrt{{l_1}^2 + {S_n}^2 - {s_1}^2}\left({l_1}^2 + {S_n}^2 - S_n\, s_1 + l_1\sqrt{{l_1}^2 + {S_n}^2 - {s_1}^2}\right)}, \tag{3.32}$$

and

$$\frac{\partial c_3}{\partial l_1} = \frac{(s_1 - S_n)\left(l_1 + \sqrt{{l_1}^2 + {S_n}^2 - {s_1}^2}\right) l_1}{\sqrt{{l_1}^2 + {S_n}^2 - {s_1}^2}\left({l_1}^2 + {S_n}^2 - S_n\, s_1 + l_1\sqrt{{l_1}^2 + {S_n}^2 - {s_1}^2}\right)}. \tag{3.33}$$

These derivative terms relate variation in a dependent or kinematic variable to the independent or engineering variables. Even for a simple problem, the closed form derivative terms can become very complex. The next section will demonstrate the use of such derivative terms in tolerance analysis.

3.3.2 Linear Variations of the Pin/Hole Problem

Previous sections have demonstrated the bounds on the nominal values in an assembly. This section will demonstrate how the DLM may be used to add small variations to the nominal values. It will show both the utility and the limitations of this method.

The derivative terms derived in closed form in the previous section can be used

as sensitivities in a statistical analysis by the following equations:

$$dc_{3_{\text{RMS}}} = \sqrt{\left(\frac{\partial c_3}{\partial s_1} ds_1\right)^2 + \left(\frac{\partial c_3}{\partial S_n} dS_n\right)^2 + \left(\frac{\partial c_3}{\partial l_1} dl_1\right)^2} \tag{3.34}$$

$$dc_{3_{\text{Worst Case}}} = \left|\frac{\partial c_3}{\partial s_1}\right| ds_1 + \left|\frac{\partial c_3}{\partial S_n}\right| dS_n + \left|\frac{\partial c_3}{\partial l_1}\right| dl_1. \tag{3.35}$$

These equations relate the variations in the independent parameters ds_1, dS_n, and dl_1 to variation in the dependent variable dc_3. If the tolerances on s_1, S_n, and l_1 are substituted for the variations ds_1, dS_n, and dl_1, equations 3.34 and 3.35 become estimates of the tolerance accumulation in the assembly. The RMS equation is purely a statistical estimate. It assumes a Gaussian distribution of the variables. The Worst Case equation is a conservative estimate of the variation in an assembly.

Both of these tolerance accumulation equations assume that the variations are linearly independent: the variables are not covariant. This is typically a valid assumption when parts are created by different processes and then assembled. If the variation among the parts is correlated, equations 3.34 and 3.35 are invalid so the the full covariance matrix must be used. They also assume that the assembly function is somewhat flat in the region of interest. This assumption will be examined later.

It is not always possible to solve for the dependent variables and calculate the

derivatives in terms of the engineering requirements or independent variables as was done in section 3.3.1. Using the linearizing vector loop equations, it is possible to compute the sensitivities using linear algebra. The linearized vector loop equations can be divided into two matrices containing the independent and dependent terms. The basic equation governing the linearized solution is

$$\boldsymbol{A}\, d\vec{X} + \boldsymbol{B}\, d\vec{U} = \vec{0}, \tag{3.36}$$

where $\boldsymbol{A}$ is the Jacobian or first derivative matrix with respect to the independent variables, $d\vec{X}$ is the variation or tolerance associated with these variables, $\boldsymbol{B}$ is the Jacobian matrix with respect to the dependent variables, and $d\vec{U}$ is the variation with respect to the dependent variables. Solving for $d\vec{U}$ gives

$$d\vec{U} = -\boldsymbol{B}^{-1}\boldsymbol{A}d\vec{X}. \tag{3.37}$$

This method can be applied to the pin-hole orientation problem. Forming the Jacobian matrix for the independent variables $\{s_1, S_n, l_1\}$ from equations 3.19 and 3.20 gives

$$\boldsymbol{A} = \begin{bmatrix} \cos(c_3) & -1 & 0 \\ -\sin(c_3) & 0 & -1 \end{bmatrix}, \tag{3.38}$$

while the Jacobian matrix of the dependent variables $\{c_3, l_2\}$ is

$$\boldsymbol{B} = \begin{bmatrix} (l_2\cos(c_3) - s_1\sin(c_3)) & \sin(c_3) \\ (-s_1\cos(c_3) - l_2\sin(c_3)) & \cos(c_3) \end{bmatrix}. \tag{3.39}$$

The inverse of $\boldsymbol{B}$ is

$$\boldsymbol{B}^{-1} = \frac{1}{l_2}\begin{bmatrix} \cos(c_3) & -\sin(c_3) \\ s_1\ \cos(c_3) + l_2\ \sin(c_3) & l_2\ \cos(c_3) - s_1\ \sin(c_3) \end{bmatrix}. \tag{3.40}$$

By performing the matrix multiplication $-(\boldsymbol{B}^{-1}\boldsymbol{A})$ the sensitivity matrix is

$$\boldsymbol{S} = \frac{1}{l_2}\begin{bmatrix} -1 & \cos(c_3) & -\sin(c_3) \\ -s_1 & s_1\,\cos(c_3) + l_2\,\sin(c_3) & l_2\,\cos(c_3) - s_1\,\sin(c_3) \end{bmatrix}. \tag{3.41}$$

The entire system is then

$$\begin{Bmatrix} dc_3 \\ dl_2 \end{Bmatrix} = \frac{1}{l_2}\begin{bmatrix} -1 & \cos(c_3) & -\sin(c_3) \\ -s_1 & s_1\cos(c_3) + l_2\sin(c_3) & l_2\cos(c_3) - s_1\sin(c_3) \end{bmatrix}\begin{Bmatrix} ds_1 \\ dS_n \\ dl_1 \end{Bmatrix}. \tag{3.42}$$

The sensitivities show how much influence a given variation has on an assembly. For example, the variation in the pin diameter, ds_1, is negatively correlated with the variation in the tilt angle. Note that the sensitivities are not always defined in terms of the independent variables. The dependent variables can be calculated either numerically or from geometric construction in a CAD model.

Multiplying through by the variation in the independent variables in equation 3.42 gives

$$d\vec{U} = \frac{1}{l_2}\begin{bmatrix} -ds_1 + dS_n\cos(c_3) - dl_1\sin(c_3) \\ -ds_1 s_1 + dl_1 l_2\cos(c_3) + dS_n s_1\cos(c_3) + dS_n l_2\sin(c_3) - dl_1 s_1\sin(c_3) \end{bmatrix}, \tag{3.43}$$

where

$$d\vec{U} = \begin{Bmatrix} dc_3 \\ dl_2 \end{Bmatrix} \tag{3.44}$$

is the vector of assembly variations.

One common linearization assumption can be made by considering small variations around the nominal (c_3 = 0). The constraint sensitivity for c_3 is then defined

as

$$dc_3 = dS_n - ds_1. \tag{3.45}$$

This is the design rule that is normally used for angular tilt of a pin in a hole. As the angle moves away from the nominal position, the error increases due to the small angle assumptions that were used to arrive at this rule.

A more general linearization can be accomplished by using the sensitivities. The sensitivities are calculated with the assembly in a given position and orientation. The sensitivities for the pin at its maximum orientation were derived in equation 3.41. These sensitivities can then be used to extrapolate the affects of small variations on the assembly function.

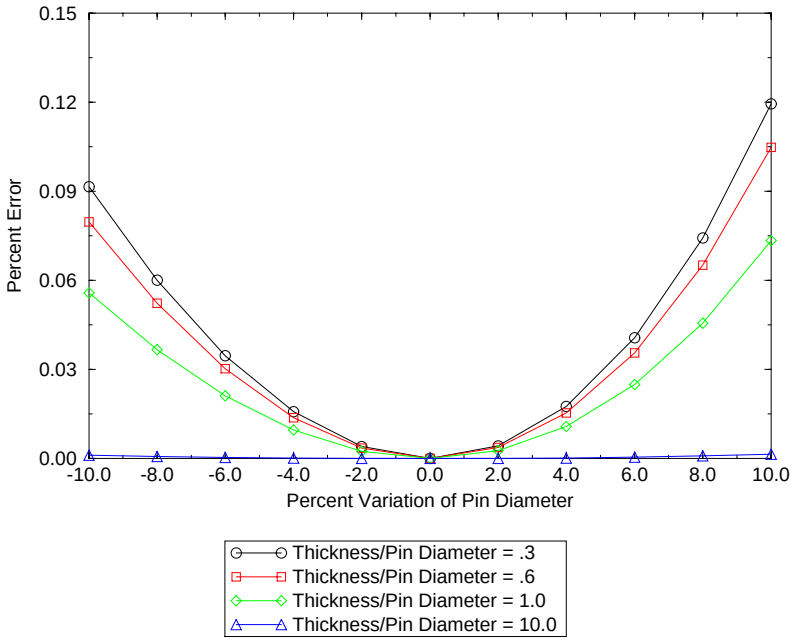

Figure 3.12: Error induced by linearization of pin/hole problem.

Figure 3.12 shows the error associated with this linearized extrapolation. Using figure 3.11, a region was selected in the nonlinear region. The values of S_h/s_1 =2.0 and l_1/s_1 =0.3 were selected as the starting location. The hole thickness l_1 was then increased for succeeding analyses. The linearized solution, equation 3.43, was compared with the closed-form solution, equation 3.30, to arrive at a percent error for each analysis. The solution at the nominal size is exact for both cases. Thus, the error at 0% variation is exactly 0. Even in the most non-linear regime, the error is less than .15%. When the ratio of the hole thickness to pin diameter is 10.0, the error over the entire range is nearly zero.

3.3.3 Linear Variations of the Tab/Slot Problem

Similar results also occur when analyzing the tab skewed in a slot. Figure 3.3 and equations 3.2 and 3.3 show that the c_2 angle is the dependent kinematic variable in this case. Referring to the geometry of the loop, the angle c_2 may be defined as

$$c_2 = \theta_1 + \theta_2. \tag{3.46}$$

The terms θ_1 and θ_2 are derived from the geometry: to be

$$\theta_1 = \cos^{-1}\left(\frac{s_w}{\sqrt{T_L^2 + T_w^2}}\right) \tag{3.47}$$

$$\theta_2 = \cos^{-1}\left(\frac{T_L}{\sqrt{T_L^2 + T_w^2}}\right). \tag{3.48}$$

Thus,

$$c_2 = \cos^{-1}\left(\frac{s_w}{\sqrt{T_L^2 + T_w^2}}\right) + \cos^{-1}\left(\frac{T_L}{\sqrt{T_L^2 + T_w^2}}\right). \tag{3.49}$$

The closed form derivatives may also be obtained from this solution.

A plot of this surface is shown in figure 3.13. A portion of this function has imaginary results. Physically, this is associated with the slot being wider than the length of the diagonal across the tab. This results in an unstable solution. The function is non-linear near this instability. Most designers instinctively understand these non-linear situations and design in the more linear regime. Once again, it should be noted that away from this non-linearity the function is flat.

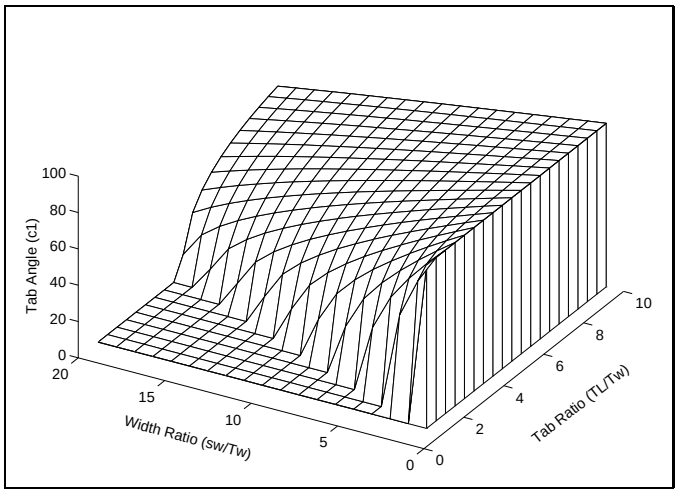

Figure 3.13: Skew angle of tab as a function of tab length/tab width and slot width/tab width.

The sensitivity matrix is derived by using equations 3.2 and 3.3. Using the

independent parameters T_w, T_L, and s_w, the $\mathbf{A}$ matrix is

$$\mathbf{A} = \begin{bmatrix} \cos(c_2) & -\sin(c_2) & 0 \\ \sin(c_2) & \cos(c_2) & -1 \end{bmatrix} \tag{3.50}$$

and the $\mathbf{B}$ matrix is

$$\mathbf{B} = \begin{bmatrix} T_w \sin(c_2) + T_L \cos(c_2) & 1 \\ -T_w \cos(c_2) + T_L \sin(c_2) & 0 \end{bmatrix}. \tag{3.51}$$

Performing the matrix manipulations $-(\mathbf{B}^{-1}\mathbf{A})$, the full system of equations is

$$\begin{Bmatrix} dc_2 \\ dl_2 \end{Bmatrix} = \frac{1}{D} \begin{bmatrix} -\sin(c_2) & -\cos(c_2) & 1 \\ -T_w & -T_L & T_w \sin(c2) + T_L \cos(c2) \end{bmatrix} \begin{Bmatrix} dT_w \\ dT_L \\ ds_w \end{Bmatrix} \tag{3.52}$$

where

$$D = T_w \cos(c2) - T_L \sin(c2). \tag{3.53}$$

An error analysis of the linearization is shown in figure 3.14. There is a discontinuity in the skew angle of the tab. If the diagonal length across the tab is too short, the tab will spin in the slot. This error analysis starts on the verge of the discontinuity in the non-linear range.

Four different cases were selected for the error analysis. The ratio of the slot width to tab width (S_w/T_w) is 4.0. The initial tab aspect ratio is 4.5. When the tab length is varied by -10%, this approaches the discontinuity. The error due to linearization at the worst case is nearly 12%. However, this error quickly becomes more manageable as the percent variation decreases and the design moves away

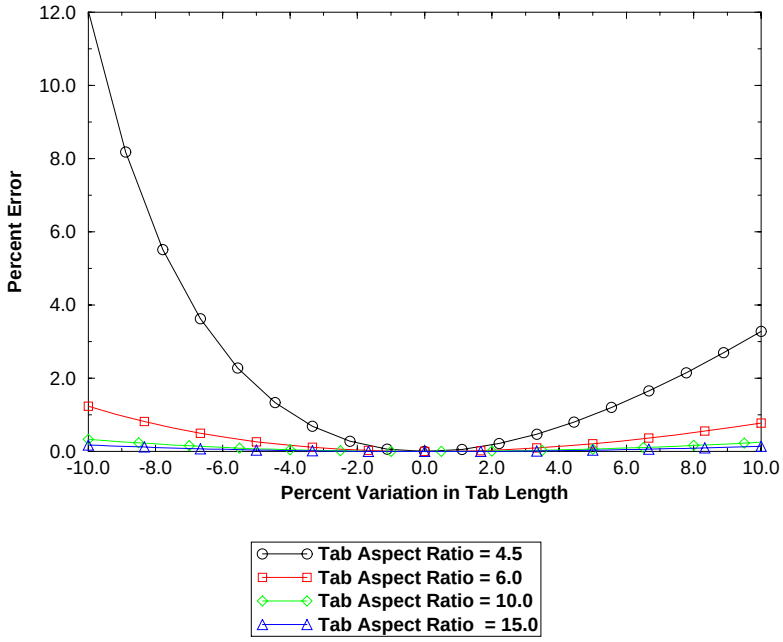

Figure 3.14: Error induced by linearization of the tab/slot problem.

from the discontinuity. With a tab aspect ratio of 15.0, the error is nearly zero for the entire range of variation.

3.3.4 Limitations of the Direct Linearization Method

The previous examples have demonstrated the application of DLM to two simple problems. For a wide range of problems, DLM is accurate and computationally efficient. These examples also point out some of the limitations of DLM:

- DLM can be inaccurate near discontinuities,
- DLM is not well suited to large variations,

- DLM can be inaccurate in highly non-linear functions.

Discontinuities in the functions are a major problem. They arise from changing boundary conditions. If contact changes among the surfaces, the vector loops change. For example, consider a plate that rests on four studs. Only three studs are required to define the plane. The fourth stud is redundant. It is not clear how the vector loops should be defined in this case.

The other two limitations occur in few cases. Tolerances are typically very small in relation to the nominal dimension. Based on the results of this and other studies, it is recommended that variations be less than 5% of the nominal for linearized analysis. Non-linearities are typically avoided by designers because of the inherent instabilities. However, if highly non-linear configurations are required by the design, Monte Carlo analysis methods are appropriate.

3.4 Summary

This chapter has demonstrated that vector loops are capable of capturing the same information as defined by Virtual Boundary Requirements. It has also shown that vector loops can be used to algorithmically derive the Conditional Tolerances associated with arbitrary functions.

This chapter has also demonstrated that linearized methods can be used to ac-

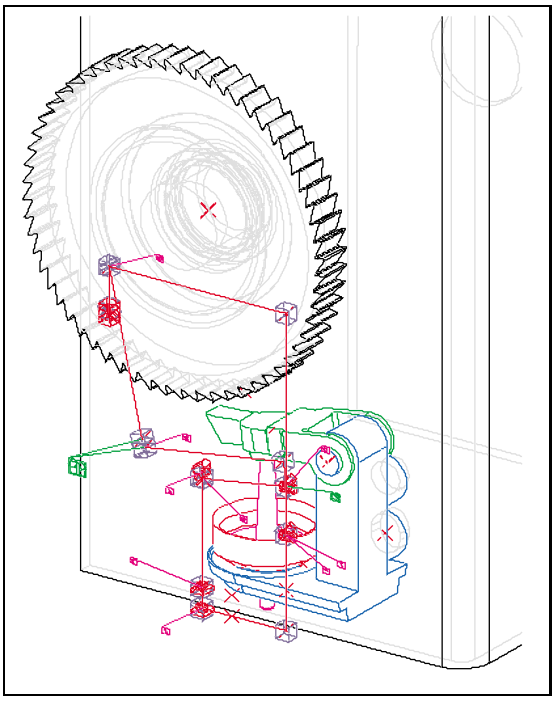

Figure 3.15: Complex ratchet-pawl assembly.

curately solve for variations in an assembly. It has shown that for certain non-linear situations, inaccuracies can arise, but designs typically avoid non-linear geometric configurations.

The application of vector loops on real engineering problems is not trivial. It takes engineering experience and judgment to determine the vector loop and gain engineering insight into the design. It is feasible that feature recognition techniques could be applied to the vector loop method to speed the definition of loops. A graphical method for defining the loops has been implemented in $AutoCAD^{TM}$, $ProEngineer^{TM}$, and $CATIA^{TM}$. In these systems the user specifies parts, datum

planes associated with the parts, joints, and the datum planes defining the joints. Once this information has been specified, the vector loops can be automatically created and solved. These tools permit the analysis of real world problems such as the ratchet-pawl assembly as shown in figure 3.15.

The examples presented in this chapter are very simplistic. However, they do allow closed form solutions. The same methods can be accurately applied to complex assemblies that include multiple parts and geometric tolerances.

Chapter 4

Compliance and Tolerance Analysis

This chapter develops theory for integrating tolerance analysis with linear finite element analysis. It shows how equilibrium methods may be used to predict assembly forces and stresses. It develops a linear method of solving certain contact problems, define the limitations, and show different implementations for tolerance analysis. This methodology can provide engineers and designers with a process for determining the effect of manufacturing tolerances early in the design process.

Chapter 3 described methods for performing tolerance analysis on rigid assemblies. In a rigid assembly, all of the necessary information can be obtained directly from the geometry. No force analysis is required. However, for assemblies of compliant parts, forces are often required to bring mating parts together.

One limitation associated with rigid body assembly methods is discontinuous

or changing boundaries. For example, the block in figure 4.1 is designed to rest on three columns. However, due to size variations it will only rest on two of the columns; the third column is redundant. It is impossible to predict which columns will support the block. In real structures, the third column will share the load as the force from either gravity or a fastener is applied, causing deformation of the other members. In statics, this type of problem is classified as an indeterminate structure. Force equilibrium does not provide sufficient information to solve the problem. Additional equations must be developed from the material properties.

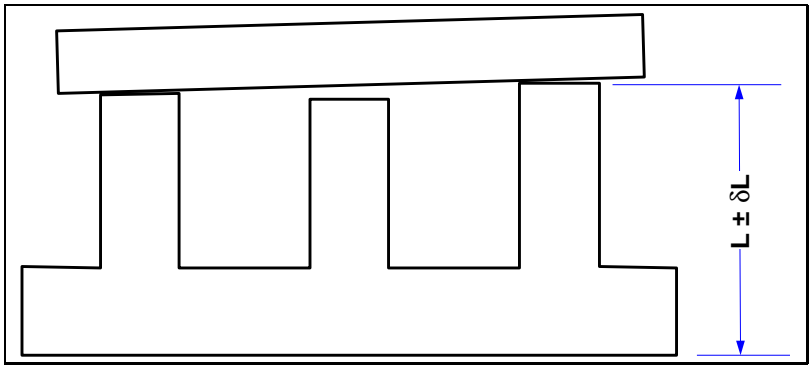

Figure 4.1: Statically indeterminate structure.

The tolerance analysis methods described in chapter 3 are equivalent to statically determinate structures. The geometry provides adequate information to solve for the tolerance stack-up. Additional equations are required to solve for tolerance stack-ups involving assembly forces or redundant supports. As in statically indeterminate structures, the needed equations arise from the material properties. These

equations and methods for using them in compliant tolerance analysis are derived in this chapter.

The problem of part compliance becomes apparent in dealing with thin shell components. An airplane skin may be slightly warped, yet it can still be riveted in place. What are the consequences of this? What are the residual assembly stresses created in the part? This question is especially important for assemblies of composite parts which can delaminate or fracture under excessive loads. How likely are composite parts to fail during assembly if they are subject to specified dimensional and surface variations?

4.1 Linear Contact Analysis

In 1975, Francavilla and Zienkiewicz (1975) published a note documenting a method of calculating contact stresses in assemblies, such as press fit cylinders, using the finite element method. This method is limited because it requires that the extent of the contact zone be known prior to the solution of the deformation problem. It also ignores the effects of friction. It provides a “steady-state” solution to the contact problem after the surfaces are fully in contact. Due to these limitations, the steady state method can not handle a wide variety of “transient” contact problems, specifically, those that are classified as “moving boundary value” problems, where

the contact zone changes as force is applied. Transient contact problems require an iterative solution to determine the boundary of the contact zone. Thus, research in the area of contact analysis has ignored this steady-state method and developed general contact elements that require non-linear solutions. Dealing correctly with non-linear elements and solutions is not a trivial problem. The non-linearities can cause convergence problems and increase both modeling and solution time.

However, the steady-state method is well suited to performing assembly solutions for tolerance analysis. It is also well matched with the DLM tolerance model described in chapter 3. The linear contact solution method requires the following assumptions:

1. Contact between mating surfaces must be enforced at the nodes so the entire contact zone is specified in advance.
2. Small geometric variations in a part will create negligible changes in the part stiffness matrices.
3. Friction must be negligible.
4. The gap/interference must be governed by small deformation theory.
5. The material must behave linearly.
6. The assembly process must be linear.

These limitations are compatible with tolerance analysis, which deals with small deviations about nominal dimensions.

A derivation of a steady-state contact analysis method follows for both one-dimensional and n-dimensional assemblies. Assume that two compliant parts, **a** and **b**, having stiffnesses k_a and k_b, are to be brought into contact by closing an assembly gap as shown in figure 4.2. The gap δ_o can be specified as the difference of the equilibrium displacements of the individual parts,

$$\delta_o = \delta_a - \delta_b. \tag{4.1}$$

This assumes that positive displacement is to the right as indicated in figure 4.2.

Hooke's Law can be written for each part,

$$\delta_a = F_a/k_a, \tag{4.2}$$

$$\delta_b = F_b/k_b. \tag{4.3}$$

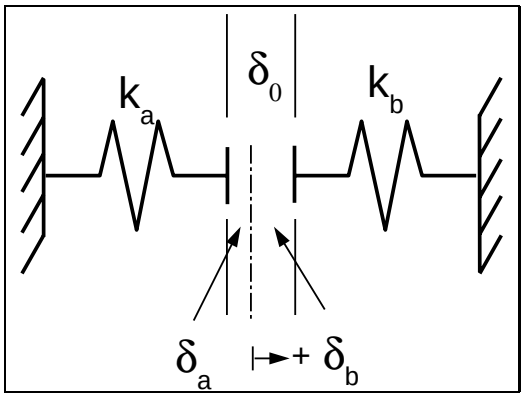

Figure 4.2: Two springs to be assembled and the resultant equilibrium point.

When the gap is closed, the forces in each spring must be in equilibrium:

$$F_a = -F_b. \tag{4.4}$$

Combining these equations, δ_o can be defined as

$$\delta_o = \frac{F_a}{k_a} - \frac{F_b}{k_b}. \tag{4.5}$$

Substituting $-F_a$ for F_b,

$$\delta_o = \left(\frac{1}{k_a} + \frac{1}{k_b}\right) F_a. \tag{4.6}$$

Since the gap is the known quantity, this equation can be solved for F_a:

$$F_a = \frac{1}{\frac{1}{k_a} + \frac{1}{k_b}} \delta_o. \tag{4.7}$$

The primary variable of interest in the gap closure problem is displacement. Substituting equations 4.4 and 4.7 into equations 4.2 and 4.3, the required displacements of the individual components can be obtained:

$$\delta_a = \frac{\frac{1}{k_a}}{\frac{1}{k_a} + \frac{1}{k_b}} \delta_o, \tag{4.8}$$

$$\delta_b = -\frac{\frac{1}{k_b}}{\frac{1}{k_a} + \frac{1}{k_b}} \delta_o. \tag{4.9}$$

Thus, the displacements of δ_a and δ_b depend inversely on the stiffnesses or (directly on the compliance) of the mating parts.

These results can be applied to complex structural models, as shown in figure 4.3, using a matrix formulation. In this case, the $\vec{\delta}$ terms represent displacement

vectors and the $\boldsymbol{K}$ terms represent the stiffness matrices associated with each structure.

By Hooke's Law

$$\vec{\delta}_a = \boldsymbol{K}_a{}^{-1}\vec{F}_a, \tag{4.10}$$

$$\vec{\delta}_b = \boldsymbol{K}_b{}^{-1}\vec{F}_b. \tag{4.11}$$

At equilibrium,

$$\vec{F}_a = -\vec{F}_b \tag{4.12}$$

and

$$\vec{\delta}_o = \vec{\delta}_a - \vec{\delta}_b. \tag{4.13}$$

Substituting the statements of Hooke's law and equation 4.12 into equation 4.13,

$$\vec{\delta}_o = \boldsymbol{K}_a{}^{-1}\vec{F}_a - \boldsymbol{K}_b{}^{-1}\vec{F}_b, \tag{4.14}$$

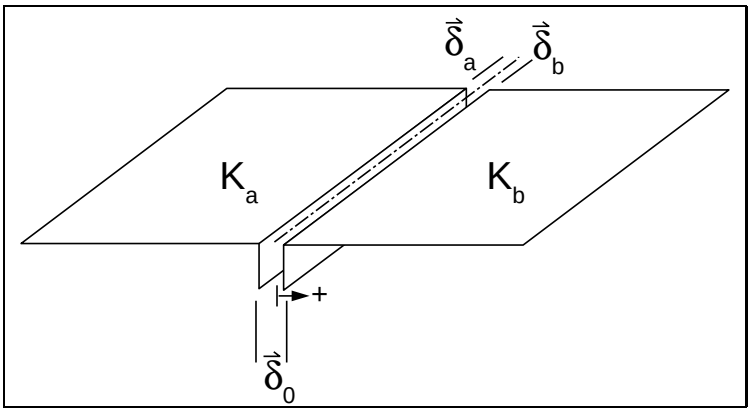

Figure 4.3: Two shells to be assembled, showing the resultant equilibrium plane.

$$= \left[\boldsymbol{K}_a{}^{-1} + \boldsymbol{K}_b{}^{-1} \right] \vec{F}_a. \tag{4.15}$$

Solving the equation for the equilibrium force,

$$\vec{F}_a = \left[\boldsymbol{K}_a{}^{-1} + \boldsymbol{K}_b{}^{-1} \right]^{-1} \vec{\delta}_o. \tag{4.16}$$

Substituting the definition of the equilibrium force into Hooke's law gives the displacement vectors associated with each part:

$$\begin{aligned} \vec{\delta}_a &= \boldsymbol{K}_a{}^{-1} \vec{F}_a, \\ &= \boldsymbol{K}_a{}^{-1} \left[\boldsymbol{K}_a{}^{-1} + \boldsymbol{K}_b{}^{-1} \right]^{-1} \vec{\delta}_o, \end{aligned} \tag{4.17}$$

$$\begin{aligned} \vec{\delta}_b &= -\boldsymbol{K}_b{}^{-1} \vec{F}_b, \\ &= -\boldsymbol{K}_b{}^{-1} \left[\boldsymbol{K}_a{}^{-1} + \boldsymbol{K}_b{}^{-1} \right]^{-1} \vec{\delta}_o. \end{aligned} \tag{4.18}$$

This is similar to the formulation that Francavilla and Zienkiewicz derive. Note the parallelism between equations 4.17 and 4.18 and the one-dimensional equations 4.8 and 4.9. In both cases, the displacements of the parts are a ratio of the inverse stiffnesses of the parts times the original gap. Also, note that the equilibrium displacements are posed in terms of the compliance matrices, the inverse stiffness matrices.

This process involves three matrix inversions so it is numerically expensive and prone to round-off error. Equations 4.17 and 4.18 can be simplified to a single matrix inversion. Starting with equation 4.17 where $\vec{\delta}_a$ is a function of $\vec{\delta}_o$,

$$\vec{\delta}_a = \boldsymbol{K}_a^{-1} \left[\boldsymbol{K}_a^{-1} + \boldsymbol{K}_b^{-1} \right]^{-1} \vec{\delta}_o,$$

$$
\begin{aligned}
&= \left[\left[\boldsymbol{K}_a^{-1} + \boldsymbol{K}_b^{-1}\right]\boldsymbol{K}_a\right]^{-1}\vec{\delta}_o, \\
&= [\underbrace{\boldsymbol{K}_a^{-1}\boldsymbol{K}_a}_{\boldsymbol{I}} + \boldsymbol{K}_b^{-1}\boldsymbol{K}_a^{-1}]^{-1}\vec{\delta}_o, \\
&= [\overbrace{\boldsymbol{K}_b^{-1}\boldsymbol{K}_b}^{\boldsymbol{I}} + \boldsymbol{K}_b^{-1}\boldsymbol{K}_a^{-1}]^{-1}\vec{\delta}_o, \\
&= \left[\boldsymbol{K}_b^{-1}\left[\boldsymbol{K}_b + \boldsymbol{K}_a\right]\right]^{-1}\vec{\delta}_o, \\
\vec{\delta}_a &= \left[\boldsymbol{K}_b + \boldsymbol{K}_a\right]^{-1}\boldsymbol{K}_b\vec{\delta}_o. \qquad (4.19)
\end{aligned}
$$

The key to this derivation is the substitution of the identity matrices, $\boldsymbol{K}_a^{-1}\boldsymbol{K}_a$, for $\boldsymbol{K}_b^{-1}\boldsymbol{K}_b$. A similar expression may be derived to describe the equilibrium position of $\vec{\delta}_b$:

$$\vec{\delta}_b = \left[\boldsymbol{K}_b + \boldsymbol{K}_a\right]^{-1}\boldsymbol{K}_a\vec{\delta}_o. \qquad (4.20)$$

This converts the equation presented by Francavilla and Zienkiewicz to a single matrix inversion, reducing numerical expense and error. In addition, this method is not iterative; there are no convergence problems. Because of the assumption of small displacements, many different cases of $\vec{\delta}_o$ may be evaluated without recalculating the stiffness matrices.

The assembly force vectors $\vec{F}_{eq}$ required to close the gap are calculated with knowledge of the displacements:

$$
\begin{aligned}
\vec{F}_{eq} &= \boldsymbol{K}_b\vec{\delta}_b, \\
&= \boldsymbol{K}_b\left[\boldsymbol{K}_b + \boldsymbol{K}_a\right]^{-1}\boldsymbol{K}_a\vec{\delta}_o. \qquad (4.21)
\end{aligned}
$$

The component stiffnesses are composed of both material and geometric

terms. Since tolerance analysis deals with small geometric variations about the nominal. Small variations in the geometry have a negligible effect on the values of the stiffness matrices.

The gap vector, $\vec{\delta}_o$, in the preceding calculations is a measure of the distance between two mating surfaces. It can represent either a gap or an interference between the parts. Figure 4.4 shows a statistical representation of $\vec{\delta}_o$. The gap vector is composed of two parts: a mean or average gap plus a random variation about the mean, as shown by the shaded tolerance band.

For tolerance analysis of compliant assemblies, $\vec{\delta}_o$ is represented algebraically as the sum of two displacement vectors:

$$\vec{\delta}_o = \vec{\delta}_{ave} \pm \vec{\delta}_i, \tag{4.22}$$

where $\vec{\delta}_{ave}$ is the average deviation due to warping and $\vec{\delta}_i$ is the $\pm 3\sigma$ random variation about the average. The plus or minus operator indicates that $\vec{\delta}_i$ represents a tolerance band about the average. These terms are graphically defined in figure

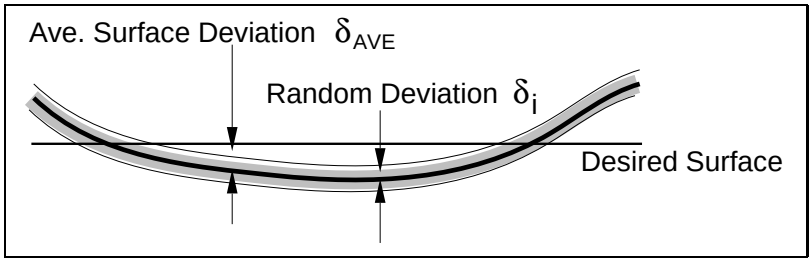

Figure 4.4: Surface variation contributing to a gap.

4.4.

The gap, $\vec{\delta}_o$, may be obtained by

1. Measuring production assemblies and calculating the mean and standard deviation at test points,
2. Performing a tolerance stack-up analysis using dimensional tolerances for each part in the assembly,
3. Estimating the assembly variation from process experience.

These equations provide a robust method for calculating forces and displacements within the limitations previously discussed.

4.2 Super-element Calculations

The stiffness matrices described in equations 4.17 and 4.18 are likely to be different sizes. This poses a problem performing the required matrix addition and multiplication. Super-elements can be used to resolve this problem. The super-element describes the equivalent stiffness for an entire part in terms of the degrees of freedom along its boundary. Figure 4.5 shows a stiffness matrix $\boldsymbol{K}_a$. Well formed stiffness matrices are typically sparse and banded. Data exists in a band around the diagonal of the matrix; the rest of the matrix has values of zero. The matrix

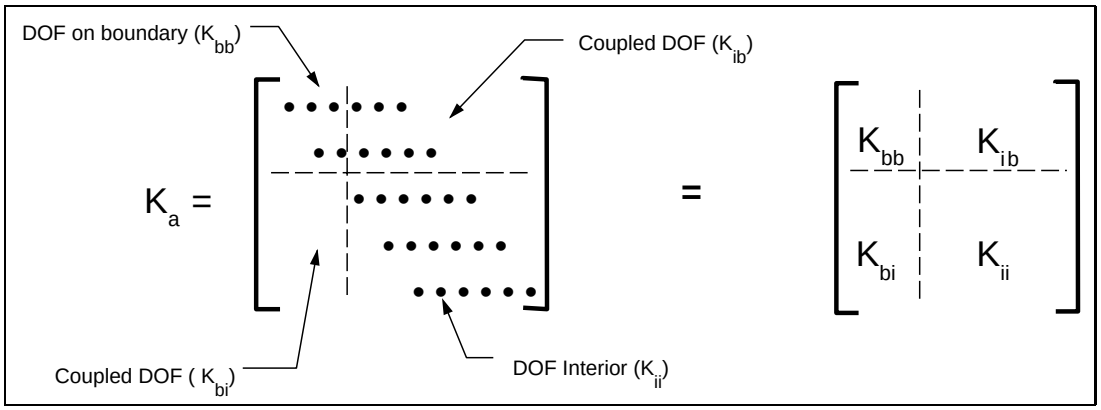

Figure 4.5: Definition of super-element.

may be sorted and partitioned so that all the degrees of freedom (DOF) that are associated with the boundary $\boldsymbol{K}_{bb}$ are in the upper left hand corner. All the degrees of freedom that are associated with the interior $\boldsymbol{K}_{ii}$ are located in the bottom right hand corner. The other two quadrants, $\boldsymbol{K}_{ib}$ and $\boldsymbol{K}_{bi}$, contain terms that couple the boundary and the interior, as shown in figure 4.5.

Partitioning the force and displacement vectors in the same manner, the linear stiffness equation can be written as

$$\left\{ \begin{array}{c} \vec{F}_{bb} \\ \hline \vec{F}_{ii} \end{array} \right\} = \left[\begin{array}{c|c} \boldsymbol{K}_{bb} & \boldsymbol{K}_{ib} \\ \hline \boldsymbol{K}_{bi} & \boldsymbol{K}_{ii} \end{array} \right] \left\{ \begin{array}{c} \vec{\delta}_{bb} \\ \hline \vec{\delta}_{ii} \end{array} \right\}, \tag{4.23}$$

where $\vec{F}_{bb}$ represents the forces on the boundary, $\vec{F}_{ii}$ represents the forces on the interior, $\vec{\delta}_{bb}$ represents the displacements on boundary, and $\vec{\delta}_{ii}$ represents the displacements on the interior. If there are no forces on the interior nodes, this

expression can be rewritten as

$$\vec{F}_{bb} = \boldsymbol{K}_{bb}\vec{\delta}_{bb} + \boldsymbol{K}_{ib}\vec{\delta}_{ii}, \tag{4.24}$$

$$\vec{0} = \boldsymbol{K}_{bi}\vec{\delta}_{bb} + \boldsymbol{K}_{ii}\vec{\delta}_{ii}. \tag{4.25}$$

Equation 4.25 can be solved for $\vec{\delta}_{ii}$:

$$\vec{\delta}_{ii} = -\boldsymbol{K}_{ii}{}^{-1}\boldsymbol{K}_{bi}\vec{\delta}_{bb}. \tag{4.26}$$

This result may be substituted into equation 4.24:

$$\vec{F}_{bb} = \boldsymbol{K}_{bb}\vec{\delta}_{bb} - \boldsymbol{K}_{ib}\boldsymbol{K}_{ii}{}^{-1}\boldsymbol{K}_{bi}\vec{\delta}_{bb}, \tag{4.27}$$

$$= (\boldsymbol{K}_{bb} - \boldsymbol{K}_{ib}\boldsymbol{K}_{ii}{}^{-1}\boldsymbol{K}_{bi})\vec{\delta}_{bb}. \tag{4.28}$$

The super-element stiffness matrix $\boldsymbol{K}_{se}$ is the term in the parenthesis:

$$\boldsymbol{K}_{se} = \boldsymbol{K}_{bb} - \boldsymbol{K}_{ib}\boldsymbol{K}_{ii}{}^{-1}\boldsymbol{K}_{bi}. \tag{4.29}$$

This matrix relates the boundary forces to the boundary displacements.

Super-elements provide a number of advantages. They are smaller than the global stiffness matrix. The size of a super-element is determined only by the number of degrees of freedom associated with the boundary. The smaller size reduces the computation time required for manipulating large matrices. Using super-elements also guarantees a set of matrices that can be multiplied and added as specified by the closure displacement equations 4.19 and 4.20. This is a necessary requirement for this method. It should be noted that while the total matrix

size is reduced, the super-element stiffness matrix is not sparse. In addition, the process of forming the super-element requires an additional matrix inversion.

The concept of super-elements corresponds well with assembly tolerance analysis. Each component is represented by a super-element. The interior details are removed, but the essential elastic behavior is retained. The reduced system allows tolerance design iterations to be performed efficiently. Since the stiffness is considered to be a constant, different gap configurations can be evaluated without recomputing the stiffness matrices.

4.3 Solution Types

The gap problem has several closure conditions that could be of interest to designers. Four have been identified: single, average, statistical, and worst case. Each requires a different closure solution.

The **single** case closure solution considers the assembly of a single set of parts. No statistical tolerance analysis is performed. A set of real or simulated parts is assembled, having dimensions that vary from the nominal, and the resulting assembly displacements are calculated. The closure displacements and forces are determined using finite element analysis. The gap is defined as the sum of the

displacements of the parts:

$$\vec{\delta}_o = \vec{\delta}_a + \vec{\delta}_b. \tag{4.30}$$

The magnitude of $\vec{\delta}_a$ and $\vec{\delta}_b$ are determined by the stiffness of the assembly.

The **average** closure solution represents the average of a set of assemblies. This is not random variation. It represents bias or offset in the assembly or manufacturing process. For example, composite parts can have an average shrinkage or warpage that affects every part. The closure solution for this case is the same as the single case closure solution with the gap vector being an average of several assemblies.

The **statistical** closure solution represents a set of assemblies analyzed simultaneously. A simplified statistical solution may be obtained by assuming the variation $\vec{\delta}_o$ is a randomly independent normally distributed value defined by a mean $\vec{\mu}_o$ and a standard deviation $\vec{\sigma}_o$. The gap definition is derived from a statistical tolerance analysis where variation in the length is determined by root sum squares. The complete statistical closure solution requires a linear superposition of the average and the statistical solutions:

$$\vec{\mu}_o = \vec{\mu}_{\delta_a} + \vec{\mu}_{\delta_b}, \tag{4.31}$$

$$\vec{\sigma}_o = \vec{\sigma}_{\delta_a} + \vec{\sigma}_{\delta_b} \tag{4.32}$$

Equation 4.32 raises a subtle point. Independently random standard deviations

typically add as root sum squares as in the dimensional variation previously mentioned. In the statistical closure solution, $\vec{\sigma}_{\delta_a}$ and $\vec{\sigma}_{\delta_b}$ are linear scale factors of $\vec{\sigma}_o$. They are not new random quantities, but linear factors of the original random gap.

The statistical method presented here is an approximation that does not include covariance. The concept of covariance is explained in chapter 5 and a full statistical solution including covariance effects is presented in chapter 6.

The **worst case** closure solution predicts the extreme range of variation for the assembly process. Stout (1997) has shown that the worst case stresses are obtained when adjacent nodes are at opposite extremes of the tolerance band.

All four solutions are extracted from the same equations for the closure displacements. They represent different ways of estimating the accumulation of assembly variation. The four expressions are summarized in table 4.1

The linear compliant closure solutions and linear tolerance analysis solutions are similar. This parallelism is clearly seen in table 4.1. In this table, $\boldsymbol{K}_a$ and $\boldsymbol{K}_b$ represent the stiffness matrices of the mating parts, $\vec{\delta}_o$ represents the gap vector for a single assembly, $\vec{\delta}_{ave}$ is the average gap between mating nodes for several assemblies, $\vec{\delta}_i$ is the randomly independent gap variation, $\vec{\delta}_a$ and $\vec{\delta}_b$ are the closure displacements at each pair of mating nodes, and *ndof* defines degrees of freedom at each FE node. Each set of equations is the sum of the contributing variations multiplied by a weight factor from the sensitivity to each variation. The

Table 4.1: A comparison mechanical tolerance and compliant assembly analysis.

Solution	Tolerances	Elastic Assembly Analysis
Single	$dU = \sum \left(\frac{\partial f}{\partial x_i} dx_i \right)$	$\vec{\delta}_a = \left[\boldsymbol{K}_a + \boldsymbol{K}_b \right]^{-1} \boldsymbol{K}_b \vec{\delta}_o$ $\vec{\delta}_b = \left[\boldsymbol{K}_a + \boldsymbol{K}_b \right]^{-1} \boldsymbol{K}_a \vec{\delta}_o$
Average	$dU = \sum \left(\frac{\partial f}{\partial x_i} dx_{ave} \right)$	$\vec{\delta}_a = \left[\boldsymbol{K}_a + \boldsymbol{K}_b \right]^{-1} \boldsymbol{K}_b \vec{\delta}_{ave}$ $\vec{\delta}_b = \left[\boldsymbol{K}_a + \boldsymbol{K}_b \right]^{-1} \boldsymbol{K}_a \vec{\delta}_{ave}$
Statistical	$dU = \sqrt{\sum \left(\frac{\partial f}{\partial x_i} \right)^2 T_i^2}$	$\vec{\sigma}_{a_i} = \sqrt{\sum_{j=1}^{ndof} \left(\left[\boldsymbol{K}_{a_{ij}} + \boldsymbol{K}_{b_{ij}} \right]^{-1} \boldsymbol{K}_{b_{ij}} \vec{\delta}_i \right)^2}$ $\vec{\sigma}_{b_i} = \sqrt{\sum_{j=1}^{ndof} \left(\left[\boldsymbol{K}_{a_{ij}} + \boldsymbol{K}_{b_{ij}} \right]^{-1} \boldsymbol{K}_{a_{ij}} \vec{\delta}_i \right)^2}$
Worst Case	$dU = \sum \left(\left\lvert \frac{\partial f}{\partial x_i} \right\rvert \lvert T_i \rvert \right)$	$\vec{\sigma}_{a_i} = (-1)^i \sum_{j=1}^{ndof} \left[\boldsymbol{K}_{a_{ij}} + \boldsymbol{K}_{b_{ij}} \right]^{-1} \boldsymbol{K}_{b_{ij}} \left\lvert \vec{\delta}_i \right\rvert$ $\vec{\sigma}_{b_i} = (-1)^i \sum_{j=1}^{ndof} \left[\boldsymbol{K}_{a_{ij}} + \boldsymbol{K}_{b_{ij}} \right]^{-1} \boldsymbol{K}_{a_{ij}} \left\lvert \vec{\delta}_i \right\rvert$

difference arises in the way the variations are summed. Note that the single and average solutions retain the signs on the sensitivities and the gap vectors, while the linear statistical and worst case are pure magnitudes. The sum of variations expressed in table 4.1 closely parallels tolerance accumulation expressions for rigid body assemblies. The principle difference arises in the definition of the sensitivity terms. For linear tolerance analysis of mechanical assemblies, the sensitivities are determined from the rigid body analysis. For elastic assemblies, the sensitivities are determined from the stiffness matrices.

The steady-state contact solution represents the final state of the assembly when all gaps are closed. After all mating finite element nodes are attached, equi-

librium is established throughout the assembly. The steady-state solution ignores peak forces that can occur during the assembly process. The peak forces occur as individual attachments are made and may be order-dependent. Although the single and average closure solutions do not consider the peak forces, they are included as random possibilities in the statistical and worst case closure solutions.

4.4 Solution Method

This section describes the process for performing tolerance analysis of compliant structures using the solutions developed in the previous section. The method presumes that the gap definition is given from either prior tolerance analysis or assembly data. The process was implemented using the commercial software packages, MSC/PATRAN^{TM}, MSC/NASTRAN^{TM}, and Matlab^{TM}.

4.4.1 Solution by Direct Manipulation of the Stiffness Matrices

This solution requires creation of a finite element (FE) model of the assembly in a FE pre-processor. The model geometry is created at the nominal size. Good modeling practice is required by the commercial analysis code. MSC/PATRAN^{TM} creates duplicate nodes along shared edges and surfaces. These nodes must be equivalenced to ensure that the degrees of freedom will match in the super-

element stiffness matrices. Boundary conditions must be established which ensure that parts are constrained and not subject to any rigid body modes. The selection of appropriate boundary conditions is essential and frequently difficult. Super-elements are defined for each mating part. The nodes along the gap define the boundary of the mating super-elements. When the model is complete, the MSC/NASTRAN^{TM} bulk data file (the analysis input file) can be created. An example model is shown in figure 4.6.

The bulk data file must be edited by hand to include two changes. The first is the declaration of the MSC/NASTRAN^{TM} OUTPUT4 file name. The super-element stiffness matrices are written to the OUTPUT4 file. This should be added at the top of the input file. Also a Direct Matrix Abstraction Program (DMAP) must be inserted into the executive section of the bulk data file to extract the super-element stiffness matrices and write them into the OUTPUT4 file. This must be inserted after the

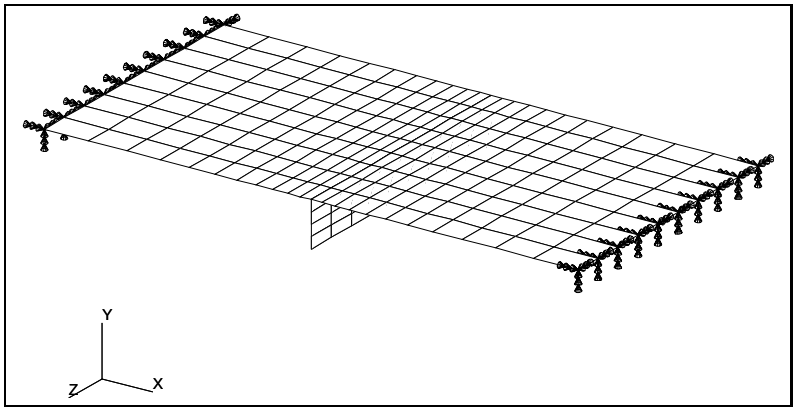

Figure 4.6: Nominally sized flanged shell finite element model.

solution type declaration Examples of these additions are shown in figure 4.7

When the analysis code is executed, the specified OUTPUT4 file will be created containing the super-element stiffness matrices.

The matrices must be translated from the OUTPUT4 format data file into a Matlab^{TM} data file. Once these files are in Matlab^{TM}, the required matrix operations, as specified in table 4.1, can be performed. Assembly forces and boundary displacements can be calculated directly at this point for a given gap vector, $\vec{\delta}_0$.

Residual stresses throughout the part can not be calculated directly with this method. Since the commercial FE code was used to generate the super-element stiffness matrices, the full stiffness matrix is not available. The residual stresses are calculated by transferring the assembly force vectors from Matlab^{TM} into the finite element pre-processor. A full analysis is performed on each part by applying

```
ASSIGN OUTPUT4='two_plate.op4', UNIT=12, FORM=FORMATTED
                    ⋮
COMPILE DMAP=SEKR,SOUIN=MSCSOU
ALTER 111
   MESSAGE //'SEID='/SEID $
   OUTPUT4 KAA,,,,//0/-12/0//16 $
ENDALTER
                    ⋮
```

Figure 4.7: Additions to the MSC/NASTRAN^{TM} Bulk Data File.

the displacement or force boundary conditions on individual parts of the assembly. The results of such an analysis are shown in figure 4.8. The full description of this problem is given in Chapter 7.

4.4.2 Solution by Internal Nodal Constraints

An alternate procedure may be used to obtain gap closure for the single case solution. Multi-point constraints (MPC) can be used to specify nodal displacement boundary conditions. An MPC defines an equation between different degrees of freedom in a finite element model. For gap or interference problems, it is possible to define an equation linking nodes along the gap and a node exterior to the model, the “reference node.” The reference node is used to store the magnitude of the gap

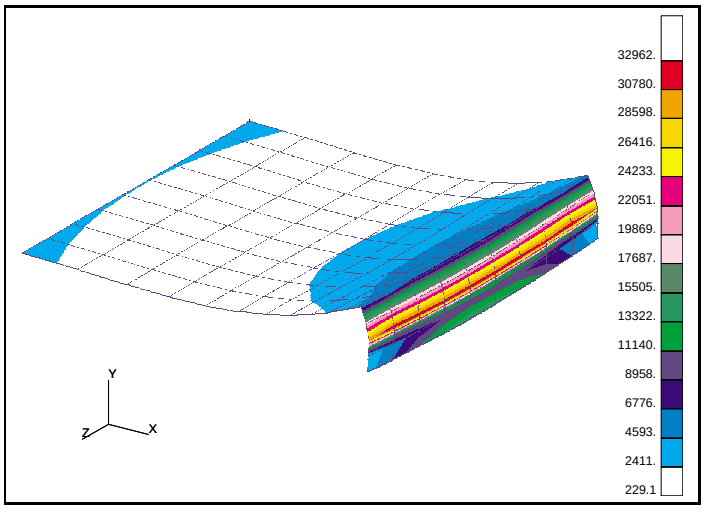

Figure 4.8: Flanged shell subject to .01” closure gap.

or interference between the parts. The actual geometry is created in its nominal shape and the MPC is used to drive the deformation. The definition of the MPC input line for MSC/NASTRAN^{TM} and a sample closure constraint are shown in figure 4.9. The MPC enforces the interference defined by the reference node and

```
MPC, ID, NODE, DOF, SCALAR, NODE, DOF, SCALAR
,,       NODE, DOF, SCALAR
```

For example,

```
MPC,5,1,1,-1.0,1000,1,1.0
,,501,1,1.0
```

Figure 4.9: MSC/NASTRAN^{TM} multi-point constraint definition.

provides the equilibrium solution that accounts for model stiffness. A similar MPC must be defined for every point of contact. An example of this method is given in chapter 7.

Multi-point constraints are fairly easy to define. Variable gaps or interferences can be defined by using multiple reference nodes. They also provide direct calculation of the the residual stresses. However, they do not provide access to the sensitivity terms that can be used to determine statistical or worst case solutions.

4.5 Summary

This chapter has presented the theory and method for combining tolerance analysis with assembly compliance. The method can predict the effects of manufacturing variation on assembly forces and stresses. A simplified form of a linear contact solution has been introduced. The method of super-elements has been used to reduce matrix size and assure the feasibility of matrix addition and multiplication. Four different solution methods, which are able to compute solutions for both one of a kind assemblies and large production runs, have been presented. Finally, two methods were given showing how to integrate this theory with commercial analysis tools. Both analysis methods are useful depending upon the desired closure solution.

Chapter 5

Random Bézier Curves

Chapter 4 developed the basic equations for tolerance analysis of compliant assemblies. However, the equations did not consider the effects of correlation or statistical covariance between assembly points. This correlation may occur if points lie on a continuous surface. The surface continuity constrains the variation between adjacent points leading to geometric covariance.

This chapter develops a fundamental tool for describing geometric covariance, the random Bézier curve. It develops the mathematics of random Bézier curves and defines bounds that can be used to relate a tolerance band about the curve to bounds on the Bézier control points. Finally, shows how random control points can be used to generate a family of random Bézier curves within a specified tolerance band.

5.1 Introduction

Random polynomials arise whenever the coefficients of a polynomial are subject to random variation. An engineering application of random polynomials occurs in the development of filters (transfer functions) for signal processing. There are sources of error in the signal processing hardware. By including these effects in the model, the designer can compensate for the error (Bharucha-Reid and Sambandham 1986).

As an example of a random power basis polynomial, consider the quadratic equation

$$y(\mu_y, s_y) = a_2 x^2 + a_1 x + a_0 \tag{5.1}$$

where the coefficients a_i are normally distributed random variables with a mean of μ_i and a standard deviation of s_i. Equation 5.1 represents a family of quadratic polynomials that also have a normal distribution, $y(\mu_y, s_y)$. The symbol s is used for standard deviation throughout this dissertation instead of σ, which we use to denote stress.

Figure 5.1 shows the quadratic polynomial described in equation 5.1 with μ_i = 0 and s_i = 1, i = 0,1,2. The mean of the polynomial is y = 0. The dashed lines represent bounds on the curve for the case where the a_i terms each have a distribution of $\pm$3s variation about the mean. The dotted curves are representative of

the random quadratic polynomials belonging to the set described by equation 5.1.

Figure 5.1 demonstrates a problem with using random power basis polynomials for computer-aided geometric design. The bounds on the polynomial diverge from the mean of the function. It is difficult to use the polynomial representation to characterize a uniform profile tolerance or envelope about the curve.

Bharucha-Reid and Sambandham (1986) overview the work that has been done in the area of random polynomials. The majority of the research involves determining the number and distribution of roots and the variances of these quantities. More recent work in this field includes random algebraic surfaces (Ibragimov and Podkorytov 1995) and better approximations of the real roots of random poly-

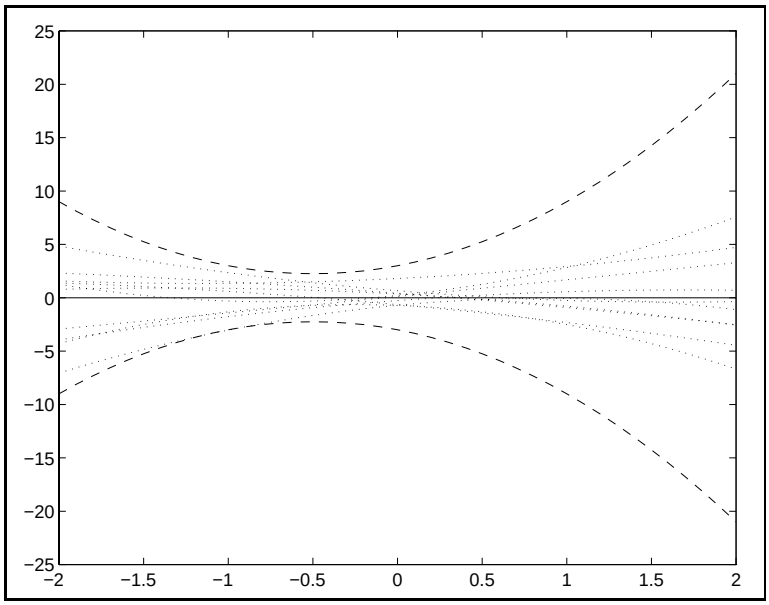

Figure 5.1: Random quadratic polynomial with a mean of 0 and a variance of 1.

nomial functions (Basilicas 1992).

Onecescu and Istrătescu (1975) defined random Bernstein polynomials. They showed that the Bernstein polynomials may be used to approximate arbitrary random functions and proved that as the order of the polynomial approaches infinity, the approximation converges uniformly to the mean of the random function. None of these sources discuss bounds on the standard deviation of algebraic polynomials.

Polynomial curve fitting techniques (Weisberg 1980) have been used to describe correlation between a set of points and goodness of fit, but they have not been used to describe random polynomials prior to this dissertation.

5.2 Covariance

If the polynomial coefficients are not randomly independent, the variables are covariant. Covariance is used to describe the correlation of random variables. For example, if a and b are random variables defined by $a = 2b$ then a and b are fully covariant. If there is some random error ϵ included in a, then $a = 2b + \epsilon$. In this case, the variables are only partially covariant.

A multivariate normal distribution can be described by its mean and covariance. In multivariate statistics, covariance is expressed in matrix format. The diagonal

terms are the variance in each random variable, and off-diagonal terms are the covariance that express how the random variables are interrelated,

$$\mathbf{\Sigma} = \begin{bmatrix} \nu_{00} & \nu_{10} & \cdots & \nu_{0n} \\ \nu_{10} & \nu_{11} & \cdots & \nu_{1n} \\ \vdots & \vdots & \ddots & \vdots \\ \nu_{n0} & \nu_{n1} & \cdots & \nu_{nn} \end{bmatrix}. \tag{5.2}$$

Throughout this dissertation the covariance matrix is denoted by the symbol $\mathbf{\Sigma}$. The square root of the variance ν_{ii} is defined as the standard deviation,

$$s = \sqrt{\nu}. \tag{5.3}$$

A standard statistical tool for evaluating normal multivariate populations is the chi-squared (χ_p^2) distribution. The chi-square distribution defines the limits for a multivariate distribution. Given a normally distributed random variable $\vec{x}$ with a mean of $\vec{\mu_x}$ and a covariance $\mathbf{\Sigma}_x$, the ellipsoid bounding the distribution is defined as

$$(\vec{x} - \vec{\mu_x})^t {\mathbf{\Sigma}_x}^{-1} (\vec{x} - \vec{\mu_x}) \leq \chi_p^2(\alpha) \tag{5.4}$$

where $\chi_p^2(\alpha)$ represents the upper (100α)th percentile of the χ_p^2 distribution (Johnson and Wichern 1988). This is analogous to the constant standard deviation s bounds for a normal distribution. The subscript p describes the number of random variables. Tables of chi-squared results are widely available. This function is used to determine the constant probability ellipses described in section 5.1. It can also be used to evaluate the bivariate distributions of the control points.

The physical interpretation of covariance can be seen by considering a random variable with a bivariate normal distribution in x and y. If the x and y values of the variable are plotted, the constant probability curve forms an ellipse. Figure 5.2 shows the 50% and 99% constant probability ellipses for the uncorrelated, partially correlated, and fully correlated cases. The major and minor axes of each ellipse is determined by the variance. The covariance affects the tilt angle and the eccentricity of the ellipse.

The variance-covariance calculation is analogous to the determination of moments and products of inertia in mechanics. Both of these quantities are mathematically defined as tensors. The first moment of a solid body describes the centroid or center of mass. The second moment of a solid body describes the moments and products of inertia. These terms define the distribution of area or

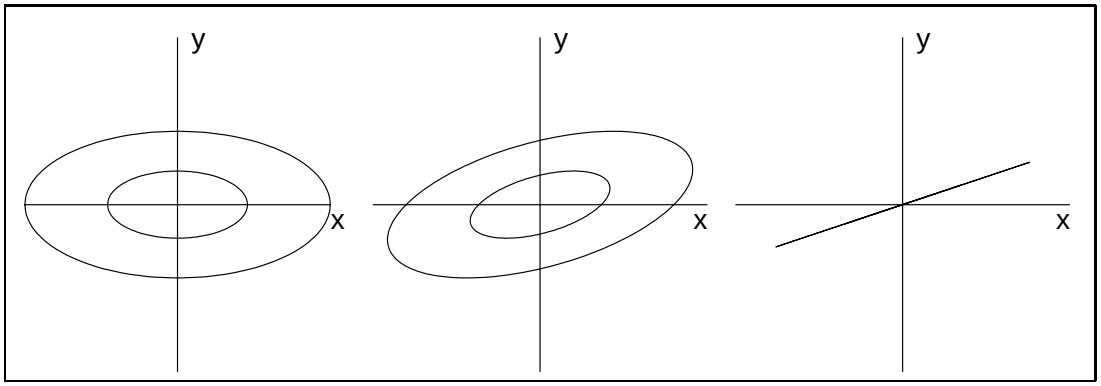

Figure 5.2: 50% and 99% constant probability ellipses for uncorrelated, partially correlated, and fully correlated bivariate normal distributions.

mass about a given axis. Frequently, the defining coordinate system is parallel to the global coordinate system through the centroid of the object.

Figure 5.3 shows two simple beam cross sections. The I-beam is symmetric about the centroid in the global coordinate system. The principle axes of the I-beam are aligned with the global coordinate system so the products of inertia are zero. The Z-beam is asymmetric about the global coordinate system. The products of inertia are non-zero due to the asymmetry. The moments of inertia are tensors that can be written in matrix form. The maximum size of the moment of inertia tensor is 3×3.

Figure 5.4 shows the analogous system for a set of 3 random variables. If the data is aligned with the global coordinate system, the covariance tensor is diagonal. If the data is skewed from the global coordinate system in each axis the covariance tensor is fully populated. The variance-covariance terms describe how data is distributed about the mean. The general covariance matrix can be $n \times n$ dimensional.

Both the moment of inertia and covariance are defined by moment calculations. The first moment of a continuous function is defined as

$$\mu_x = E[x_i] = \int_{-\infty}^{\infty} x_i f(x) dx_i \tag{5.5}$$

where x_i is the random variable and $f(x_i)$ is a probability density function describ-

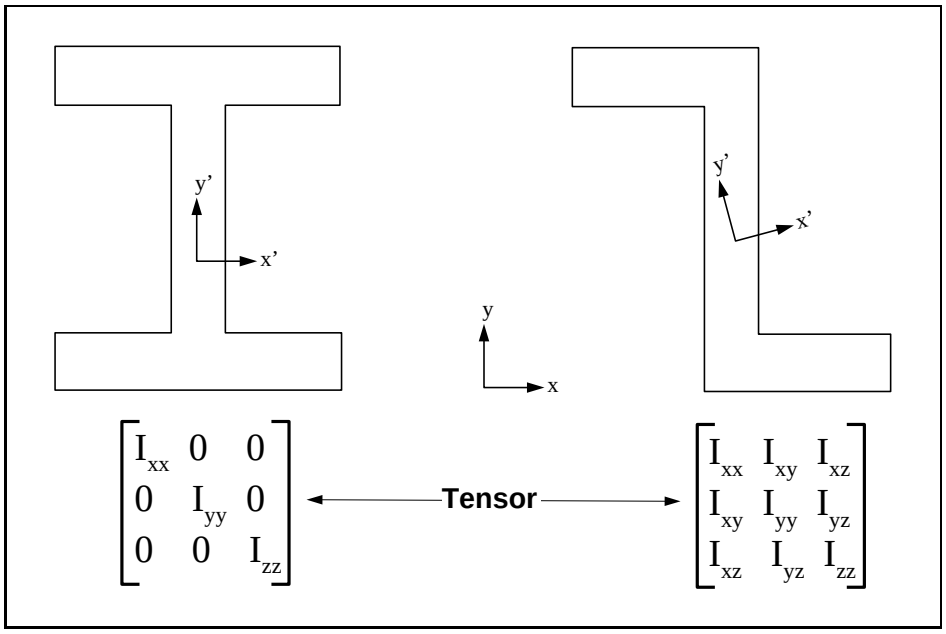

Figure 5.3: Geometric interpretation of the moment of inertia tensor.

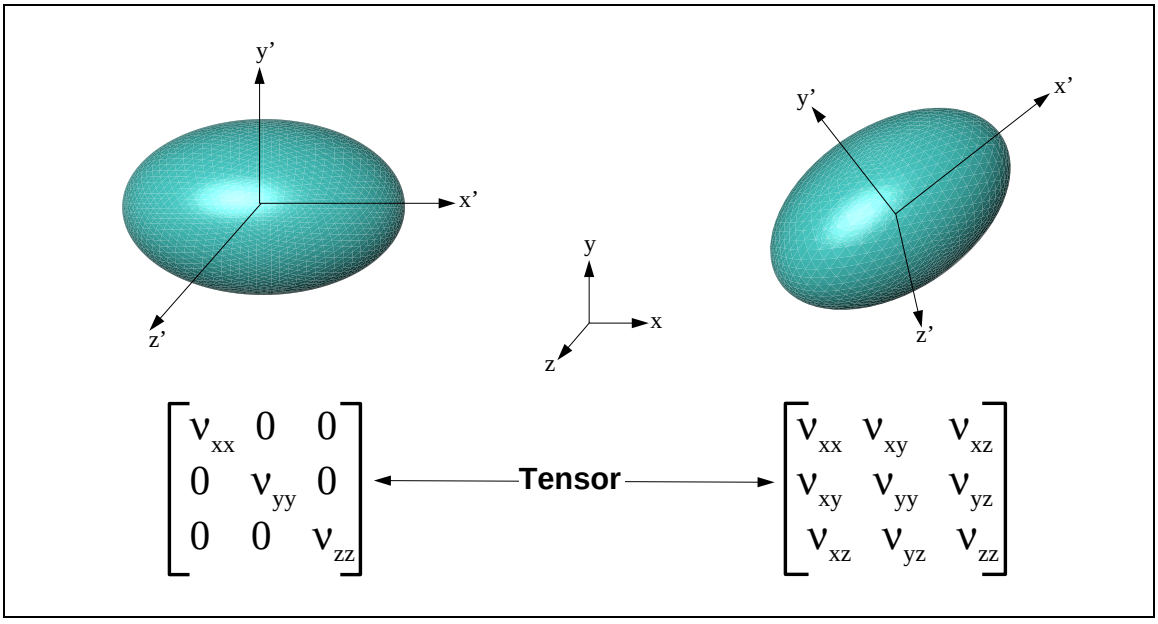

Figure 5.4: Geometric interpretation of the covariance tensor.

ing the distribution of the random variable. Equation 5.5 is related to the centroid or center of mass of a solid body, or the mean, μ_x, of a set of data. The integration is defined by the expectation operator $E[]$. This is a linear operator that describes the "expected" value of a function.

The second moment of the data is the variance. The variance measures the distribution of random data about the mean of the data. The definition of variance is

$$Var(x_i) = \int_{-\infty}^{\infty} (x_i - \mu_i)^2 f(x_i) dx_i \tag{5.6}$$

where $f(x_i)$ is the probability density function.

Covariance describes asymmetry in multi-variable data. The definition of covariance is

$$Cov(x_i, x_j) = \int_{-\infty}^{\infty} \int_{-\infty}^{\infty} (x_i - \mu_i)(x_j - \mu_j) f(x_i, x_j) dx_i dx_j \tag{5.7}$$

where $f(x_i, x_j)$ is the joint probability density function of x_i and x_j. The variance defined in equation 5.6 is a special case of the covariance where $i = j$.

Calculations for the variance and covariance are critical to the definition of random Bézier curves.

5.3 Bounded Bézier Curves

Offset curves have been widely studied because of their utility, not only to tolerance analysis, but also other applications, such as toolpath generation for numerically controlled milling. This section describes the mathematics of offset Bézier curves.

A Bézier curve of degree n is defined by

$$\vec{f}(t) = \sum_{i=0}^{n} B_i^n(t)\vec{P}_i, \tag{5.8}$$

where $B_i^n(t)$ is the ith Bernstein basis function of degree n defined as

$$B_i^n = \frac{n!}{(n-i)!i!}t^i(1-t)^i \tag{5.9}$$

and control points $\vec{P}_i$ lie in R^3,

$$\vec{P}_i = \left\{ \begin{array}{c} x \\ y \\ z \end{array} \right\}_i . \tag{5.10}$$

As the parameter t varies from 0 to 1, equation 5.8 describes a smooth curve that starts at the first control point P_o and ends at the last control point P_n. Intermediate control points act as handles that allow the curve to be stretched into the desired shape.

Each vector component $\{x, y, z\}$ is independent so the vector function $\vec{f}(t)$ can be decomposed into three separate scalar equations:

$$\vec{f}(t) = \left\{ \begin{array}{c} x(t) \\ y(t) \\ z(t) \end{array} \right\}. \tag{5.11}$$

Since all three scalar functions have the same B_i^n coefficients, relations that are derived for one of the scalar equations also apply to the others.

Figure 5.5 shows an example of a Bézier curve. The lines connecting the control points constitute the control polygon. The Bézier curve is drawn as a solid line. Two dashed lines are drawn on either side of the Bézier curve representing a tolerance band which bounds the curve.

The tolerance bands represent design limits or manufacturing tolerances. Since real surfaces cannot be manufactured precisely, they will be subject to error. Engineers apply tolerance bands to indicate the precision required from production processes necessary for proper performance.

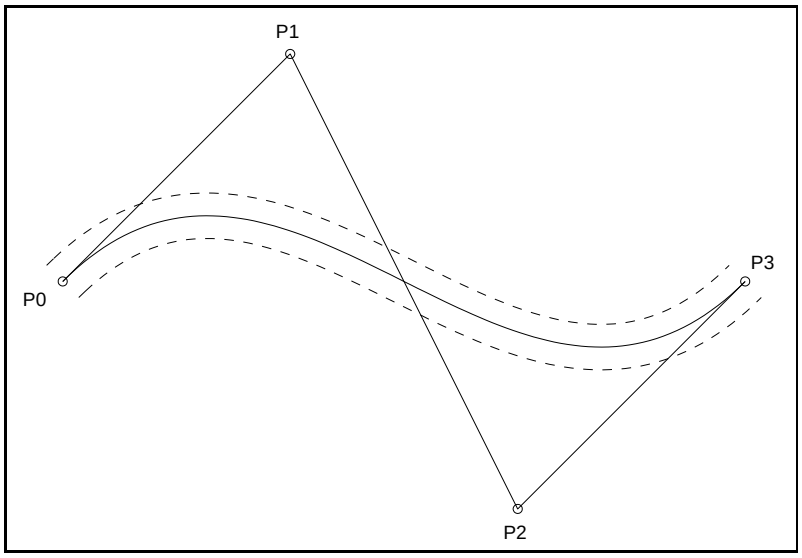

Figure 5.5: Planar Bézier curve with normal offsets.

The bounding curves shown in figure 5.5 are the *normal offset curves* which are at a fixed distance from the curve at all points. The normal offset curve is specified by a normal vector $\vec{N}(t)$ and a scalar offset value T,

$$\vec{f}(t) = \sum_{i=0}^{n} B_i^n(t)\vec{P}_i + T\frac{\vec{N}(t)}{\sqrt{N(t)_x^2 + N(t)_y^2}}. \tag{5.12}$$

Unless $N(t)_x^2 + N(t)_y^2$ is a perfect square (Farouki and Sakkis 1990), this equation cannot be expressed in the form of equation 5.8. Thus, the normal offset curves cannot generally be described by a rational Bézier curve.

Consider now, a Bézier curve that is defined by the nominal control points P_i and a variation about the control points $\vec{\epsilon_i}$,

$$\vec{f}(t) = \sum_{i=0}^{n} B_i^n(t)\left(\vec{P}_i + \vec{\epsilon_i}\right). \tag{5.13}$$

Applying the distributive law of algebra, this curve can be separated into two distinct parts, the nominal curve $\vec{f}_n(t)$ and the error curve $\vec{f}_{\mathrm{err}}(t)$,

$$\vec{f}(t) = \vec{f}_n(t) + \vec{f}_{\mathrm{err}}(t) = \sum_{i=0}^{n} B_i^n(t)\vec{P}_i + \sum_{i=0}^{n} B_i^n(t)\vec{\epsilon_i}. \tag{5.14}$$

Note that the error curve is a Bézier polynomial of the same degree as the nominal curve.

The error curve, $\vec{f}_{\mathrm{err}}(t)$ does not define the normal offset curve as defined in equation 5.12. However, the error curve does provide a method for introducing perturbations into the nominal curve. Equation 5.14 forms the basis for developing

bounded random Bézier curves. By considering the variation in the control points, $\vec{\epsilon_i}$, to be a random variable, the error curve defines a statistical offset about the nominal curve. Although, Sederberg (1992) has shown that the offset curve can be bounded within a rectangular interval, the concept of a statistically defined offset is not addressed in the literature.

This chapter develops methods to describe a statistically defined offset curve in terms of Bézier polynomials. The boundary curves will define the Gaussian probability that a random curve exists inside the boundary envelope. It will also explore the relationship between the statistical bounds on the curve and the statistical bounds on the control points.

The following sections:

- Develop mathematical expressions for the mean and covariance of a random Bézier curve.
- Develop a statistical definition of variation in Bézier curves, where offsets represent a normally distributed variation about the nominal Bézier curve.
- Develop a relationship between the control point variation and the manufacturing profile tolerance on a curve.
- Show that bounded control points describe a bounded Bézier curve.

5.4 Random Bézier Curves

The equation of a Bézier curve is a linear expression in terms of the control points $\vec{P}_i$. Considering the control points, $\vec{P}_i$, to be random variables, a family of random curves can be represented by the mean value and covariance of the control points.

Section 5.2 showed the effect of covariance on a set of random variables and described the physical meaning of correlation of the random variables. Random Bézier curves also exhibit covariance by virtue of their continuity. If a single point on the curve is displaced, surrounding points must also be displaced to preserve continuity. Thus, there is a covariant relationship between all the points on a continuous curve subject to random variation. The random curves are described by a mean or nominal curve and a band representing a normally distributed variation about the mean. Covariance is a measure of the spread of the distribution. As with dimensional variations of size, tolerance limits are generally taken to be $\pm 3s$ limits. So also with variation of curves or surfaces, the tolerance band represents a set of $\pm 3s$ limits.

The vector representation of a Bézier curve provides a more convenient notation for calculating the mean and covariance. The vector notation for the x compo-

nent of the curve is

$$x(t) = \begin{bmatrix} B_0^n(t) & B_1^n(t) & B_2^n(t) \cdots B_n^n(t) \end{bmatrix} \begin{bmatrix} X_0 \\ X_1 \\ X_2 \\ \vdots \\ X_n \end{bmatrix} = \vec{B}^n \vec{P}_X \tag{5.15}$$

where $\vec{B}^n$ represents the vector of Bernstein polynomials of degree n and $\vec{P}_X$ is the vector of the x components of the control points $\vec{P}_i$. The y and z components have similar definitions:

$$y(t) = \vec{B}^n \vec{P}_Y, \tag{5.16}$$

$$z(t) = \vec{B}^n \vec{P}_Z. \tag{5.17}$$

Equations 5.15, 5.16, and 5.17 are three independent expressions that represent a position in space for any value of t where 0 $\leq t \leq$ 1.

A multivariate normal distribution can be described by its mean and covariance. The mean can be described by the first moment of $f(\vec{x})$ using the expectation operator, $E[\vec{X}]$.

The first moment of $x(t)$ is

$$E[x(t)] = E\left[\vec{B}^n \vec{P}_X\right] \tag{5.18}$$

$$= \vec{B}^n E\left[\vec{P}_X\right] \tag{5.19}$$

$$= \mu_{x(t)} = \vec{B}^n \vec{\mu}_{P_X} \tag{5.20}$$

where $\vec{\mu}_{P_X}$ is the mean value of the X_i components of $\vec{P}_X$. Similar expressions exist for the $y(t)$ and $z(t)$ components of the curve. The first moment defines the mean value of the random Bézier curves in terms of the mean value of the control points. Given a Gaussian distribution of the control points, the mean of the control points describe the mean of the entire curve.

The second moment of the equation is the variance. For a single component $x(t)$ the variance is defined as

$$Var(x(t)) = E\left[(\vec{B}^n\vec{P}_X - \vec{B}^n\vec{\mu}_{P_X})(\vec{B}^n\vec{P}_X - \vec{B}^n\vec{\mu}_{P_X})^t\right] \tag{5.21}$$

$$= E[\vec{B}^n(\vec{P}_X - \vec{\mu}_{P_X})(\vec{B}^n(\vec{P}_X - \vec{\mu}_{P_X}))^t] \tag{5.22}$$

$$= E[\vec{B}^n(\vec{P}_X - \vec{\mu}_{P_X})(\vec{P}_X - \vec{\mu}_{P_X})^t\vec{B}^{nt}] \tag{5.23}$$

$$= \vec{B}^n E[(\vec{P}_X - \vec{\mu}_{P_X})(\vec{P}_X - \vec{\mu}_{P_X})^t]\vec{B}^{nt} \tag{5.24}$$

$$= \nu_{x(t)} = \vec{B}^n\mathbf{\Sigma}_{P_X}\vec{B}^{nt} \tag{5.25}$$

where $\mathbf{\Sigma}_{P_X}$ is the covariance matrix of the x components of the control points.

Equation 5.25 shows that the variance of $x(t)$, $\nu_{x(t)}$, is described by the covariance of the control points, $\mathbf{\Sigma}_{P_X}$. The $y(t)$ and $z(t)$ variance is described in a similar manner:

$$\nu_{y(t)} = \vec{B}^n\mathbf{\Sigma}_{P_Y}\vec{B}^{nt} \tag{5.26}$$

$$\nu_{z(t)} = \vec{B}_n\mathbf{\Sigma}_{P_Z}\vec{B}_n{}^t \tag{5.27}$$

Each covariance matrix, $\mathbf{\Sigma}_{P_x}$, $\mathbf{\Sigma}_{P_y}$, and $\mathbf{\Sigma}_{P_z}$, is an $n \times n$ matrix that describes the

variance of each control point and the associated covariance. The equations for $x(t)$, $y(t)$, and $z(t)$ are completely independent. While there may be covariance between the control points for a given component direction, there is no covariance between the components. Thus, the variance statement relating the curve variance to the control point covariance for a random Bézier curve of degree n is

$$\nu_{x(t)} = \nu_{y(t)} = \nu_{z(t)} = \begin{bmatrix} B_0^n(t) & B_1^n(t) & \cdots & B_n^n(t) \end{bmatrix} \begin{bmatrix} \nu_{00} & \nu_{01} & \cdots & \nu_{0n} \\ \nu_{01} & \nu_{11} & \cdots & \nu_{1n} \\ \vdots & \vdots & \ddots & \vdots \\ \nu_{0n} & \nu_{n1} & \cdots & \nu_{nn} \end{bmatrix} \begin{bmatrix} B_0^n(t) \\ B_1^n(t) \\ \vdots \\ B_n^n(t) \end{bmatrix}. \tag{5.28}$$

The diagonal terms are the variance, while the off-diagonal terms are the covariance. If the control points were independent of one another, the covariance terms would vanish yielding a diagonal matrix. Thus, covariance is a measure of dependency or correlation of the terms.

As stated previously, continuity constraints on a curve imply covariance between points in random curves. This, in turn, places constraints on the control point variation of random Bézier curves. There is a dependent relationship between the variation of control points. The next section demonstrates the effects of covariance in a bounded random Bézier curve.

5.5 Bounded Random Bézier Curves

For manufacturing, limits of variation about a curve are typically specified as a band or profile tolerance about the curve. This section will describe methods for defining a relationship between the profile tolerance and the control point bounds of a random Bézier curve.

The curve variance $\nu_{f(t)}$ forms a bound on the curve and describes how points are clustered about the mean curve. The curve variance is defined by

$$\nu = s^2_{f(t)} = s^2_{x(t)} = s^2_{y(t)} = s^2_{z(t)}. \tag{5.29}$$

Note that $s^2_{x(t)}$, $s^2_{y(t)}$, and $s^2_{z(t)}$ are independent (not covariant) since the equations for each of the coordinate directions are independent.

Solving for the standard deviation, s, in equation 5.29 defines a statistical sphere of random variation about every point t in the curve. Figure 5.6 shows a representation of this in a planar Bézier curve. The standard deviation of the uncorrelated bivariate distribution defines bounds on the curve measured normal to the mean curve. The distance of the offset is measured in standard deviations. Common practice is to define the band at a $3s$ offset from the mean. The number of standard deviations determines the percent of scatter points falling within the bounds.

Equation 5.29 requires that the values of ν_{ij} from equations 5.25, 5.26, and 5.27

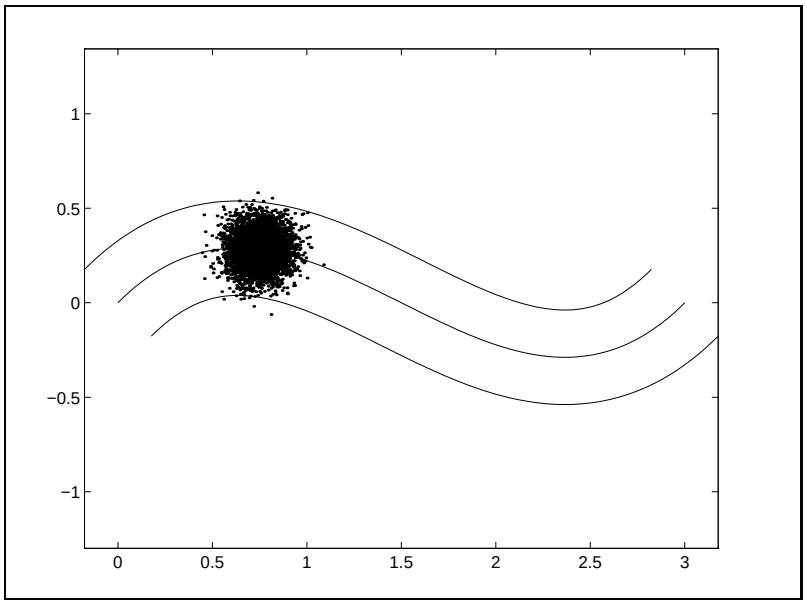

Figure 5.6: Bivariate distribution defining a normal offset to a Bézier curve.

must be determined for $x(t)$, $y(t)$, and $z(t)$. Since each component is independent and the distribution is spherical, the covariance matrices for each of the equations are equivalent,

$$\mathbf{\Sigma}_{P_X} = \mathbf{\Sigma}_{P_Y} = \mathbf{\Sigma}_{P_Z}\,. \tag{5.30}$$

Therefore, the values of ν_{ij} only need to be determined once.

Equation 5.28 defines the covariant relationship between control points in a Bézier curve. Ideally, the ν_{ij} terms would define $\nu_{f(t)}$ such that it is a constant for all values of t. There may be an infinite number of solutions to the covariance matrix defined by equation 5.28.

Two methods have been developed for determining the values of the covariance

matrix. The first method finds a constant standard deviation of random curves for a given parametric value. This method can currently only be applied to quadratic Bézier curves and only gives the desired bounds at one parametric value. This method is described in Appendix A.

The second method defines random Bézier curves based on linear regression techniques. This method gives a bounding envelope about the entire nominal curve that can be used to describe tolerance variation in the curve.

5.6 Polynomial Regression in Bézier Space

This section develops a method for describing the family of random Bézier curves that exists within a statistical tolerance envelope. The primary tool used in this section is polynomial regression.

Regression techniques fit a curve to a set of points. One common regression technique is the *least squares* fit which minimizes the sum of the square error in the vertical direction. Although this method can be expanded to handle a 3-D space curve, the derivations given in this section will be limited to planar curves.

Assume a set of m points x_i defined by Bézier curves of degree n evaluated at t_i points

$$x_0 = B_0^n(t_0)P_0 + B_1^n(t_0)P_1 + \cdots + B_n^n(t_0)P_n \tag{5.31}$$

$$x_1 = B_0^n(t_1)P_0 + B_1^n(t_1)P_1 + \cdots + B_n^n(t_1)P_n \tag{5.32}$$

$$\vdots \quad \vdots \tag{5.33}$$

$$x_m = B_0^n(t_m)P_0 + B_1^n(t_m)P_1 + \cdots + B_n^n(t_m)P_n. \tag{5.34}$$

Let $\boldsymbol{A}$ be defined as the $m \times n$ matrix of Bernstein polynomials evaluated at t_i points

$$\boldsymbol{A} = \begin{bmatrix} B_0^n(t_0) & B_1^n(t_0) & \cdots & B_n^n(t_0) \\ B_0^n(t_1) & B_1^n(t_1) & \cdots & B_n^n(t_1) \\ \vdots & \vdots & \ddots & \vdots \\ B_0^n(t_m) & B_1^n(t_m) & \cdots & B_n^n(t_m) \end{bmatrix}. \tag{5.35}$$

Equations 5.34 can then be written in matrix form as

$$\vec{X} = \boldsymbol{A}\vec{P}_x \tag{5.36}$$

where $\vec{X}$ is the vector of points x_i and $\vec{P}_x$ is the vector of control points P_i associated with x_i.

In a least squares problem, the points $\vec{X}$ are known and the coefficients (or control points in a Bézier curve) are unknown. Simple inversion can not be generally used to solve for $\vec{P}_x$ since matrix $\boldsymbol{A}$ is not guaranteed to be square. The least squares solution to equation 5.36 is

$$\vec{P}_x = (\boldsymbol{A}^t\boldsymbol{A})^{-1}\boldsymbol{A}^t\vec{X}. \tag{5.37}$$

$$\tag{5.38}$$

Similarly, the expression for the y components of the control points is

$$\vec{P}_y = (\boldsymbol{A}^t\boldsymbol{A})^{-1}\boldsymbol{A}^t\vec{Y} \tag{5.39}$$

where $\vec{P}_y$ are vectors of control points for the Bézier curve, $\vec{Y}$ is measured variation at a selected number of points, and $\boldsymbol{A}$ is an $m \times n$ matrix of the Bernstein polynomials evaluated at corresponding t_i points. The solution of these equations requires that $m \geq n$.

Weisberg (1980) notes that the covariance of the regression terms is defined as

$$\boldsymbol{\Sigma} = \nu(\boldsymbol{A}^t\boldsymbol{A})^{-1}. \tag{5.40}$$

Covariance is typically used to determine the variance of the regression terms and the correlation that exists between them. By defining ν as the target variance of the tolerance band and $\boldsymbol{A}$ as the matrix of the Bernstein basis functions, equation 5.40 defines variance-covariance of the random Bézier control points. The control points define the family of random Bézier curve that exist within the tolerance band.

5.6.1 Monte Carlo Simulation

A Monte Carlo simulation has been created to model the random Bézier curves that exist within a given tolerance band. A base curve is described and random variations about the curve are defined. A least squares fit is made through each set of random points generating a Bézier curve, and the corresponding control points are plotted.

Figure 5.7 shows the nominal curve with random vectors emerging from it. The

origins of the vectors include the curve end-points (t = 0 and t = 1) and uniformly distributed random values of t with $0 < t < 1$. The magnitude of the vectors represent normally distributed random offset values in both the x and y directions. The magnitudes have a mean of 0 and a $3s$ standard deviation equal to the curve tolerance. The vector end-points are used in equations 5.37 and 5.39 to define variations for the least squares fit.

The results of 10,000 polynomial regressions are shown in figure 5.8. This case is defined by a quadratic Bézier curve with control points at $\{0,0\}$, $\{5,3\}$, and $\{10,-1\}$. Random values of t plus the endpoints were chosen as sample points. Points were generated with a standard deviation of 1/3 in both the x and y directions about the sample points. These points were then fit using the polynomial

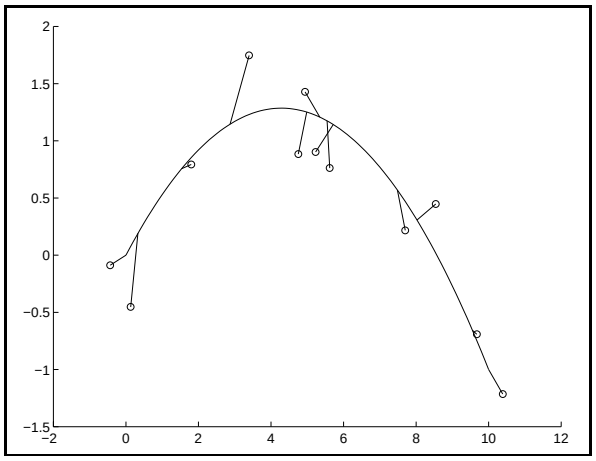

Figure 5.7: Random linear regression points. Vectors have normally distributed lengths and uniformly distributed origins.

regression equations 5.37 and 5.39.

Histograms of the analysis results in figure 5.8 show that the control point distributions are normally distributed without any bias or skew. Section 5.5 showed that there is covariance between the control points, P_i, for a given component. However, there is no covariance between the x and y components of the curve: the components are uncorrelated. Thus, the distributions of the control points is circular. The circles about the control points represent a 99.0% chi-squared value based on the analytical results from equation 5.40. This corresponds to approximately a $3s$ distribution. The means of the distributions are the nominal Bézier control points, which agrees with the values calculated for the first moment in equation 5.20.

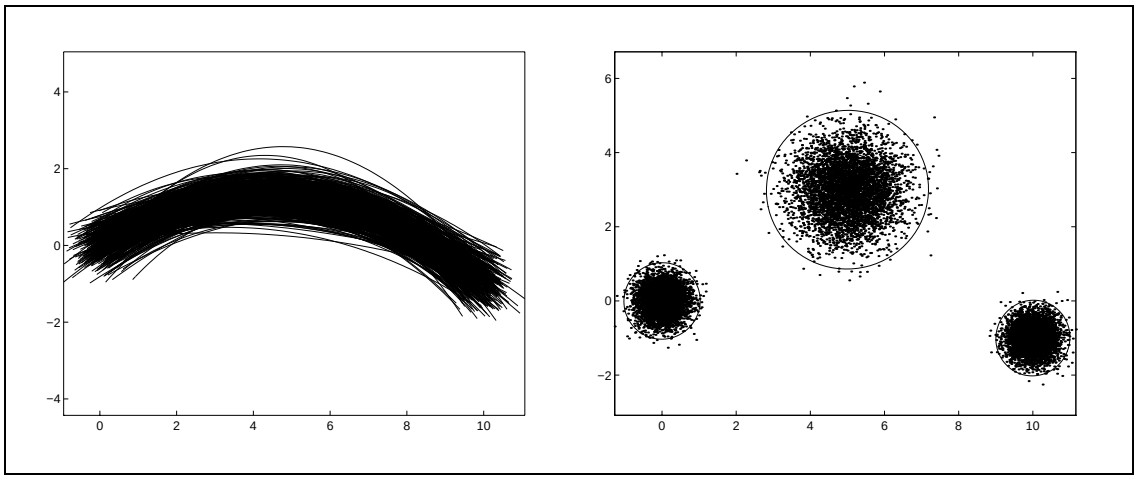

Figure 5.8: Random quadratic Bézier curves (left) and associated control points with the 99% chi-square circular analytical bounds (right).

This example determined the control points based on Bézier curves within a given bound. Knowing the control point covariance, it is also possible to reverse this process and define a family of random Bézier curves that exist within a given bound.

If quadratic Bézier curves are fit through three Gaussian distributions centered on the curve at $t = \{0, 1/2, 1\}$, the 99% chi-squared radius values of the left, middle, and right control points in figure 5.8 are 1.0071, 2.1126, and 1.0013, respectively. This compares with the analytical results of 1.0000, 2.1213, and 1.0000. The analytic and Monte Carlo results are very comparable. The results indicate that 99% of all the control points lie within the circles.

As the middle distribution is moved away from the parametric center of a quadratic curve, $t = 1/2$, the chi-squared radius of the center control point increases. For example, if points are fit about $t = \{0, 1/4, 1\}$, the chi-squared radius of the center control point is 3.027. The value of the standard deviation grows rapidly as t approaches 0 or 1 due to numerical instability in the regression equations which occurs when sample points are too close together.

Numerical instability can be avoided if a sufficient number of points are selected to perform the least squares fit. The Monte Carlo simulation shows that at least $4n$ random points (where n is the degree of the curve) must be chosen to avoid problems of numerical stability in the regression analysis. Thus, eight points were

chosen for the example in figure 5.8.

The least squares approximation converges to the nominal curve as the number of sample points increase. Similarly, the variance of the control points converges to the mean. Thus, the lower bound of the variance approaches 0 as the number of sample points approaches infinity. This reflects the error in the curve fit. If the curve is evaluated at infinite locations, the error in the curve fit is zero.

The Bézier regression with the least numerical error occurs when the sample points are evenly distributed. The maximum variance for the fewest number of points occurs when values of t are evenly distributed such that

$$t = \frac{i}{n}, \text{ for } i = 0 \text{ to } n \tag{5.41}$$

where n is the degree of the curve. For a quadratic curve, n is 2, therefore t = {0, 1/2, 1}. Similarly, for a cubic curve n is 3 and t = {0, 1/3, 2/3, 1}. When more points are added, a least squares fit is required and the variance of the curve decreases.

Figure 5.9 shows the convergence of the center two control points of a cubic Bézier curve as the number of samples increases. The variance of the two internal control points of a cubic Bézier curve is equal. The covariance matrix was calculated using 5.40 with the variance of the curve, ν, equal to 1 and values of t evenly

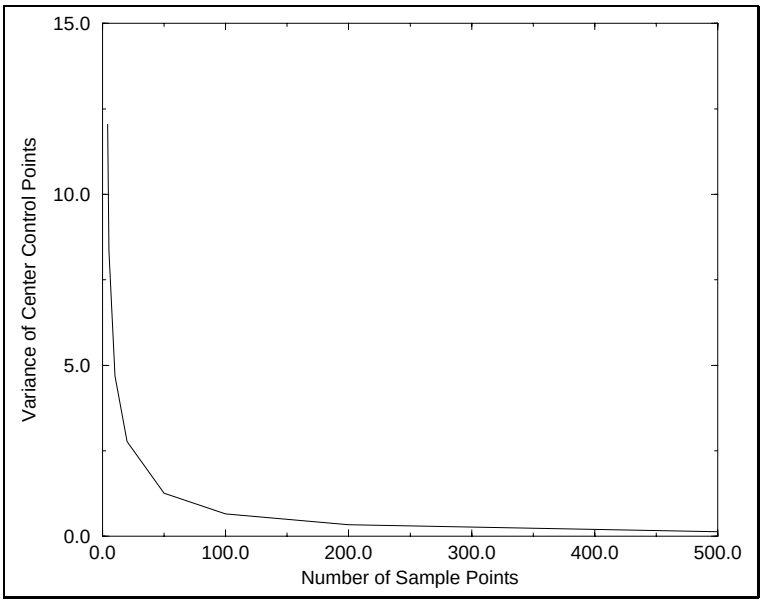

Figure 5.9: Variance of center control points of a cubic Bézier curve.

distributed such that

$$t = \frac{i}{N-1}, \text{ for } i = 0 \text{ to } N-1 \tag{5.42}$$

where N is equal to the number of sample points in the set. The maximum bound occurs when the number of samples equals the degree of the curve plus one ($N = n+1$). For a cubic curve, the covariance matrix for the maximum bound is,

$$\mathbf{\Sigma} = \begin{bmatrix} 1 & -\frac{5}{6} & \frac{1}{3} & 0 \\ -\frac{5}{6} & \frac{217}{18} & -\frac{86}{9} & \frac{1}{3} \\ \frac{1}{3} & -\frac{86}{9} & \frac{217}{18} & -\frac{5}{6} \\ 0 & \frac{1}{3} & -\frac{5}{6} & 1 \end{bmatrix}. \tag{5.43}$$

Random samples in figure 5.9 were started at $N = 12$, (corresponding to $4n$) since

fewer samples could create numerically unstable results. At $N = 12$, the variance of the internal control points from Monte Carlo analysis is 11.48 as compared with 12.055 (217/18) from equation 5.43.

The covariance matrix, $(\boldsymbol{A}^t\boldsymbol{A})^{-1}$, can be considered a sensitivity matrix. It shows how sensitive the system is to changes in a given parameter. In the case of a Bézier regression, the $\boldsymbol{A}$ matrix is dependent on the Bernstein basis functions and the parametric values, t, as shown in equation 5.35. The sensitivities are independent of the physical coordinates (x and y), thus the covariance matrix is independent of the control points. Monte Carlo simulations were performed to verify that the variance of the control points is independent of translation, rotation, and scale.

Table 5.1 documents the results of the Monte Carlo analyses. A Bézier curve with control points at $\{0,0\}$, $\{1,1\}$, $\{2,-1\}$, and $\{3,0\}$ was created. The control points were then scaled, rotated, and translated and random variation was introduced onto each new curve. A least squares fit was performed on the perturbed points to create a new Bézier curve. The standard deviation of the second control point, P_1 of the random Bézier curves was calculated and reported in table 5.1. In all cases, the standard deviation of the second control point is approximately the same, and the variation between each case is relatively small.

Table 5.1: Control Point Variation with Respect to Scale, Rotation and Translation.

Monte Carlo Analysis of 2500 Random Samples with tolerance of .1							
Scale							
Scale Factor	1.0	2.0	4.0	8.0	10.0	Mean	Std. Dev.
Std. Dev.	.0849	.0851	.0841	.0833	.0839	.0841	7.4027e-04
Rotation							
Angle (deg.)	0	45	90	135	180	Mean	Std. Dev.
Std. Dev.	.0849	.0844	.0849	.0820	.0831	.0831	0.0013
Translation							
Distance	{0,0}	{1,3}	{2,6}	{3,9}	{4,12}	Mean	Std. Dev.
Std. Dev.	.0849	.0856	.0855	.0851	.0819	0.0846	0.0015

5.7 Bounding Curves from Covariate Control Points

This section demonstrates the effects on the curve bounds by using the covariate control points described in section 5.6.

The covariance matrix, $(\boldsymbol{A}^t\boldsymbol{A})^{-1}$, provides a mapping between the profile tolerances on a curve and the bounds on the control points. Assuming the profile tolerance T represents a 3s limit, the control point variance is

$$\nu_{P_i} = \frac{T^2}{9}\boldsymbol{\Sigma}_{P_i} \tag{5.44}$$

where $\boldsymbol{\Sigma}_{P_i}$ is the covariance term for each Cartesian component of the Bézier

curve.

However, this mapping does not define a constant variation about the curve at every value of t. An expression for the standard deviation of the curve may be found by evaluating equation 5.25 using the covariance matrix from equation 5.43 where n=3 and s = 1:

$$s_{f(t)} = \pm\sqrt{405t^6 - 1215t^5 + \frac{2709}{2}t^4 - 684t^3 + \frac{301}{2}t^2 - 11t + 1.} \tag{5.45}$$

The standard deviation for a cubic Bézier curve represents the statistical bounds on the curve. The limits represented by equation 5.45 are plotted in figure 5.10.

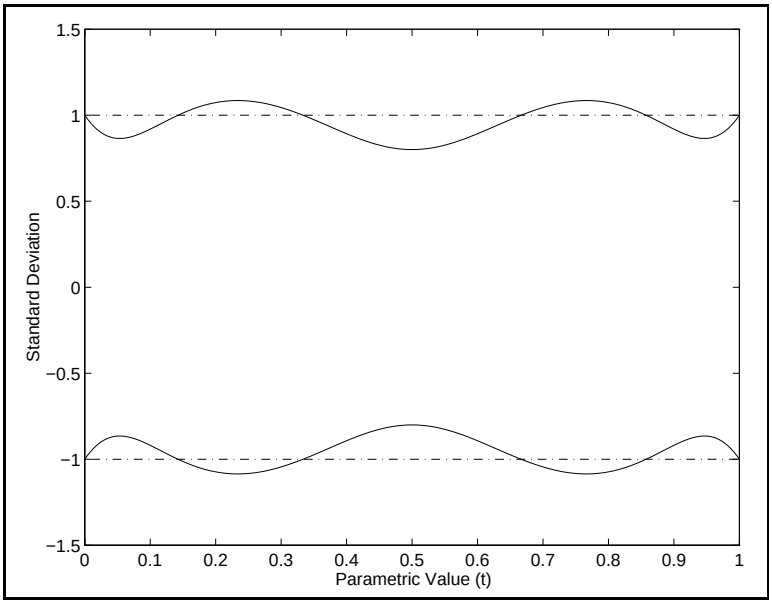

Figure 5.10: Standard deviation of points along a random cubic Bézier curve.

The minimum standard deviation for the curve is $\pm$.8004 while the the maximum standard deviation is $\pm$1.085. It is equal to 1.0 at the four selected values of t,

$t = \{0, 1/3, 2/3, 1\}$. Since equation 5.45 is a sixth order polynomial in t, there are six roots where s =1 exactly. In general, the standard deviation is guaranteed to be 1 for a polynomial of degree n at values of t where $t = i/n$ for $i = 0$ to n. There will also be $n - 1$ additional locations where the standard deviation will be one; however, it is difficult to generalize these locations for a polynomial of degree n.

Figure 5.11 shows the effect of mapping these bounds onto a cubic Bézier curve. The control points, P_i, may now exist anywhere within a bivariate normal distribution of the circular regions. Cubic curves lie within the statistical limits defined by the dashed bounds. The mean of these curves is defined by the solid curve. This solid curve also represents the nominal curve.

This method describes a family of bounded statistical curves. It relates a toler-

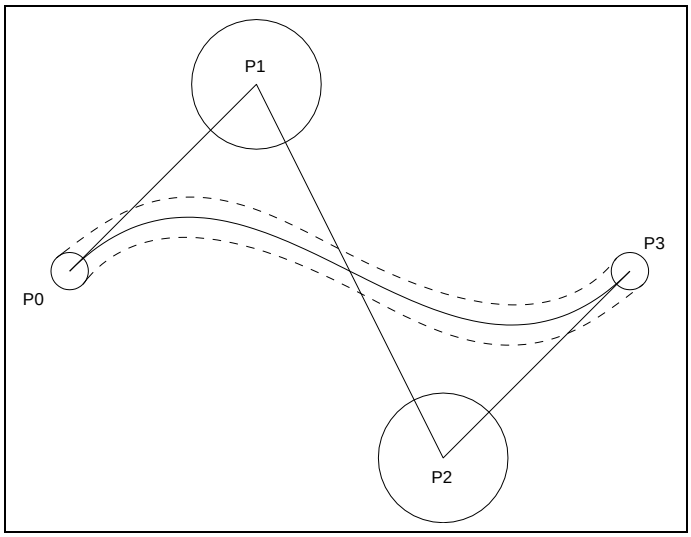

Figure 5.11: Statistical bounds for a cubic random Bézier curve.

ance band on a curve to the bounds on the control point variation. Although the bounds generated by the random control points are not constant, they do conform to the nominal curve and they are predictable.

One advantage of using Bézier curves is that the random curves have a physical relation with the random control points. This does not occur with simple random polynomials. Another advantage of random Bézier curves is that they may be added or subtracted to define a new curve. Also, since variances add linearly, the covariance matrices of the curves may be added to define the variation about the new curve. This technique will be demonstrated in Chapter 6.

5.8 Summary

This chapter has developed the concept of random Bézier curves. It has shown that linear regression techniques can be used to develop a covariance matrix that relates variation of the curve to variation of the control points. Upper and lower bounds were established that relate variation about the curve to bivariate distributions at the control points. Chapter 6 demonstrates how random Bézier curves may be used to describe geometric covariance between two mating surfaces.

Chapter 6

Covariance and Compliant Tolerance Analysis

This chapter will discuss the effects of material and geometric covariance on tolerance analysis of compliant assemblies. Covariance occurs when variations are correlated rather than independently random. The statistical closure equations derived in chapter 4 were noted as approximate because they did not account for covariance. The complete definitions are derived in this chapter.

Material covariance arises from elastic coupling within a compliant assembly. For example, as fasteners are applied to close a gap, the first fastener not only closes the gap at its location, but also decreases the gap at nearby gap locations. Thus, adjacent points will require less closure force. The interdependence between closure points may be described statistically by using material covariance. This

chapter will demonstrate how the part stiffness matrices can be used to correctly describe material covariance.

Geometric covariance describes the correlation of surface errors at adjacent points on a curve or surface. At microscopic scales, such as measuring surface roughness, adjacent points have very little correlation. At a slightly larger scale, machine scallops can cause a repeating pattern. This pattern can cause correlation between points in the scallops. At macroscopic scales, such as a warped metal sheet, a strong correlation exists between points on the surface. A point that is warped in one direction will have adjacent points that tend to be are warped in the same direction. Geometric covariance is independent of material covariance. The errors are randomly dependent simply because they are derived from a continuous surface.

The macroscopic effects of geometric covariance are examined in this chapter. The random Bézier curves developed in Chapter 5 are used to describe the variation in mating parts. An example of the geometric covariance matrix based on random Bézier curves is also provided.

6.1 Covariance of Compliant Assembly Equations

The closure solutions defined in Chapter 4 are based on a ratio of the mating component stiffness matrices in an assembly. As was shown there, the stiffness ratio K_r is defined as

$$\boldsymbol{K}_{r_a} = \left[\boldsymbol{K}_a + \boldsymbol{K}_b\right]^{-1} \boldsymbol{K}_b \tag{6.1}$$

or

$$\boldsymbol{K}_{r_b} = \left[\boldsymbol{K}_a + \boldsymbol{K}_b\right]^{-1} \boldsymbol{K}_a \tag{6.2}$$

where the subscripts a and b correspond to the components being assembled. These ratios relate the gap displacements, $\vec{\delta}_o$, to the closure displacement of $\vec{\delta}_a$ and $\vec{\delta}_b$ respectively,

$$\vec{\delta}_a = \boldsymbol{K}_{r_a} \vec{\delta}_o, \tag{6.3}$$

$$\vec{\delta}_b = \boldsymbol{K}_{r_b} \vec{\delta}_o. \tag{6.4}$$

The mean displacement of the parts ($\vec{\mu}_a$, $\vec{\mu}_b$) and the covariance of the parts ($\boldsymbol{\Sigma}_a$, $\boldsymbol{\Sigma}_b$) can be found using the statistical expectation operator E. The expectation operator is a linear mathematical operator.

Assume that the gap vector, $\vec{\delta}_o$, is a normally distributed random variable which introduces variation into the system. The output displacements, $\vec{\delta}_a$, can then be described as a multivariate normal distribution in terms of the mean and the co-

variance,

$$N_{\vec{\delta}_a}\left(\vec{\mu}_a, \boldsymbol{\Sigma}_a\right). \tag{6.5}$$

The first moment can be described as

$$E[\vec{\delta}_a] = E[\boldsymbol{K}_{r_a}\vec{\delta}_o], \tag{6.6}$$

$$= \boldsymbol{K}_{r_a}E[\vec{\delta}_o] \qquad \text{where } \boldsymbol{K}_{r_a} \text{ is not random,} \tag{6.7}$$

$$\vec{\mu}_a = \boldsymbol{K}_{r_a}\vec{\mu}_o. \tag{6.8}$$

This result shows that the mean of the part displacement, $\vec{\mu}_a$, is linearly related to the mean of the gap vector $\vec{\mu}_o$.

In addition, the second moment can be described as

$$Cov(\vec{\delta}_a) = E[(\boldsymbol{K}_{r_a}\vec{\delta}_o - \boldsymbol{K}_{r_a}\vec{\mu}_o)(\boldsymbol{K}_{r_a}\vec{\delta}_o - \boldsymbol{K}_{r_a}\vec{\mu}_o)^t], \tag{6.9}$$

$$= E[\boldsymbol{K}_{r_a}(\vec{\delta}_o - \vec{\mu}_o)((\boldsymbol{K}_{r_a}(\vec{\delta}_o - \vec{\mu}_o))^t)], \tag{6.10}$$

$$= E[\boldsymbol{K}_{r_a}(\vec{\delta}_o - \vec{\mu}_o)(\vec{\delta}_a - \vec{\mu}_o)^t\boldsymbol{K}_{r_a}{}^t], \tag{6.11}$$

$$= \boldsymbol{K}_{r_a}E[(\vec{\delta}_o - \vec{\mu}_o)(\vec{\delta}_a - \vec{\mu}_o)^t]\boldsymbol{K}_{r_a}{}^t, \tag{6.12}$$

$$\boldsymbol{\Sigma}_a = \boldsymbol{K}_{r_a}\boldsymbol{\Sigma}_o\boldsymbol{K}_{r_a}{}^t \tag{6.13}$$

where $\boldsymbol{\Sigma}_o$ is the covariance matrix of the gap vector $\vec{\delta}_o$ and $\boldsymbol{\Sigma}_a$ is the resultant covariance matrix for the closure displacements $\vec{\delta}_a$. $\boldsymbol{\Sigma}_a$ includes the covariance effects of both the material terms $\boldsymbol{K}_{r_a}$ and the geometric term $\boldsymbol{\Sigma}_o$. If $\boldsymbol{\Sigma}_o$ is diagonal, there will be no geometric covariance, but $\boldsymbol{\Sigma}_a$ may still be non-diagonal due to the

off diagonal terms in $\boldsymbol{K}_{r_a}$. When $\boldsymbol{\Sigma}_a$ is non-diagonal, the part displacements, $\vec{\delta}_a$, are covariant.

6.2 Material Covariance

Material covariance arises from the elastic coupling of materials. Figure 6.1 shows the necking that occurs in a piece of material when it is stretched. The strain in the x direction is defined by

$$\epsilon_x = \frac{\sigma}{E} \tag{6.14}$$

where σ represents stress and E represents Young's modulus. The strain in the y direction is defined by

$$\epsilon_y = -n\frac{\sigma}{E} = -n\epsilon_x \tag{6.15}$$

where n represents Poisson's ratio. The variable n is used to avoid confusion with variance, ν. The strain in the x and the y direction are fully correlated.

The stiffness ratio matrix, $\boldsymbol{K}_r$, relates assembly gap distances to closure displacements. It can be viewed as a sensitivity matrix that shows how sensitive each part displacement is to each given gap input value. Closing a gap in one location can cause motion all along the gap due to the elastic coupling. The sensitivity described by the $\boldsymbol{K}_r$ matrix is the sensitivity to gap displacement. This sensitivity may not be entirely intuitive, since the elastic coupling relates to the assembly and

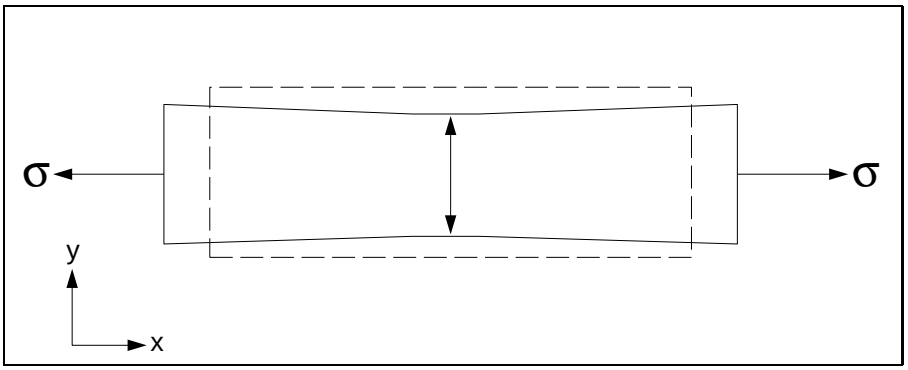

Figure 6.1: Material covariance occurs due to elastic coupling.

not simply one part.

Since $\boldsymbol{K}_r$ is created using super-element techniques, it is not sparse. There are few, if any, zero values in the matrix. Thus, even if the gap vector is randomly independent (so that Σ_o is a diagonal matrix), the part displacement covariance matrix, Σ_a, is generally a fully populated matrix.

It can also be proven that the $\boldsymbol{K}_r$ matrix is not symmetric.

If

$$\boldsymbol{K}_a \neq \boldsymbol{K}_b \neq 0 \tag{6.16}$$

and

$$\boldsymbol{K}_a = \boldsymbol{K}_a{}^t, \qquad \boldsymbol{K}_b = \boldsymbol{K}_b{}^t, \tag{6.17}$$

then,

$$\boldsymbol{K}_{r_a} = [\boldsymbol{K}_a + \boldsymbol{K}_b]^{-1}\boldsymbol{K}_b \tag{6.18}$$

and

$$\boldsymbol{K}_{r_a}{}^t = ([\boldsymbol{K}_a + \boldsymbol{K}_b]^{-1}\boldsymbol{K}_b)^t \tag{6.19}$$

$$= \boldsymbol{K}_b{}^t([\boldsymbol{K}_a + \boldsymbol{K}_b]^{-1})^t \tag{6.20}$$

$$= \boldsymbol{K}_b([\boldsymbol{K}_a + \boldsymbol{K}_b]^t)^{-1} \tag{6.21}$$

$$= \boldsymbol{K}_b[\boldsymbol{K}_a + \boldsymbol{K}_b]^{-1}; \tag{6.22}$$

therefore,

$$\boldsymbol{K}_{r_a}{}^t \neq \boldsymbol{K}_{r_a} \tag{6.23}$$

since matrix multiplication is not commutative.

6.3 Geometric Covariance

Geometric covariance arises from surface continuity conditions. Figure 6.2 shows a surface that is warped from the nominal position. If the variations from the nominal $\vec{\delta}_2$ and $\vec{\delta}_4$ are positive, $\vec{\delta}_3$ will also tend to be positive due to the surface continuity.

The definition of covariance for macroscopic variation is difficult. The definition needs to be robust enough to handle complex surface variation. It needs to define both the nominal shape and variations about the nominal.

Bézier curves are widely used in computer-aided geometric design. They have the ability to define complex shapes. The concepts developed in this section

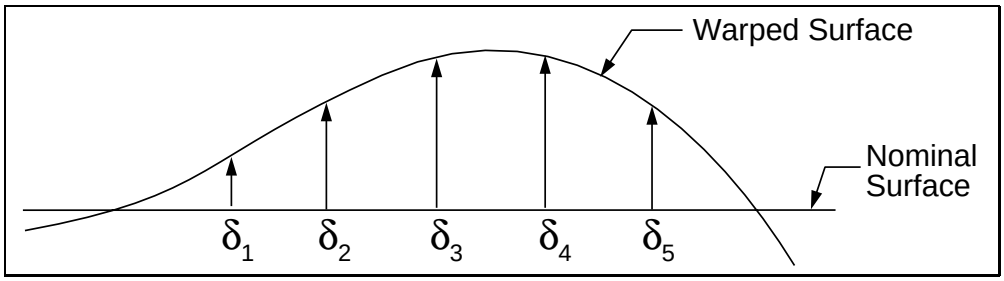

Figure 6.2: Geometric covariance occurs due to surface continuity.

will demonstrate how to use random Bézier curves as described in Chapter 5 to describe the covariant gap function that occurs when two complex surfaces are joined.

6.3.1 Using Bounded Random Bézier Curves

Bounded random Bézier curves may be used to define the statistical gap or interference between mating curves that have random variation or tolerance. The difference between two Bézier curves may be defined by the difference between the control points. Similarly, the difference between the means of two random Bézier curves, $g(t)$, is defined by the difference of the means of the control points, $\vec{\mu}_{1i}$ and $\vec{\mu}_{2i}$, of the two curves:

$$\begin{aligned} g(t) &= \sum \beta_i^n \vec{\mu}_{1i} - \sum \beta_i^n \vec{\mu}_{2i} \\ &= \sum \beta_i^n (\vec{\mu}_{1i} - \vec{\mu}_{2i}). \end{aligned} \tag{6.24}$$

The function, $g(t)$, is defined as the gap function. Since variances add linearly,

the covariance matrix of the gap function, $\Sigma_{g(t)}$, is defined by the sum of the covariance matrices of the mating random Bézier curves,

$$\Sigma_{g(t)} = \Sigma_1 + \Sigma_2. \tag{6.25}$$

Equations 6.24 and 6.25 imply that the curves being combined must be of the same order, having the same number of control points. The technique of degree elevation may be used to modify the order of mismatched curves so that they can be combined (Farin 1988b).

6.3.2 Gap Function Example

Figure 6.3 shows two mating cubic Bézier curves and the gap that is defined between these two curves. Curve 1 has mean Bézier control points at

$$P_0 = \{0, 0\}, \qquad P_1 = \{-.25, 1\}, \qquad P_2 = \{.5, 2\}, \qquad P_3 = \{0, 3\}, \tag{6.26}$$

and a profile tolerance, T_1, of 0.1.

Curve 2 has mean Bézier control points at

$$P_0 = \{0, 0\}, \qquad P_1 = \{0, 1\}, \qquad P_2 = \{.25, 2\}, \qquad P_3 = \{0, 3\}, \tag{6.27}$$

and a profile tolerance, T_2, of .05.

Random Bézier curves can be easily added or subtracted. The mean of the gap function is found by taking the difference of the mean control points of the

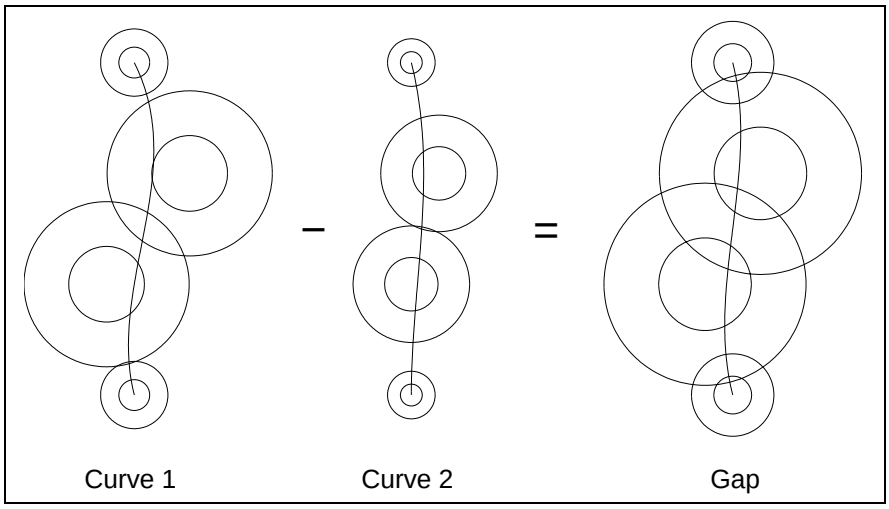

Figure 6.3: Gap defined as the difference between mating random Bézier curves. Circles represent 50% and 99% chi-squared distributions.

two curves. In this example, the gap function varies about X = 0. In figure 6.3, both endpoints of the gap function are located at X = 0. Values to the right of the endpoints indicate a gap while values to the left indicate interference or overlap between the curves.

Each curve has a mean position and a defined variation about the mean. The circles represent the 50% and 99% chi-squared bivariate distributions of the control points about the means. In this case, there is variation only in the X component of the curves. For visualization purposes, the difference operation is performed only on the X component. If there are variations in both components, the results must be mapped into parametric space to view the mean curve and to perform further

calculations.

The bivariate distributions of the control points are circular since there is no covariance between the X and Y coordinates. The different radii of the bivariate distributions within a curve is indicative of the covariance that exists between the control points in a given Bézier curve. The magnitude of the interior control point variance is dependent on the magnitude of the endpoint variances.

It is assumed that tolerances T_1 and T_2 represent a 3σ distribution. By the theory of random Bézier curves presented in Chapter 5, the bounding covariance matrix for the control points of the cubic Bézier curve labeled **Curve 1** in figure 6.3 is

$$\mathbf{\Sigma}_1 = \left(\frac{T_1}{3}\right)^2 \mathbf{\Sigma} = \frac{.01}{9} \begin{bmatrix} 1 & -\frac{5}{6} & \frac{1}{3} & 0 \\ -\frac{5}{6} & \frac{217}{18} & -\frac{86}{9} & \frac{1}{3} \\ \frac{1}{3} & -\frac{86}{9} & \frac{217}{18} & -\frac{5}{6} \\ 0 & \frac{1}{3} & -\frac{5}{6} & 1 \end{bmatrix}. \tag{6.28}$$

Similarly, the covariance matrix for the control points in the cubic Bézier curve labeled **Curve 2** in figure 6.3 is

$$\mathbf{\Sigma}_2 = \left(\frac{T_2}{3}\right)^2 \mathbf{\Sigma} = \frac{.0025}{9} \begin{bmatrix} 1 & -\frac{5}{6} & \frac{1}{3} & 0 \\ -\frac{5}{6} & \frac{217}{18} & -\frac{86}{9} & \frac{1}{3} \\ \frac{1}{3} & -\frac{86}{9} & \frac{217}{18} & -\frac{5}{6} \\ 0 & \frac{1}{3} & -\frac{5}{6} & 1 \end{bmatrix}. \tag{6.29}$$

The covariance matrices of the two curves are summed to determine the covariance matrix of the gap, $g(t)$,

$$\boldsymbol{\Sigma}_{g(t)} = \boldsymbol{\Sigma}_1 + \boldsymbol{\Sigma}_2, \tag{6.30}$$

$$= \frac{.1^2}{9}\boldsymbol{\Sigma} + \frac{.05^2}{9}\boldsymbol{\Sigma}, \tag{6.31}$$

$$= \frac{.0125}{9}\boldsymbol{\Sigma}. \tag{6.32}$$

The variance of the gap function is then $\frac{.0125}{9}$. This corresponds to a 3σ profile tolerance of approximately 0.112.

6.4 Closure Displacement Covariance Matrix

The previous section developed the gap covariance matrix $\boldsymbol{\Sigma}_o$ as a function of t. This covariance matrix is required in equation 6.13,

$$\boldsymbol{\Sigma}_a = \boldsymbol{K}_{r_a}\boldsymbol{\Sigma}_o{\boldsymbol{K}_{r_a}}^t$$

which is used to determine the closure displacement covariance. However, the matrices are not generally compatible for multiplication due to the differing sizes of the matrices. Typically, $\boldsymbol{\Sigma}_o$ must be expanded for the solution of equation 6.13.

The size of the $\boldsymbol{K}_{r_a}$ matrix is defined by the number of nodes along the boundary times the degrees of freedom that exist at each node. For most finite element analysis codes, the degrees of freedom in the stiffness matrix occur in the following

order, translations in X, Y, and Z and then rotations about X, Y, and Z. Not all degrees of freedom are present for every finite element type. Care must be used to select the correct degrees of freedom in Σ_o for a given element type.

The surface variations defined by Σ_o are characterized by measuring translational displacements. Rotations arise due to the displacements but are not characterized by independent variations. Thus, the gap between mating surfaces is defined in terms of translation. Therefore, the rotational degrees of freedom found in shell type finite elements are always assigned to zero in the geometric covariance matrix Σ_o.

The variation of the gap function and the Bézier curve describing the mating surfaces are both functions of the parametric value t. To map this variation to specific points or finite element nodes on the curve, the variance must be evaluated at specific parametric values of the Bézier curve. This is done in the following manner:

Define a matrix $\boldsymbol{C}$ such that

$$\boldsymbol{C} = \begin{bmatrix} \beta_0^n(t_0) & \beta_1^n(t_0) & \cdots & \beta_n^n(t_0) \\ \beta_0^n(t_1) & \beta_1^n(t_1) & \cdots & \beta_n^n(t_1) \\ \vdots & \vdots & \ddots & \vdots \\ \beta_0^n(t_m) & \beta_1^n(t_m) & \cdots & \beta_n^n(t_m) \end{bmatrix} \tag{6.33}$$

where each term t_i represents a parametric value of a point or finite element node on the Bézier curve. The covariance matrix of each of these points ,t_i, is then

defined by

$$\boldsymbol{\Sigma}_o = \boldsymbol{C}\boldsymbol{\Sigma}\boldsymbol{C}^t \tag{6.34}$$

where

$$\boldsymbol{\Sigma} = (\boldsymbol{A}^t\boldsymbol{A})^{-1} \tag{6.35}$$

is the covariance matrix of the control points of the random Bézier curve as defined in Chapter 5.

It should be pointed out that the $\boldsymbol{C}$ matrix is of the same form as the $\boldsymbol{A}$ matrix defined in chapter 5. The difference between $\boldsymbol{A}$ and $\boldsymbol{C}$ is that they are typically evaluated at different points t_i. If they happen to be evaluated at the same points t_i, then $\boldsymbol{C} = \boldsymbol{A}$. If the number of points, t_i, is equal to the order of the curve, then $\boldsymbol{C}$ is square. In that case,

$$\boldsymbol{\Sigma}_p = \boldsymbol{C}\boldsymbol{\Sigma}\boldsymbol{C}^t, \tag{6.36}$$

$$= \boldsymbol{A}\nu(\boldsymbol{A}^t\boldsymbol{A})^{-1}\boldsymbol{A}^t, \tag{6.37}$$

$$= \nu(\boldsymbol{A}\boldsymbol{A}^{-1}\boldsymbol{A}^{t^{-1}}\boldsymbol{A}^t), \tag{6.38}$$

$$= \nu\boldsymbol{I} \tag{6.39}$$

assuming that the variance of the curve, ν, is constant along the curve. This implies that the variance at these points is exactly the variance of the curve and that the variation between each point is independent.

Since the covariance in the different coordinate directions is independent, the

expanded covariance matrices must be interweaved to match the degrees of freedom as specified in the stiffness matrix.

6.5 Combined Material and Geometric Covariance

Previous sections have shown the physical and mathematical sources of covariance and provided methods for accounting for this covariance in compliant tolerance analysis.

The complete equation describing the closure displacement covariance for a given component a can be defined as

$$\boldsymbol{\Sigma}_a = \boldsymbol{K}_{r_a} \boldsymbol{\Sigma}_o{}^t \boldsymbol{K}_{r_a}{}^t. \tag{6.40}$$

where the geometric covariance term $\boldsymbol{\Sigma}_o$ is determined through production process control procedures or

$$\boldsymbol{\Sigma}_a = \boldsymbol{K}_{r_a} \boldsymbol{C} \boldsymbol{\Sigma} \boldsymbol{C}^t \boldsymbol{K}_{r_a}{}^t. \tag{6.41}$$

where the geometric covariance term is estimated using a random Bézier curves of order n $\boldsymbol{\Sigma}$, and $\boldsymbol{C}$ is used to expand $\boldsymbol{\Sigma}$ to account for the actual degrees of freedom in $\boldsymbol{K}_{r_a}$. These equations define the variance and covariance of nodes along the gap boundary. They include material covariance, geometric covariance, and the tolerance band in the gap.

The assembly forces required to close the gap may be found from the displacement results

$$\boldsymbol{F}_{\mathrm{a}} = \boldsymbol{K}_a \vec{\delta}_a = \boldsymbol{K}_a \boldsymbol{K}_{r_a} \vec{\delta}_o = \boldsymbol{K}_{F_a} \vec{\delta}_o \tag{6.42}$$

where

$$\boldsymbol{K}_{F_a} = \boldsymbol{K}_a \boldsymbol{K}_{r_a} = \boldsymbol{K}_a \left[\boldsymbol{K}_a + \boldsymbol{K}_b\right]^{-1} \boldsymbol{K}_b = -\boldsymbol{K}_{F_b}. \tag{6.43}$$

using the estimated geometric covariance matrix equation 6.41.

The covariance matrix of the assembly forces for component a using an estimated geometric covariance matrix is then

$$\boldsymbol{\Sigma}_{F_a} = \boldsymbol{K}_{F_a} \boldsymbol{C} \boldsymbol{\Sigma} \boldsymbol{C}^t {\boldsymbol{K}_{F_a}}^t. \tag{6.44}$$

If the variation in assembly forces are the final required result, the standard deviations may be extracted from the square root of the diagonal elements. The covariance terms can add insight into the correlation of the forces, but they do not affect the variation of the forces directly. The diagonal terms of $\boldsymbol{\Sigma}_{F_a}$ contain many off-diagonal terms of the $\boldsymbol{K}_{F_a}$ and $\boldsymbol{C}$ matrices, which account for effects of covariance.

6.6 Result Recovery within a Single Component

The previous section described methods for determining the statistical closure displacements or assembly forces required to assemble two components. The as-

sembly forces due to a random gap are defined by the mean vector and the covariance matrix of the assembly forces. The statistical solution of the displacement or stress field within a given component is found by returning to the original component stiffness matrix from which the super-element stiffness matrix was derived. By applying the covariant assembly displacements to the boundaries of each part, the displacements, forces, and stresses at interior points may be determined by FEA on each part.

Stochastic finite element analysis (SFEA) includes random effects in the finite element analysis. SFEA requires two separate analyses, one to calculate the mean and another to calculate the variances or standard deviations. SFEA normally is used to compute the effects of random material properties in structures such as earth filled dams or concrete structures. SFEA with random boundary conditions and constant material properties has not been found in the literature. The derivation of the appropriate equations follows the same expectation methods as described in section 6.1.

For a linear static analysis, the mean displacement field is defined using the standard FEA equations based on Hooke's law

$$\vec{\mu}_\delta = \boldsymbol{K}^{-1}\vec{\mu}_F \tag{6.45}$$

where $\vec{\mu}_\delta$ is the vector of mean displacements at each degree of freedom, $\boldsymbol{K}$ is the stiffness matrix, and $\vec{\mu}_F$ is the vector of mean assembly forces. This calculation

may be performed using a commercial FEA code.

The calculation of the standard deviations requires a separate calculation. Since the stiffness matrix is not a random variable in this analysis, the covariance matrix of the internal displacements at each degree of freedom is determined by

$$\boldsymbol{\Sigma}_{\delta} = \boldsymbol{K}^{-1}\boldsymbol{\Sigma}_{F}\boldsymbol{K}^{-1^{t}} \tag{6.46}$$

where $\boldsymbol{\Sigma}_{\delta}$ is the covariance matrix of the displacements, and $\boldsymbol{\Sigma}_{F}$ is the covariance matrix of the assembly forces determined by the closure equations. $\boldsymbol{\Sigma}_{F}$ may have to be modified to make the degrees of freedom in the covariance matrix match the degrees of freedom in the stiffness matrix. The standard deviation of each degree of freedom is determined by the square root of the corresponding diagonal element of $\boldsymbol{\Sigma}_{\delta}$.

Stress recovery within an element requires the use of the element constitutive matrix $\boldsymbol{D}$ and the element shape function matrix $\boldsymbol{B}$. These matrices are different for each finite element type and material type. The constitutive matrix for a plane stress problem is defined as

$$\boldsymbol{D} = \frac{E}{1-n^{2}}\begin{bmatrix} 1 & n & 0 \\ n & 1 & 0 \\ 0 & 0 & \frac{1-n}{2} \end{bmatrix} \tag{6.47}$$

where E is Young's Modulus and n is Poisson's ratio. The element shape function

matrix for a linear triangular element is

$$\boldsymbol{B} = \frac{1}{2A}\begin{bmatrix} (y_2 - y_3) & 0 & (y_3 - y_1) & 0 & (y_1 - y_2) & 0 \\ 0 & (x_3 - x_2) & 0 & (x_1 - x_3) & 0 & (x_2 - x_1) \\ (x_3 - x_2) & (y_2 - y_3) & (x_1 - x_3) & (y_3 - y_1) & (x_2 - x_1) & (y_1 - y_2) \end{bmatrix} \tag{6.48}$$

where A is the area of the triangular element and x_i, y_i are the coordinate positions of node i.

The mean stresses are calculated at points interior to the finite element (Gauss points) by

$$\vec{\mu}_{\sigma_e} = \boldsymbol{D}\boldsymbol{B}\vec{\mu}_{\delta} \tag{6.49}$$

The covariance matrix of the stresses at the Gauss points is determined by

$$\boldsymbol{\Sigma}_{\sigma_e} = \boldsymbol{D}\boldsymbol{B}\boldsymbol{\Sigma}_{\delta_e}\boldsymbol{B}^t\boldsymbol{D}^t \tag{6.50}$$

where $\boldsymbol{\Sigma}_{\sigma_e}$ is the covariance matrix of the stresses and $\boldsymbol{\Sigma}_{\delta_e}$ is the covariance matrix of the nodal displacements for a given element.

The diagonal elements of the stress covariance matrix, $\boldsymbol{\Sigma}_{\sigma_e}$, contain the variance of the stress components. The stress values, $\boldsymbol{\Sigma}_{\sigma_e}$, are calculated internal to each element and must be extrapolated to the nodes for post-processing. Standard deviations may not be computed until the extrapolation and nodal averaging for post-processing is completed.

The standard deviation of the stresses or strains may not be computed using most commercial codes since the formulation of the $\boldsymbol{B}$ matrix is considered propri-

etary information. A numerical example of this process using a custom FE analysis code is provided in Chapter 7.

6.7 A Test for Statistically Significant Covariance

Section 6.2 noted that because the super-element stiffness matrices, $\boldsymbol{K}$, are full, the part displacement covariance matrices, Σ, are also full. Due to the nature of the elasticity equations, the displacement correlation between points along the gap should decrease with distance. If points in close proximity are numbered consecutively, the covariance matrix should be banded: the terms near the diagonal should be significant, and the terms far from the diagonal should be zero. However, calculated results show that these distant covariance terms are very small, though not zero. This result raises a question. What value of covariance is significant? How small does the covariance term need to be before it can be ignored?

The statistical test proposed here is based on the geometric definition of covariance. Each covariance term can be considered as the correlation factor between two random variables. The variance of these two random variables and the associated covariance define a bivariate distribution of the variables. Geometrically, this is related to taking a planar cut through the hyper-ellipsoid representing the multi-variate distribution. In this context, the geometric definition of covariance is

associated with the angular tilt and the eccentricity of the ellipse in a planar cross section.

Figure 6.4 shows a Mohr's circle for covariance between two finite element nodes. The horizontal axis represents variance and the vertical axis represents covariance. The variance values νii and ν_{jj} are plotted on the horizontal axis, and the midpoint between the variance values is determined:

$$\nu_{mid} = \frac{\nu_{ii} + \nu_{jj}}{2}. \tag{6.51}$$

The covariance value ν_{ij} is plotted on the vertical axis, and the line $\bar{CD}$ is constructed. The circle is defined using the midpoint and the endpoints of line $\bar{CD}$. The intersections of the circle with the variance axis represent the major and minor principle axes of the covariance ellipse.

The tilt angle can be calculated from the triangle abr. The length of side a is

$$a = \frac{\nu_{ii} - \nu_{jj}}{2}. \tag{6.52}$$

The length of b is simply ν_{ij}.

The definition of the tilt angle, θ, in terms of the variance ν_{ii}, ν_{jj}, and the covariance ν_{ij} is

$$\tan(2\theta) = \frac{2\nu_{ij}}{\nu_{ii} - \nu_{jj}}. \tag{6.53}$$

If θ is 45^o, the i and j variables have equal variance. The covariance is then defined by the radius of the Mohr's circle.

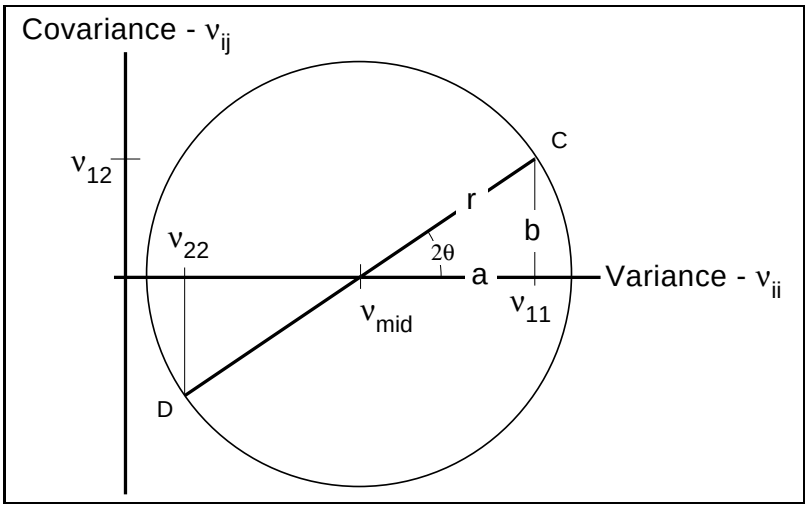

Figure 6.4: Mohr's circle solution for covariance.

This result indicates that if the covariance term is 0, the variables are uncorrelated, and if the covariance term is small it has little effect on the angle. Thus, the tilt angle of the ellipse can be used to define the statistical significance of the covariance value:

$$\theta < \frac{1}{2}\tan^{-1}\left(\frac{2\nu_{ij}}{\nu_{ii}-\nu_{jj}}\right). \tag{6.54}$$

The difference between lengths a and r is a measure of the effect of covariance. This quantity has the value $r - r\cos(2\theta)$ and can be used to determine the error due to neglecting the covariance. The test that is proposed here uses the ratio of this error term and the value of the major principle variance,

$$\hat{\nu}_{err} = \frac{r - r\cos(2\theta)}{r + \nu_{mid}}. \tag{6.55}$$

Evaluation of equation 6.55 has shown that values of $\hat{\nu}_{err} \leq .005$ are statistically

insignificant.

In covariance matrices where many terms may be small, error can accumulate causing larger deviations. The test suggested in this section is more useful for determining form than creating a sparse matrix in such cases.

6.8 Conclusion

This chapter has discussed the effects of covariance on compliant assembly tolerance analysis. It has demonstrated that both material and geometric covariance can affect the statistical analysis of joining parts separated by a statistical gap. Methods for defining both material and geometric covariance matrices were developed. It was also shown how these matrices effect the calculation of the statistical closure solution.

Chapter 7

Results

This chapter will present a series of examples that demonstrate the methods developed in this dissertation. The problems range from simple, closed form solutions to complex real-world manufacturing problems.

7.1 Example 1: One dimensional springs.

The springs shown in figure 7.1 represent the simplest compliant assembly problem. The physical model is composed of two springs with stiffnesses k_a and k_b separated by a gap. When the gap is closed, the equilibrium position is determined by the spring stiffnesses. The springs are displaced by δ_a or δ_b, respectively, to reach equilibrium. The gap, δ_o, is a statistical quantity with a mean and a standard deviation due to assembly tolerance stack-ups. The nominal value of δ_b can

be determined from the nominal dimensions of the tolerance model,

$$\delta_o = L + L_a - L_b. \tag{7.1}$$

Assuming that the tolerances of the lengths, T_L, T_a, and T_b, represent the standard deviations associated with each dimension, the variation of the gap can be determined using the root-sum squares of the tolerance values,

$$s_o = \sqrt{T_L^2 + T_a^2 + T_b^2} \tag{7.2}$$

As derived in Chapter 4, the equilibrium position of the closed gap is a function of the spring stiffness. The same equations also hold for the standard deviations. The standard deviation of the equilibrium point is a function of the gap standard

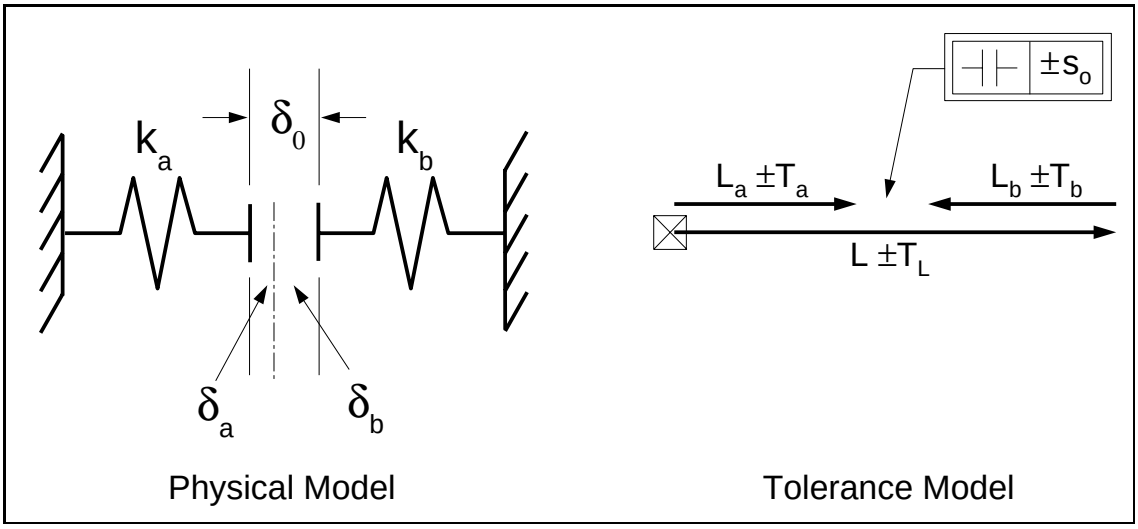

Figure 7.1: One-dimensional spring problem.

deviation,

$$s_a = \frac{k_b}{k_a + k_b} s_o \tag{7.3}$$

and

$$s_b = \frac{k_a}{k_a + k_b} s_o. \tag{7.4}$$

Also, the sum of the standard deviations of the springs must equal the standard deviation of the entire gap,

$$s_o = s_a + s_b \tag{7.5}$$

where s_o, s_a, and s_b represent the standard deviations of δ_o, δ_a, and δ_b respectively. The compliance of the springs distributes the variation between the two parts.

This problem can be solved using both the linearized compliant assembly model and Monte Carlo simulation. Using values of k_a = 1, k_b = 4, δ_o = 0 and s_o = 1, the linearized compliant solution yields

$$s_o = 1.0, \qquad s_a = .8, \qquad s_b = .2, \qquad 3s_F = 2.4,$$

while the Monte Carlo simulation yields

$$s_o = .9963, \qquad s_a = .7971, \qquad s_b = .1992, \qquad 3s_F = 2.3912.$$

Here, s_F represents the standard deviation of the equilibrium force or the standard deviation of the force required to assemble the two springs.

Figure 7.2 shows the force distribution of a 100,000 sample Monte Carlo analysis. The distribution is normal, the mean equilibrium force is zero, and the standard

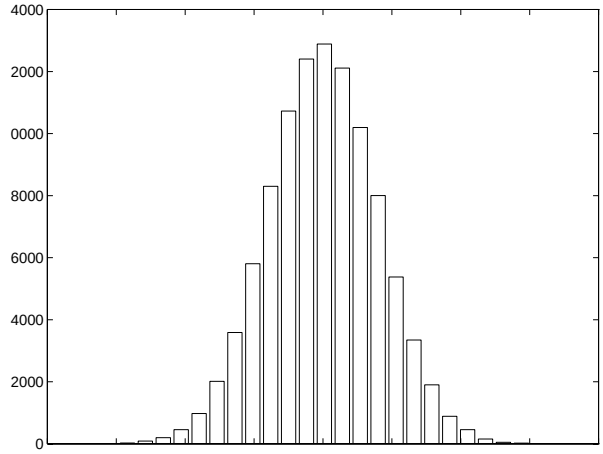

Figure 7.2: One-dimensional simple spring problem.

deviations correspond to the linearized model results.

There is no covariance since there are no surface continuity constraints or material coupling.

7.2 Example 2: One dimensional series springs.

Consider the linear assembly of springs shown in figure 7.3. It is composed of two sub-assemblies A and B. The spring lengths are subject to random manufacturing variations. Each spring in sub-assembly A has an unloaded length of L/4 $\pm$.01, and each spring in sub-assembly B has an unloaded length of L/3 $\pm$.01. Assume that each tolerance T represents a 3s (standard deviation) variation in the length. In this simple one-dimensional problem, the component tolerances may be added

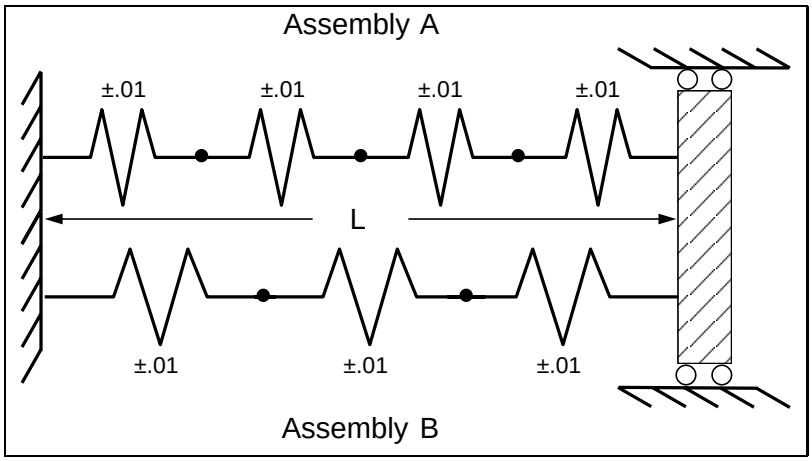

Figure 7.3: An assembly of linear springs.

by root-sum-squares to obtain a statistical estimate of the variation in each assembly. Thus, the statistical assembly variation due to the accumulated component tolerances is

$$T_{asm} = \sqrt{\sum {T_i}^2} \tag{7.6}$$

where T denotes the dimensional tolerance. For assembly A the tolerance stack-up is

$$T_a = \sqrt{4(.01)^2} = \pm.02, \tag{7.7}$$

and for assembly B it is

$$T_b = \sqrt{3(.01)^2} = \pm.0173. \tag{7.8}$$

The standard deviation of the gap between the free length of these two spring assemblies can be defined by the root mean squares of the variation of each as-

sembly:

$$s_o = \sqrt{T_a^2 + T_b^2} = \sqrt{4(.01)^2 + 3(.01)^2} = \pm .0265. \tag{7.9}$$

If the nominal lengths of A and B are equal, this value can be visualized as the maximum probable difference between the ends of the springs due to manufacturing errors. If the nominal lengths are *not* the same, then the average gap must be calculated from the nominal lengths.

If the two sets of springs are assembled as shown in figure 7.3, one will be stretched and the other compressed until they are the same length. This deformation will create a resultant force in the springs that depends on the gap size. The equilibrium position of the combined assembly must be a function of the stiffnesses of the springs.

If the springs are assumed to act as simple trusses, the stiffness matrices for each assembly can be defined as

$$\boldsymbol{K}_a = \frac{EA}{L_a} \begin{bmatrix} 1 & -1 & 0 & 0 & 0 \\ -1 & 2 & -1 & 0 & 0 \\ 0 & -1 & 2 & -1 & 0 \\ 0 & 0 & -1 & 2 & -1 \\ 0 & 0 & 0 & -1 & 1 \end{bmatrix} \tag{7.10}$$

and

$$\boldsymbol{K}_b = \frac{EA_2}{L_b} \begin{bmatrix} 1 & -1 & 0 & 0 \\ -1 & 2 & -1 & 0 \\ 0 & -1 & 2 & -1 \\ 0 & 0 & -1 & 1 \end{bmatrix}. \tag{7.11}$$

If the matrices are reduced via matrix condensation techniques (super-elements)

they become

$$\boldsymbol{K}_a = \frac{EA}{L_a}\begin{bmatrix} \frac{1}{4} & -\frac{1}{4} \\ -\frac{1}{4} & \frac{1}{4} \end{bmatrix} \tag{7.12}$$

and

$$\boldsymbol{K}_b = \frac{EA_2}{L_b}\begin{bmatrix} \frac{1}{3} & -\frac{1}{3} \\ -\frac{1}{3} & \frac{1}{3} \end{bmatrix}. \tag{7.13}$$

When the ground nodes are constrained, this is reduced even further to

$$K_a = \frac{EA}{4L_a} \qquad \text{and} \qquad K_b = \frac{EA_2}{3L_b}. \tag{7.14}$$

These results may be substituted into equations 4.17 and 4.18:

$$s_a = \frac{K_a^{-1}}{K_a^{-1} + K_b^{-1}} s_o = \frac{4L_aA_2}{4L_aA_2 + 3L_bA} s_o, \tag{7.15}$$

$$s_b = \frac{K_b^{-1}}{K_a^{-1} + K_b^{-1}} s_o = \frac{3L_bA}{4L_aA_2 + 3L_bA} s_o, \tag{7.16}$$

Let $A_2 = 2A$. Since $L_a = L/4$ and $L_b = L/3$, then

$$s_a = \frac{2}{3} s_o \qquad \text{and} \qquad s_b = \frac{1}{3} s_o \tag{7.17}$$

Assembly **A** has more components and a larger variation than assembly **B**. The resulting deformations represent a statistical variation in the displacement of the springs in each sub-assembly. The standard deviations, s_a and s_b, become boundary conditions applied to the gap surfaces.

The assembly force required to close the gap is proportional to the statistical displacement of the springs. The nominal force in each sub-assembly of springs is zero when the ideal length of each subset is equal to L. However, accounting for the 3s variation in the lengths induces an equilibrating force of

$$F_{eq} = K_a s_a = K_b s_b \tag{7.18}$$

$$F_{eq} = \pm .0176 \frac{EA}{L} \tag{7.19}$$

in each sub-assembly.

Thermal stress calculations are frequently performed because these stresses have been shown to be significant, while manufacturing stresses have been ignored. However, the displacements due to manufacturing variation are on the same order of magnitude as thermal expansion. For example, given steel trusses 10 inches long and 1 inch in area, the 3s statistical axial stress in each sub-assembly is 53,900 psi.

In contrast, assuming that a steel part is subjected to 100$^o F$ temperature rise,

$$\begin{aligned} \alpha_{steel} &= 6 \times 10^{-6} \\ \sigma &= E\alpha\Delta T \\ &= (30 \times 10^6)(6 \times 10^{-6})100 \\ &= 18,000 \text{ psi}. \end{aligned} \tag{7.20}$$

This example shows that the thermal stresses and the manufacturing stresses can be of the same order of magnitude. This indicates that more emphasis should be placed on quantifying the effects of manufacturing variation.

7.3 Example 3: Beam Assembly

In this example, consider an assembly of six planar beams as shown in figure 7.4. The end of each beam has three degrees of freedom: translation in the x and y axes and rotation about the z axis. The assembly points are labeled 1 and 2.

Nominally the two halves assemble without any gap or interference. However, the design specifications permit a $\pm$.01 variation in the horizontal and vertical directions at the assembly points. The variation is assumed to be a $\pm$3 standard deviation limit.

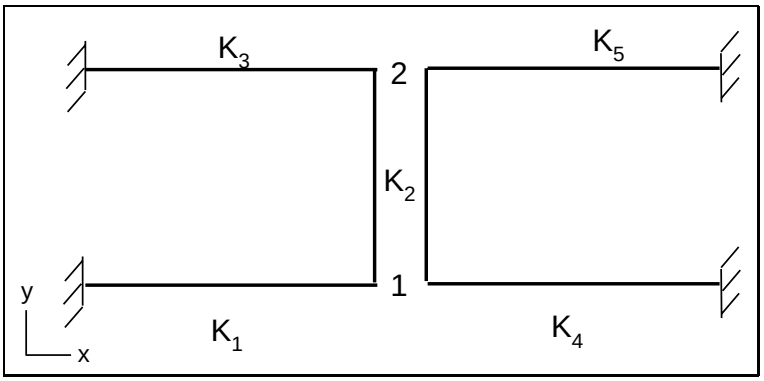

Figure 7.4: Two planar beam assemblies.

Random variations may occur at these points, but the physics of the assembly problem must be satisfied:

$$\sum F_x = 0, \tag{7.21}$$

$$\sum F_y = 0, \tag{7.22}$$

$$\sum M_z = 0. \tag{7.23}$$

A Monte Carlo analysis of this assembly indicates that the distribution of the forces is normal. The sum of the distributions on each side is zero; equilibrium is satisfied. The results of the Monte Carlo analysis are shown in figure 7.5.

The beam assembly may also be analyzed using a linearized statistical approach by the root mean squares equation,

$$s_{F_i} = \sqrt{\sum_{j=1}^{ndof} \left(\left[\boldsymbol{K}_{a\,ij} + \boldsymbol{K}_{b\,ij} \right]^{-1} \boldsymbol{K}_{b\,ij} s_i \right)^2} \tag{7.24}$$

where $\boldsymbol{K}_a$ and $\boldsymbol{K}_b$ represent the stiffnesses of each frame assembly.

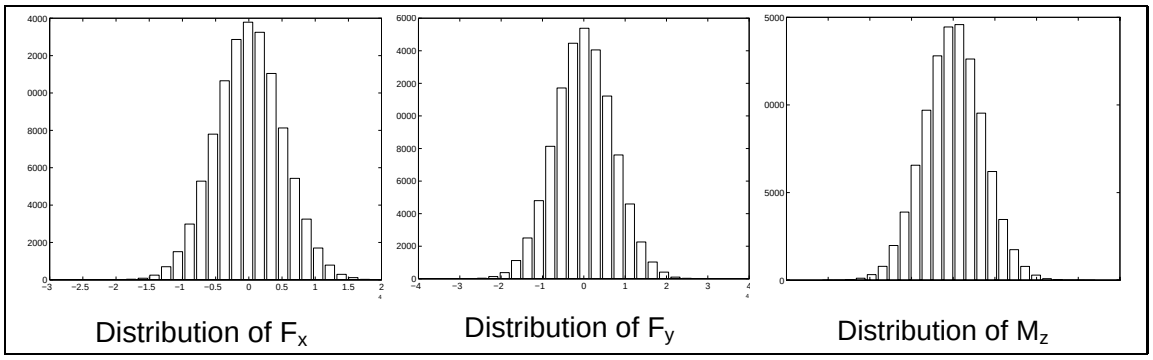

Figure 7.5: Monte Carlo force results for the beam assemblies.

The three standard deviation results at point 1 for the linearized compliant assembly model are

$$3s_{F_x} = \pm 15151, \qquad 3s_{F_y} = \pm 21266, \qquad 3s_{M_z} = \pm 1061.0.$$

This compares with the Monte Carlo analysis results of

$$3s_{F_x} = \pm 15172, \qquad 3s_{F_y} = \pm 21237, \qquad 3s_{M_z} = \pm 1061.0.$$

Once again, the results of the Monte Carlo analysis and the linearized compliant assembly solution are comparable. In addition, the linear solution requires similar calculations as one Monte Carlo iteration. So in this case, the linearized compliant solution is approximately 100,000 times faster than the Monte Carlo solution.

If covariance is included in the problem, the fundamental equation becomes

$$\boldsymbol{\Sigma}_F = \boldsymbol{K}_{ra} \boldsymbol{\Sigma}_o \boldsymbol{K}_{ra}{}^t \tag{7.25}$$

where $\boldsymbol{K}_{ra}$ is defined as

$$\boldsymbol{K}_{ra} = \boldsymbol{K}_a (\boldsymbol{K}_a + \boldsymbol{K}_b)^{-1} \boldsymbol{K}_b \tag{7.26}$$

and $\boldsymbol{\Sigma}_o$ is the geometric covariance term.

Since the assembly points are at the beam ends, there is no surface continuity

between the assembly points. Thus, Σ_o is a diagonal matrix of the form

$$\mathbf{\Sigma}_o = \left(\frac{.01}{3}\right)^2 \begin{bmatrix} 1 & 0 & 0 & 0 & 0 & 0 \\ 0 & 1 & 0 & 0 & 0 & 0 \\ 0 & 0 & 0 & 0 & 0 & 0 \\ 0 & 0 & 0 & 1 & 0 & 0 \\ 0 & 0 & 0 & 0 & 1 & 0 \\ 0 & 0 & 0 & 0 & 0 & 0 \end{bmatrix}. \tag{7.27}$$

Note that there is variation in the x and y degrees of freedom, but not in the rotational degree of freedom about the z axis.

Performing the multiplication in equation 7.25 yields a nearly full 6×6 matrix. Some of the values are very small, but many are non-zero. The test for statistical significance for covariance can be applied to Σ_F to simplify the terms and clarify the results. This process yields a banded matrix which is common in physically dependent covariance analysis,

$$\mathbf{\Sigma}_F = 10^7 \times \begin{array}{c} \\ F_{x1} \\ F_{y1} \\ M_{z1} \\ F_{x2} \\ F_{y2} \\ M_{z2} \end{array} \begin{array}{c} \begin{array}{cccccc} F_{x1} & F_{y1} & M_{z1} & F_{x2} & F_{y2} & M_{z2} \end{array} \\ \begin{pmatrix} 2.5505 & 0 & 0 & -0.0505 & 0 & 0 \\ 0 & 5.0251 & 0 & 0 & -5.0250 & 0 \\ 0 & 0 & 0.0125 & 0 & 0 & 0.0125 \\ -0.0505 & 0 & 0 & 2.5505 & 0 & 0 \\ 0 & -5.0250 & 0 & 0 & 5.0251 & 0 \\ 0 & 0 & 0.0125 & 0 & 0 & 0.0125 \end{pmatrix} \end{array}. \tag{7.28}$$

The diagonal terms of Σ_F are the variances. The square root of the diagonal terms $\Sigma_{F_i i}$ are the standard deviations. Thus, the 3 standard deviation values, $3s$, are computed by

$$3s_i = 3\sqrt{\Sigma_{F_{ii}}} \tag{7.29}$$

yields

$$3s_{F_x} = \pm 15151, \qquad 3s_{F_y} = \pm 21266, \qquad 3s_{M_z} = \pm 1061.0.$$

This result is exactly the same as obtained from equation 7.24. In addition, this solution demonstrates the correlation between the top and bottom assembly points. If there is a force in the x direction at the top point F_{x1}, there is a tendency to create a negative force of the same magnitude at the bottom point F_{x2}. Similarly, if there is a force F_{y1}, there is an equal and opposite force generated at F_{y2}. The y forces are fully correlated. Since there is no rotational variation to the assembly, the moment is created due to a couple, forces acting across a moment arm. The couple creates the same moment at the top and the bottom assembly points. Thus, the moments, M_{z1} and M_{z2} are fully correlated in the same direction.

Note that other covariance terms exist, but they are small in relation to those discussed here. The test for statistical significance of covariance set the other terms to zero.

Covariance does not change the standard deviation of the forces, but it does give additional insight into the physical nature of the problem.

7.4 Example 4: Two flanged plates

The following example demonstrates joining two flanged plates and shows the displacement effects on the gap closure problem. This result represents a single case solution and is *not* a statistical result. Figure 7.6 shows the two plates separated by a gap vector, δ_o. The vector is defined by the distance between the corresponding

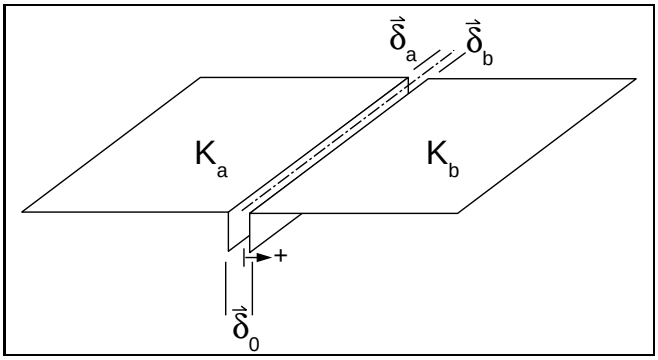

Figure 7.6: Two flanged plates with a defined gap, δ_o.

nodes at each plate. Each node represents a fastener location. Each plate has a defined stiffness, $\boldsymbol{K}$, determined by the plate thickness and material properties. The final flange positions are determined by the vectors $\vec{\delta}_a$ and $\vec{\delta}_b$.

The finite element model of this problem is shown in figure 7.7. The geometry is constructed at the nominal size. A gap is not defined in the geometry definition; the opposite edges are completely constrained.

This example examines the effects of a .05 inch gap and the same material and

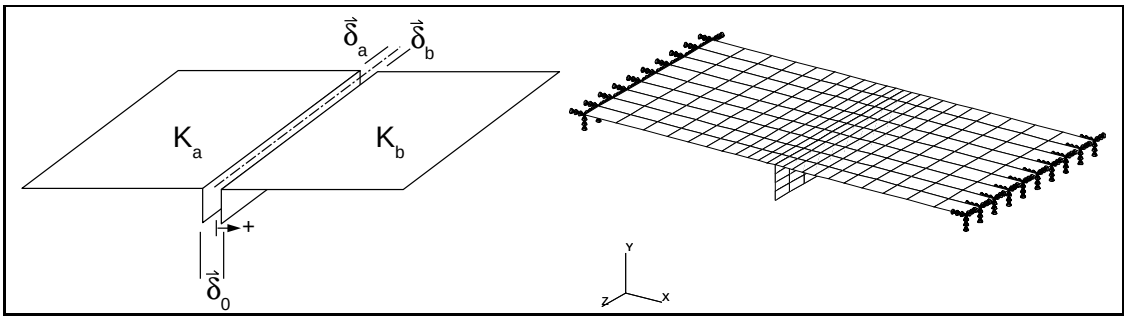

Figure 7.7: Finite element model of two flanged plates.

thickness for each plate. The final results are shown in figure 7.8. The component displacements, $\vec{\delta}_a$ and $\vec{\delta}_b$, each deformed .025 inches to close the gap. The plates also deformed upward due to the moment caused by joining the plates at the flange, below the edge constraints. Since the stiffnesses are equal in each plate, this is the anticipated result.

Similar results hold for different material properties. The compliant assembly tolerance model correctly predicts the effects of the bending moment and the material variation.

7.5 Example 5: Plane stress plates

This example develops the complete statistical covariance solution for two plates separated by a normally distributed random gap $\delta_o(\mu_o, \nu_o)$ as shown in figure 7.9. Each plates has a stiffness $\boldsymbol{K}_a$ and $\boldsymbol{K}_b$ respectively, that is determined by the

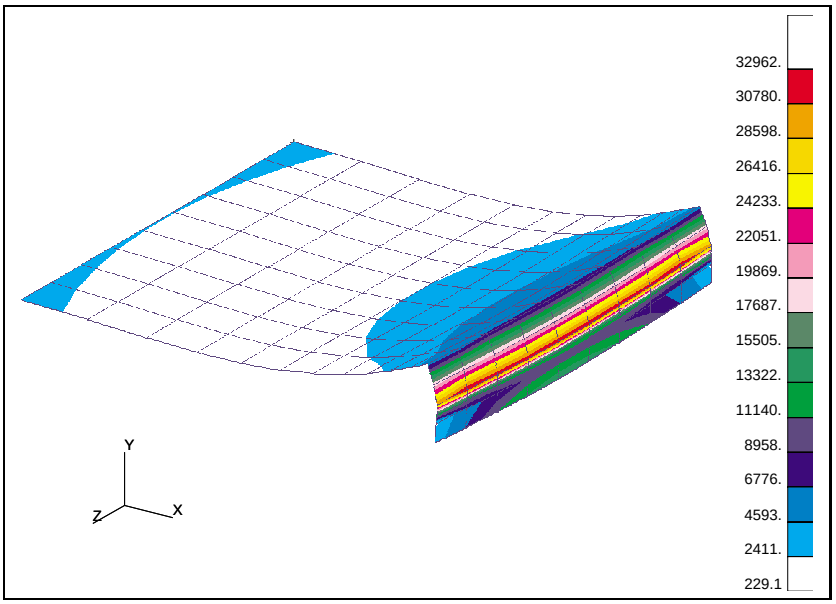

Figure 7.8: Finite element result of flanged plate.

geometry and the material properties.

Figure 7.9 also shows the finite element model of this assembly. The geometry is built at nominal size, and the finite element model is defined as a 4x4 grid on each plate. The boundary conditions are applied and super-elements are defined. The five nodes that are circled define the super-element boundary. A plane stress element has two degrees of freedom at each node, so the super-element matrices have ten degrees of freedom (size 10x10).

This example examines the specific case where the stiffnesses of each plate are equal, and the gap is defined with a mean $\mu_o = 0$ and a variance $\nu_o = 4/9$ ($3s = 2$).

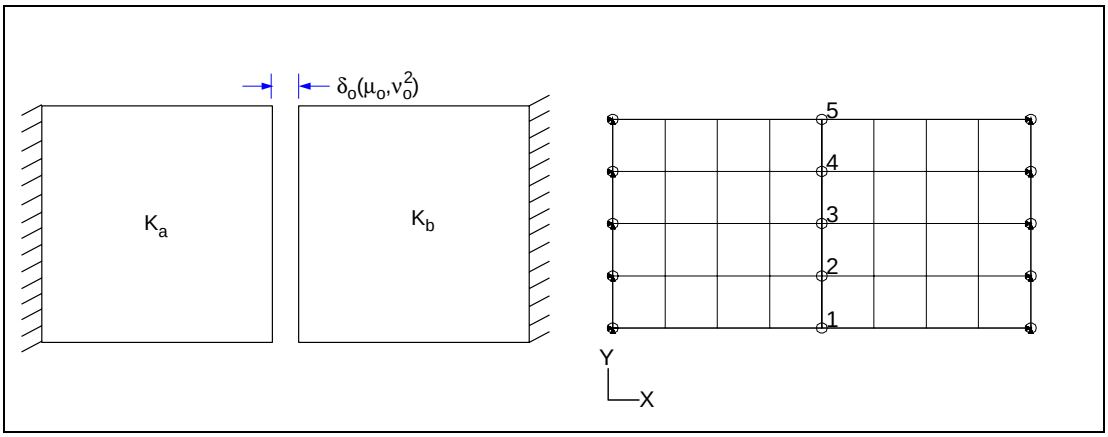

Figure 7.9: Plane strain blocks with a random gap.

Figure 7.10 shows a representation of the super-element stiffness matrices K_a and K_b. The stiffness matrices are defined in a 10x10 grid, and the value of each grid is displayed as a vertical bar. The two matrices are symmetric and very similar. There are negative values in the off-diagonal terms of the super-element stiffness matrices. The differences in $\boldsymbol{K}_a$ and $\boldsymbol{K}_b$ arise from the location of the fixed boundary conditions.

The super-element stiffness matrices are compatible for multiplication, so the stiffness ratio $\boldsymbol{K}_{r_a}$ can be defined:

$$\boldsymbol{K}_{r_a} = [\boldsymbol{K}_a + \boldsymbol{K}_b]^{-1} \boldsymbol{K}_b \tag{7.30}$$

The stiffness ratio matrix is shown in figure 7.11. It is not symmetric and there are negative values in the matrix.

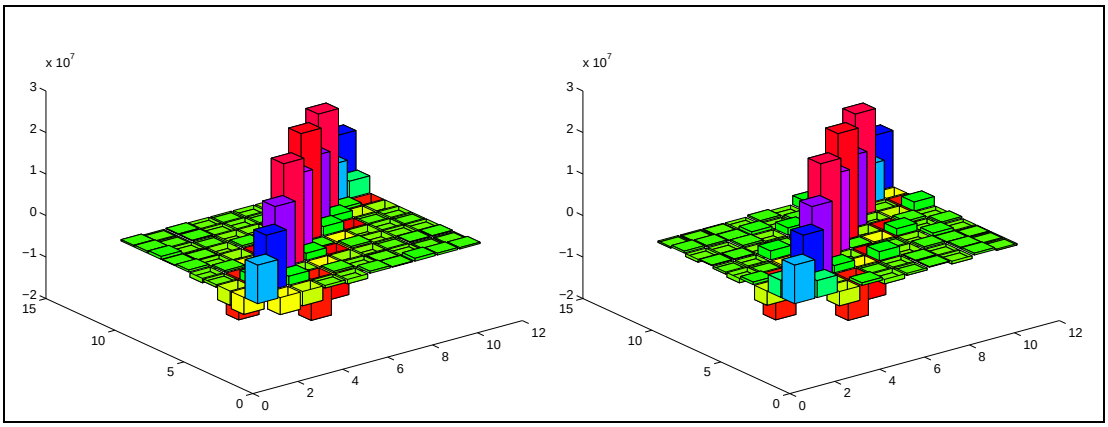

Figure 7.10: Super-element stiffness matrices $\boldsymbol{K}_a$ (left) and $\boldsymbol{K}_b$ (right).

7.5.1 Randomly independent variation in x with no covariance

The statistical solution to this problem can be solved in several ways. The first case will consider randomly independent variation in the x direction at each node and no variation in the y direction. The mean is zero and the variance is 1. The gap variance vector can be specified as

$$\nu_{\delta_o} = \frac{4}{9}[1 \quad 0 \quad 1 \quad 0 \quad 1 \quad 0 \quad 1 \quad 0 \quad 1 \quad 0]^t. \tag{7.31}$$

Ignoring the covariance that occurs due to material effects, the variance of the nodes along the gap in component **a** can be defined by

$$\vec{\nu}_{\delta_a}(i) = \sum_{j=1}^{ndof} \left(\boldsymbol{K}_{r_a}(i,j)\,\nu_{\delta_o}(j)\right)^2 \tag{7.32}$$

The results of this calculation, tabulated as 3 standard deviations, or $3\sqrt{\vec{\nu}_{\delta_a}(i)}$, are displayed in table 7.1. Since the stiffnesses are equal, the variance in the

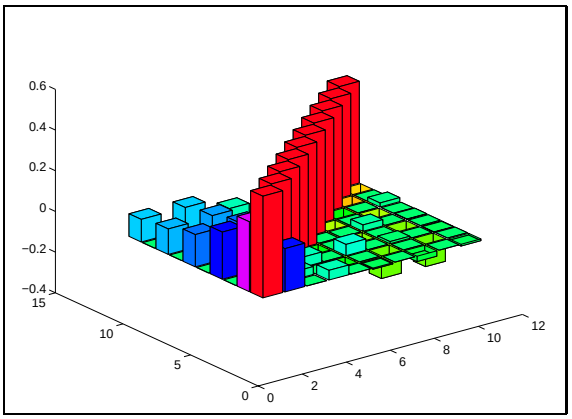

Figure 7.11: Non-covariant stiffness ratio matrix $\boldsymbol{K}_{r_a}$ for component **a**.

x direction is distributed equally between the two components, $\nu = \frac{1}{9}$. The $3s$ standard deviation is defined as the square root of the variance times 3, thus the standard deviation of x is $3s = 1$. In addition, the y variation is symmetric about the center node with the minimum variation occurring at the center point. Once again, this matches the intuitive interpretation of a flexible sheet being pulled to close the gap. The direction orthogonal to the applied variation is pulled in with the maximum deformation occurring at the edges.

Table 7.1: 3 Standard Deviations of component **a** due to statistical gap closure.

DOF	1-x	1-y	2-x	2-y	3-x	3-y	4-x	4-y	5-x	5-y
3 Sigma	1.0	0.761	1.0	0.657	1.0	0.6397	1.0	0.657	1.0	0.761

This same problem can also be solved using Monte Carlo analysis for compari-

son. Figures 7.12 and 7.13 compare the results of the linear solution posed above versus 500 finite element analyses. The results are nearly identical. The greater error is actually associated with the Monte Carlo solution since 500 samples is insufficient to generate a $3s$ sample equal to exactly 1.0. In addition, the computation time required by the linearized solution is much less than the 500 finite element analyses.

7.5.2 Covariant variation in x with material and geometric covariance

The full covariance solution includes covariance between the nodes due to surface continuity and the material effects. This example will specify a quadratic variation across the nodes to represent the surface continuity or geometric covariance constraint.

The bounding covariance matrix for a random quadratic Bézier curve is found using the A matrix described in chapter 5 by evaluating Bernstein basis functions at $t = \{0, 1/2, 1\}$

$$\boldsymbol{A} = \begin{bmatrix} 1 & 0 & 0 \\ \frac{1}{4} & \frac{1}{2} & \frac{1}{4} \\ 0 & 0 & 1 \end{bmatrix}. \tag{7.33}$$

The covariance matrix for the regression equations including the variance of

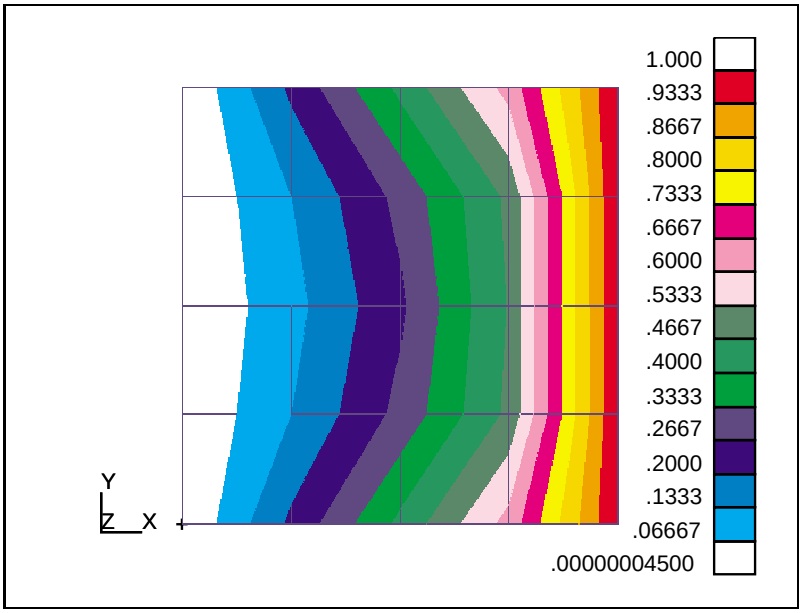

Figure 7.12: 3s x displacement results from linear compliant tolerance analysis.

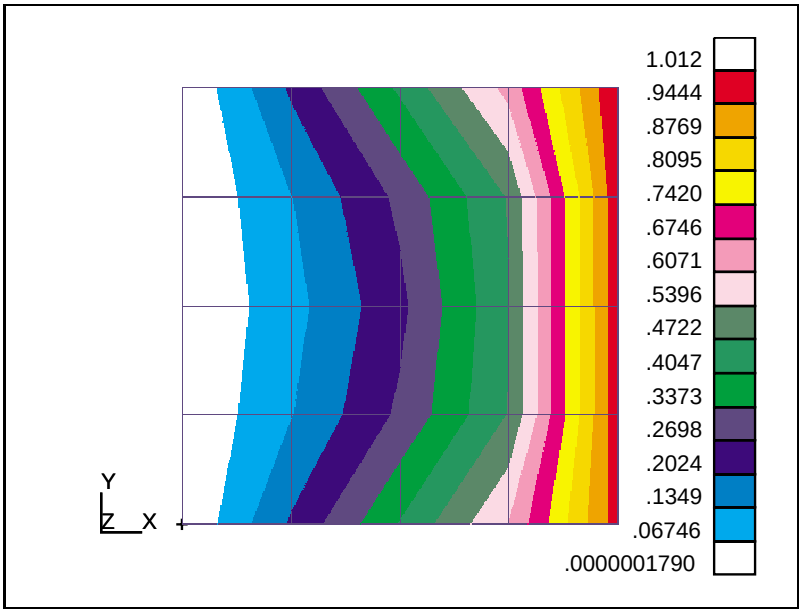

Figure 7.13: 3s x displacement results from 500 finite element analyses.

the tolerance is then

$$\boldsymbol{\Sigma} = T(\boldsymbol{A}^t\boldsymbol{A})^{-1} = \frac{4}{9}\begin{bmatrix} 1 & -\frac{1}{2} & 0 \\ -\frac{1}{2} & \frac{9}{2} & -\frac{1}{2} \\ 0 & -\frac{1}{2} & 1 \end{bmatrix}. \tag{7.34}$$

The covariance matrix $\boldsymbol{\Sigma}$ is not compatible for multiplication with the stiffness ratio matrix, so it must be expanded to contain the same degrees of freedom.

Assume that the random Bézier curve extends from node 1 to node 5. The nodes are located at parametric values of $t = \{0, .25, .5, .75, 1\}$ along the random Bézier curve. Also assume that the y degree of freedom is independent (0) of the x degree of freedom. Evaluating the Bernstein basis functions at each parametric point yields

$$\boldsymbol{B} = \begin{bmatrix} 1.0000 & 0 & 0 \\ 0 & 0 & 0 \\ 0.5625 & 0.3750 & 0.0625 \\ 0 & 0 & 0 \\ 0.2500 & 0.5000 & 0.2500 \\ 0 & 0 & 0 \\ 0.0625 & 0.3750 & 0.5625 \\ 0 & 0 & 0 \\ 0 & 0 & 1.0000 \\ 0 & 0 & 0 \end{bmatrix}. \tag{7.35}$$

The gap covariance matrix $\boldsymbol{\Sigma}_o$ can be defined by

$$\boldsymbol{\Sigma}_o = \boldsymbol{B}\boldsymbol{\Sigma}\boldsymbol{B}^t. \tag{7.36}$$

This defines a 10×10 covariance matrix that is compatible for multiplication with

the super-element stiffness matrices defining the plates. This matrix is shown as a 3-D bar chart in figure 7.14. The three highest values represent the x components of nodes 1, 3, and 5. These DOF's are randomly independent. All other DOF's in the model depend upon them. This matrix defines a statistical boundary condition that is be applied to the finite element solution.

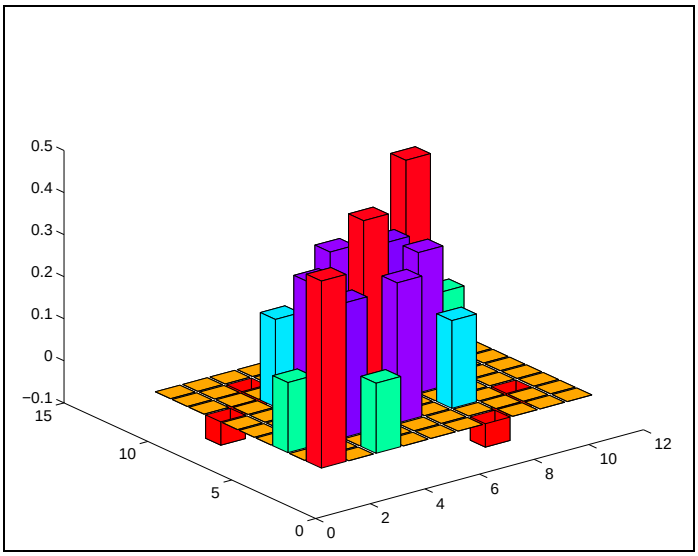

Figure 7.14: Geometric covariance matrix, Σ_o.

The complete covariance matrix, including both geometric and material covariance effects, for component **a** is defined by

$$\Sigma_a = \boldsymbol{K}_{r_a} \Sigma_o \boldsymbol{K}_{r_a}{}^t. \tag{7.37}$$

Figure 7.15 shows the covariance matrix Σ_a describing the displacements of part **a**. The diagonal elements represent the variance of the displacements due to

the geometric and material covariance in assembling the plates. The off-diagonal terms show the correlation between the displacements of each degree of freedom.

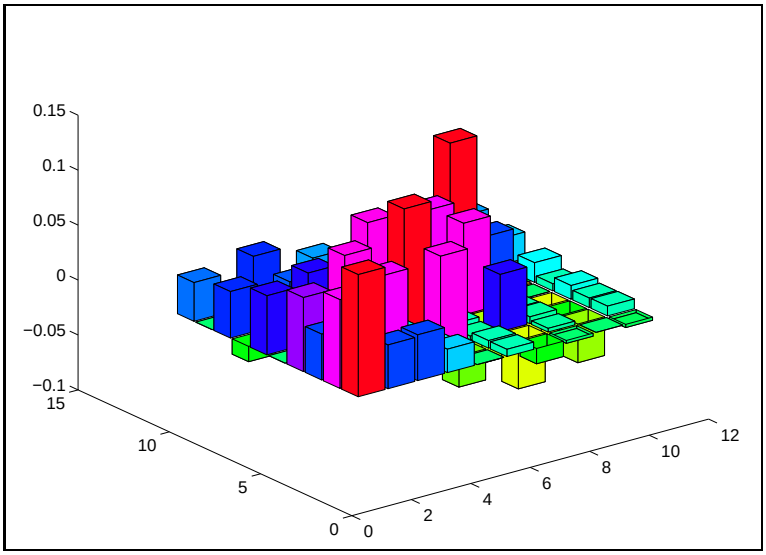

Figure 7.15: Displacement covariance matrix of part **a**, Σ_a

The $3s$ values of the x displacements are shown in table 7.2. In this case only the three independent DOF's have a $3s$ distribution of 1.0. All other degrees of freedom are dependent. This is also manifest by examining the eigenvalues of the Σ_a matrix. There are only three non-zero eigenvalues. This again indicates that only 3 degrees of freedom are independent.

Once again, this problem can also be solved using Monte Carlo analysis for comparison. Figures 7.16 and 7.17 compare the results of the linear solution posed above versus 500 finite element analyses. The results are again nearly

Table 7.2: 3 Standard Deviations of plate **a** due to statistical gap closure including both geometric and material covariance.

DOF	1-x	1-y	2-x	2-y	3-x	3-y	4-x	4-y	5-x	5-y
3 Sigma	1.0	0.52	0.85	0.34	1.0	0.24	0.85	0.34	1.0	0.52

identical. The greater error is again associated with the Monte Carlo solution since 500 samples is inaccurate.

7.6 Example 6: Simple block assembly

Figure 7.18 shows a mechanical assembly of three different sized blocks that fit inside a U-shaped base. The parts, when considered as rigid bodies, constitute a a one-dimensional tolerance stack-up; however, when deformations are considered, it becomes a two-dimensional problem. The nominal dimensions on the assembly are specified such that the blocks are press fit into the base with a nominal interference of .025 inches. The tolerance on this interference is specified to be no more than $\pm$.025 inches. Summing the nominal and variable interference gives a range from 0 to .05 inches. The parts are aluminum with a yield strength of 70 ksi. There is a design requirement that the parts be assembled without exceeding the yield strength. It is possible to predict how many parts will be rejected with the given

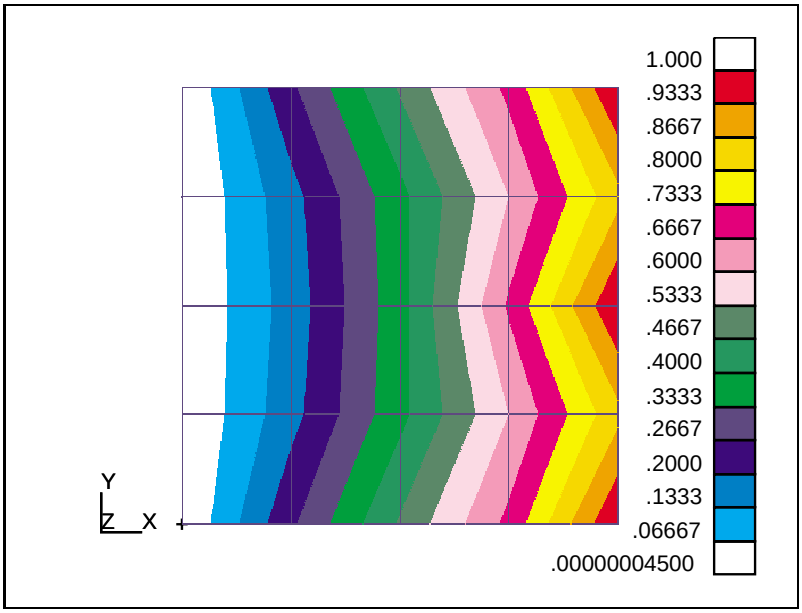

Figure 7.16: 3s x displacement results from linear compliant tolerance analysis.

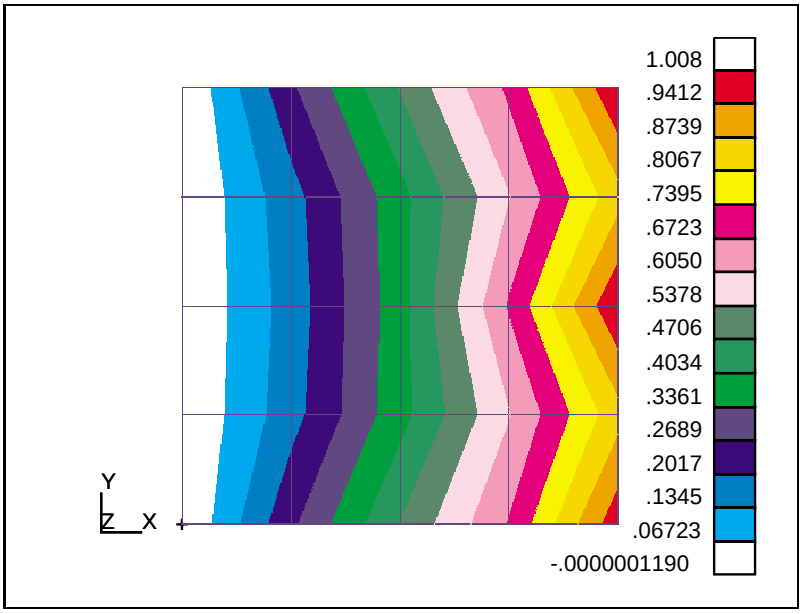

Figure 7.17: 3s x displacement results from 500 finite element analyses.

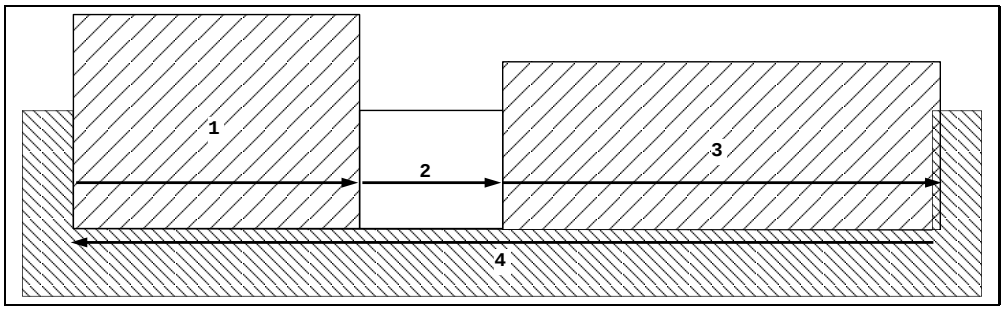

Figure 7.18: One-dimensional stacked block problem with an interference fit.

design specifications.

The finite element model is constrained in the X and Y directions at the mid-point of the base. The rest of the base is on rollers. There are also rollers between the blocks and base to allow kinematic adjustments. It is assumed that the frictional effects are very high between the mating surfaces on the left and right edges so that the nodes on the vertical edges will move together. The blocks are also assumed to be thick relative to their length and width, so this is a plane strain problem.

The model is constructed so that the blocks fit exactly inside the base. The nominal interference will be accounted for in the displacement boundary condition applied at the gap. This simplifies the construction process and corresponds with the assumption that small variations in geometry will create negligible changes in the stiffness of the parts.

This problem can be broken into two parts, the nominal solution and the statis-

tical solution. The nominal solution occurs with an interference of .025 inches. The peak mean σ_{xx} stress in the blocks is -55,488 psi. The peak mean σ_{xx} stress in the base is 49,882 psi. The interference fit places the blocks in compression and the base in tension.

Figures 7.19 and 7.20 show deformation and fringe plots of the analysis. The deformation represents the mean deformation. The base has expanded horizontally due to pressure from the blocks, with the greatest deflection occurring in the side rails. The blocks have contracted horizontally due to the clamping force of the base, with the greatest contraction occurring near the base. The stress fringes represent the mean σ_{xx} stress plus the 3 standard deviation σ_{xx} values. The predicted statistical stresses are well beyond the desired 70 ksi limits. The maximum statistical σ_{xx} stress occurs in the base with a value of 289 ksi. In reality, the material at this level has exceeded the plastic limit and would never really reach 289 ksi. This analysis can only be used to describe the deformations that will be in the linear range. However, a great deal of information can be obtained by examining the linear data.

Assuming a normal distribution, and knowing the mean and the 3s stresses, it is possible to determine the number of assemblies that will fall within the linear material limits of the assembly. Figure 7.21 shows a plot of the normal distribution of the σ_{xx} stresses in the base. The darkened areas exceed the design specification

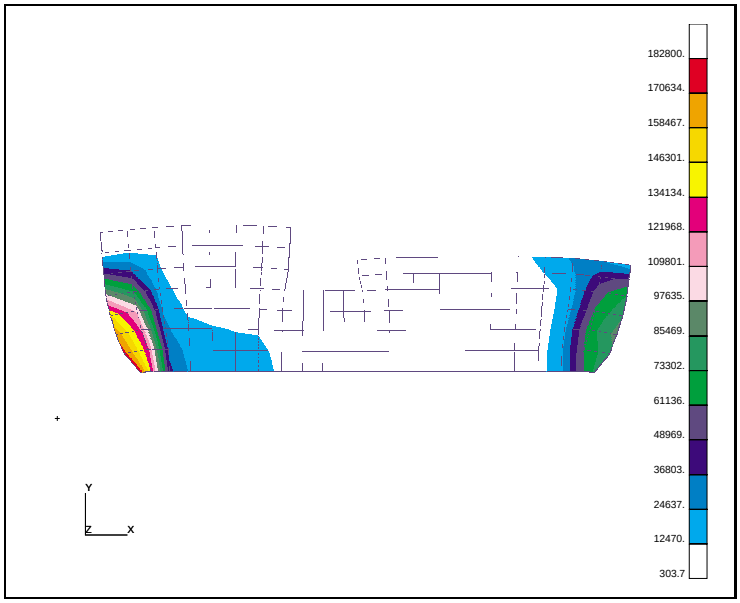

Figure 7.19: Deflection and stresses in blocks due to a $\pm$3s interference fit.

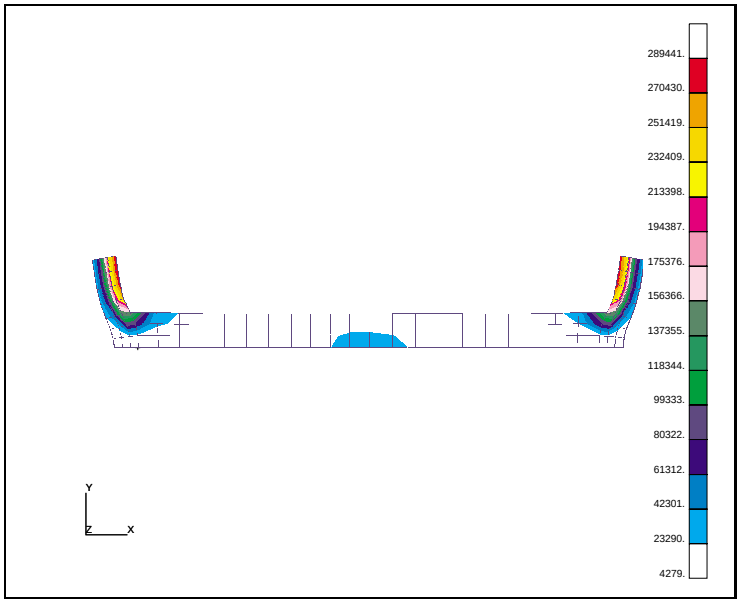

Figure 7.20: Deflection and stresses in base due to a $\pm$ 3s interference fit.

of $\pm$70 ksi. The white region represents the set of acceptable assemblies.

The mean of the distribution is $\mu = 49882$. A single standard deviation is $s = 96480.3$. The data is normalized by calculating the *z-score*. For the right hand area the z-score z_1 is

$$z_1 = \frac{x - \mu}{s}, \tag{7.38}$$

$$= \frac{70000 - 49882}{96480.33}, \tag{7.39}$$

$$= .2085. \tag{7.40}$$

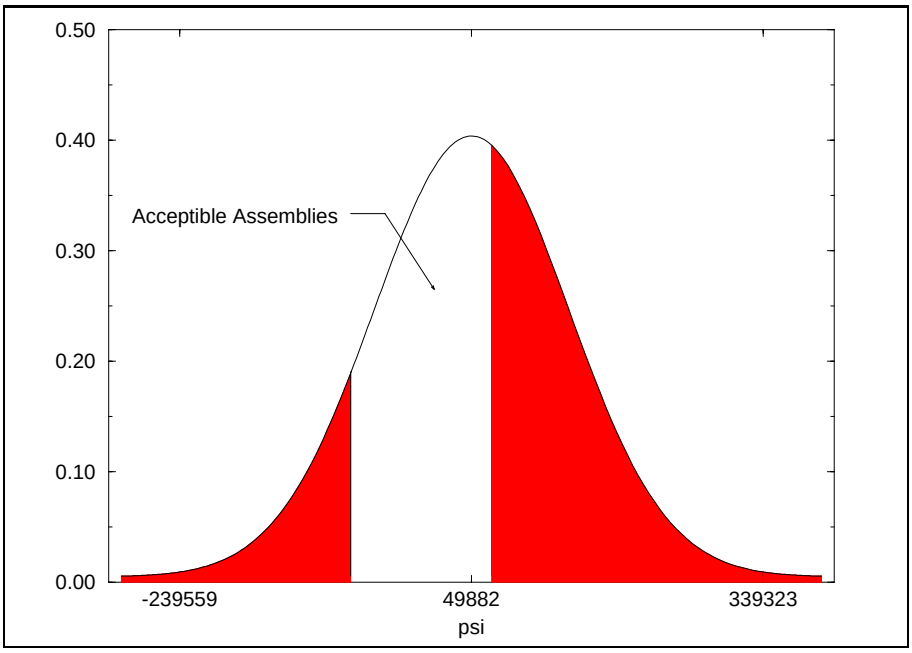

Figure 7.21: Statistical distribution of maximum σ_{xx} stress in the base.

Similarly, for the left hand region the z-score z_2 is

$$z_1 = \frac{x - \mu}{s}, \tag{7.41}$$

$$= \frac{-70000 - 49882}{96480.33}, \tag{7.42}$$

$$= -1.243. \tag{7.43}$$

By using a standard statistical table for normal distributions, the values in the tails correspond to 41.68% and 10.75% respectively. Thus, 52.43% of all assemblies will exceed the design limits and be rejected due to improperly assigned tolerances.

Note that even though the material stresses extended into the plastic region, only the linear results were used to predict the number of parts that exceeded the yield strength. A non-linear analysis was not required. This type of design constraint is a common occurrence where members, such as bolts, are taken just to the yielding point or where composite members may not exceed interlaminar shear limits due to delamination problems.

Chapter 4 noted that the mean results can be obtained by using multi-point constraint (MPC) equations. The MPC model is shown in figure 7.22. The nodes on the blocks are related to the nodes on the base, but there is one more node that is added into the equation. A fictitious node at the top of figure 7.22 is used to store the gap or interference data. An enforced displacement constraint of .050

inches has been placed on this node.

Table 7.3 shows that the results using the direct stiffness matrix and the multi-point constraint are very similar. Nodes 1 through 5 are located on the right hand interface of the stacked blocks with the base. Nodes 6 though 10 are on the opposite side. The maximum error in the two solutions is less than one percent. This occurs at node 6 which is located at the upper left hand interface. The error in this analysis is possibly due to the coupling of the Y components (via Poisson's ratio) in the stiffness matrices that was not enforced in the MPC equations.

It is important to note that only the mean may be obtained in this manner. Even though the interference is at its maximum value of .05 inches, this does not represent a "worst-case" analysis. The maximum stresses in this case are approximately 120 ksi which is less than 50% of the predicted $3s$ stresses. This method cannot be used to predict statistical rejects as was incorrectly done in (Merkley, Chase, and

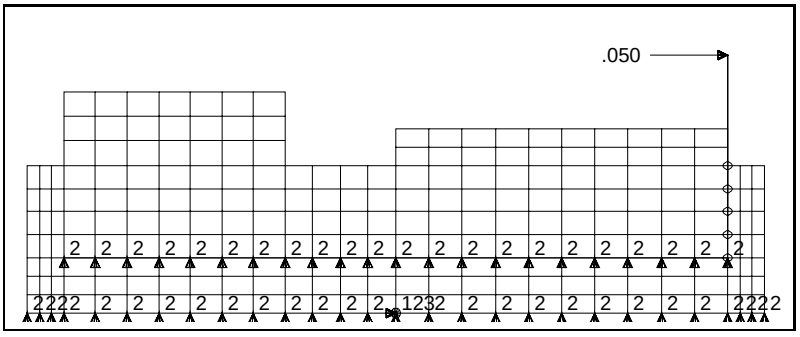

Figure 7.22: Model defined using MPC's.

Table 7.3: A Comparison of Stiffness Matrix Manipulation vs. MPC's for the Single-case Closure Solution.

Node Number	X Displacement with MPC's	X Displacement with Stiffness Matrices	Percent Error
1	0.0212	0.0212	0.1641
2	0.0204	0.0203	0.6665
3	0.0192	0.0191	0.6611
4	0.0175	0.0175	0.1395
5	0.0142	0.0143	0.4437
6	-0.0209	-0.0211	0.9689
7	-0.0200	-0.0202	0.7092
8	-0.0189	-0.0190	0.4728
9	-0.0175	-0.0175	0.1482
10	-0.0142	-0.0142	0.0128

Perry 1996) and (Merkley and Chase 1997). However, this method can give good results in cases where covariance can be ignored, such as very small statistical variation about the mean and widely spaced fasteners.

7.7 Example 7: Railway passenger compartment.

The final example shows results that were computed for a railway passenger compartment shown in figure 7.23. This assembly is composed of nine steel reinforced fiberglass panels. The finite element model is composed of linear shell elements. This precludes an accurate statistical analysis of stresses since the stochastic finite element code developed in this dissertation only analyses plane strain and plane

stress problems. However, it is possible to use the MPC method to demonstrate areas of concern in the design.

The analysis in this section focuses on the the three panels comprising the left side assembly. This assembly is shown in figure 7.24.

The maximum gaps were determined by using 3 standard deviation values from tolerances on the drawings. These values corresponded to the actual variations that were obtained during manufacturing due to warpage and shrinkage of the fiberglass panels.

The failure criteria for fiberglass is the maximum principle stress. Since the fibers are randomly oriented, some of them will always fall in the direction of the maximum stress. Once some of the fibers fail, others quickly follow. For this material, the failure stress occurs at 8000 psi tension and 16000 psi compression.

The maximum principle assembly stresses for the panels are shown in figure 7.25. All along the connecting flanges high stresses occur. However, the stresses are particularly high in the radius in the upper corner and the base, indicating problem areas. During the manufacturing process problems were encountered assembling the cap of the luggage rack onto these three panels. This is indicative of the kinds of problems that can occur due to improper tolerance specifications in compliant assemblies.

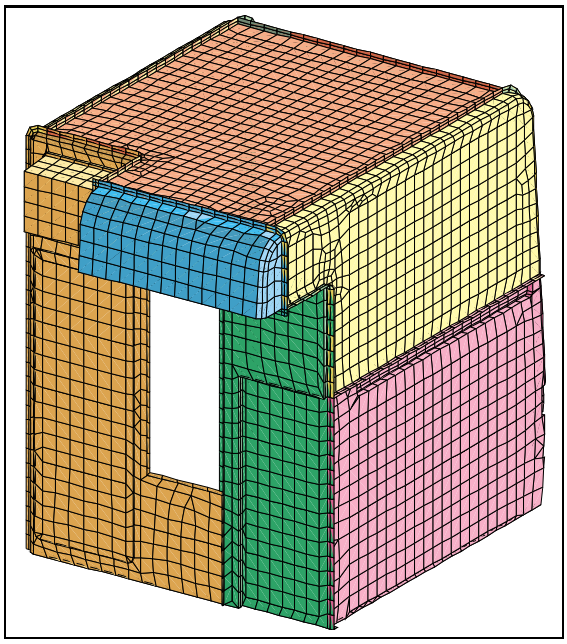

Figure 7.23: Finite element model of a railway passenger compartment.

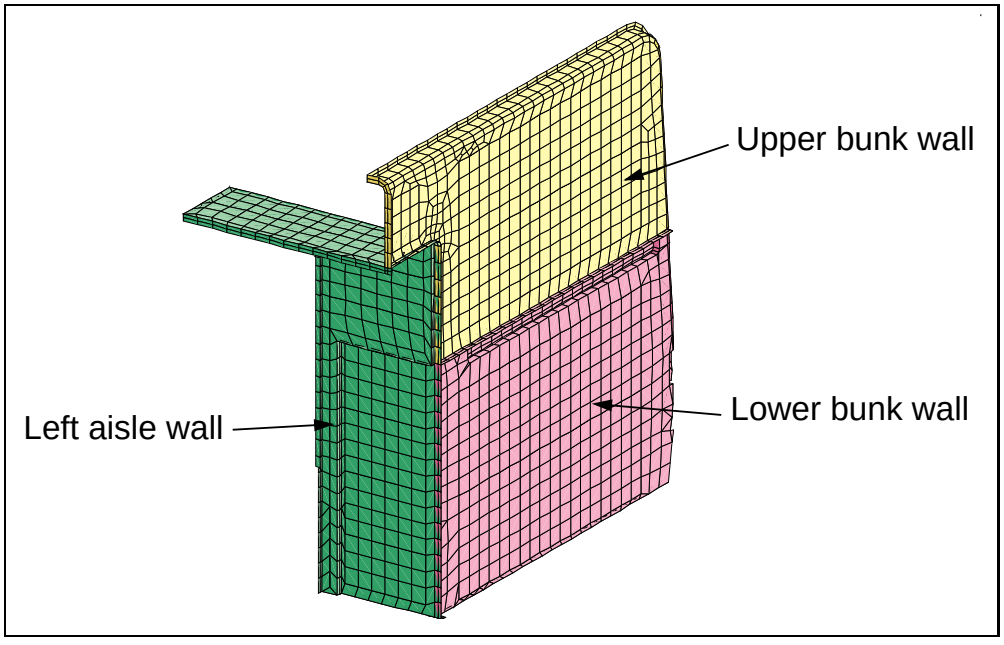

Figure 7.24: Left side assembly of a railway passenger compartment.

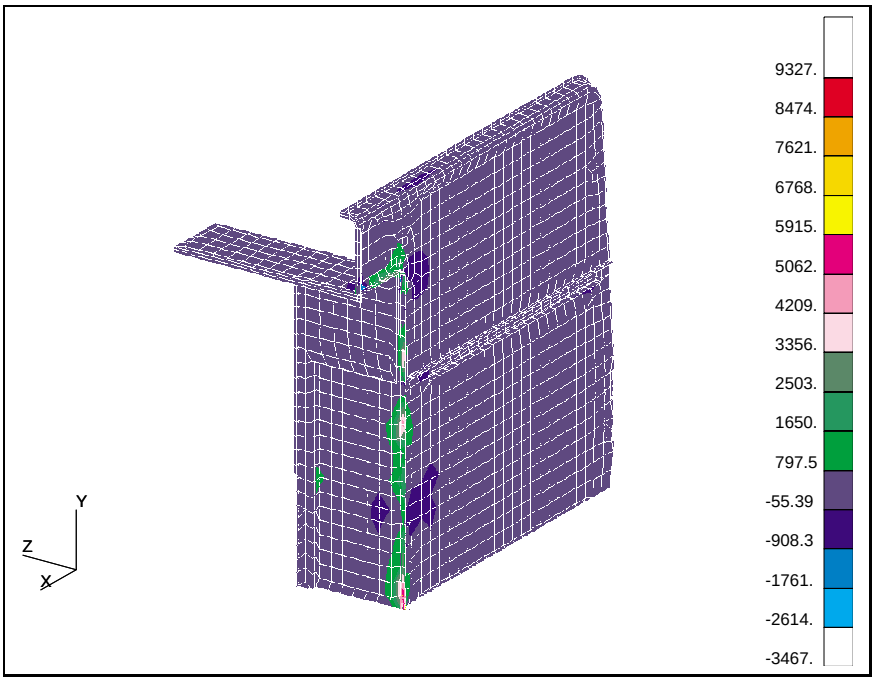

Figure 7.25: Maximum principle stresses in the left side assembly.

One other result that came out of this analysis is that assembly order can be critical. By specifying a different order of assembly, the part stresses changed significantly. This is an area that should be researched further.

7.8 Summary

This chapter has presented the results of tolerance analyses that include the assembly compliance. Compliant tolerance analysis can be verified with simple problems. It can also be applied to complex real-world problems. In addition, the linear

compliant tolerance analysis techniques outlined in this dissertation correlate well with Monte Carlo simulation results. The effects of neglecting material and geometric covariance have been demonstrated. Finally, it has shown that compliant tolerance analysis can be used to predict the consequences of manufacturing variations on assembly stresses.

Chapter 8

Conclusions

8.1 Conclusion

This dissertation has developed the theory and methods defining compliant tolerance analysis. This work has merged research in the areas of tolerance analysis, finite element analysis, computer-aided geometric design, and statistics. Compliant tolerance analysis should prove useful for a wide variety of design and manufacturing tasks including:

- Predicting the closure forces in assemblies of misaligned parts.
- Predicting the final location of mating surfaces.
- Predicting distortion due to internal assembly stresses.

- Predicting internal residual stress and force due to assembly of off-nominal parts.
- Predicting percent of assemblies which will not meet design limits.
- Performing “what-if” studies and assigning tolerances throughout an assembly to minimize production/maintenance problems.
- Performing sensitivity studies to identify the critical sources of variation.

This analysis method helps engineers and designers understand the effects and the importance of manufacturing tolerance early in the design process. It provides a tool for evaluating the consequences of manufacturing tolerances on assembled products.

The methods developed in this dissertation are also useful in productions. Manufacturing problems can be analyzed, such as the effect of an out-of-spec part on a current product line. Fixturing problems could also be evaluated with these methods.

Compliant tolerance analysis can serve as a design tool by using estimated process variation to assign tolerances. It can also be used with actual process data to determine the affects of manufacturing variation on assemblies.

8.2 Contributions

This dissertation includes a number of original contributions:

- A method for including component compliance in a tolerance analysis of assemblies has been developed. The fundamental equations for performing a steady-state contact solution were simplified and numerically improved by reducing the number of required matrix inversions.

- A firm theoretical foundation has been established for applying Vector Assembly Modeling to tolerance analysis of compliant assemblies. The Vector Assembly Model meets all the criteria for a valid tolerance theory and provides an algorithmic tool for developing the kinematic constraints needed to describe the propagation of variation in assemblies.

- The linearization assumptions of the Vector Assembly Model have been validated. For simple assembly models, the function space is primarily linear, except in certain regimes which are normally avoided in design practice. Linearized tolerance analysis is well matched with linearized FEA.

- Steady-state contact solutions of finite element analysis were expanded to include random variation in the system. The concepts of material and geometric covariance were introduced and corresponding algebraic terms were

derived and explained.

- Super-elements have been identified as a robust method of creating the component stiffness matrices. Representing each part in an assembly as a super-element is a natural application of finite element analysis and reduces computation for design iteration.

- The concept of random Bézier curves was developed. Bounds on these curves were established that relate variation in the curve to variation in the control points. It was demonstrated that Bézier curve mathematics can be used to add and subtract random Bézier curves. The geometric covariance matrix was derived from random Bézier curves.

- A new test for the statistical significance of covariance terms was introduced which allows large covariance matrices to be simplified.

- Compliant tolerance analysis was applied to several assemblies ranging from simple springs to complex geometry. It provided correct results on the simple intuitively understood assemblies and agreed with simulated manufacturing results on complex assemblies.

- Monte Carlo simulation was used as a verification tool. It showed that care must be exercised in representing mating surface variations. Assuming independent random variation ignores surface continuity constraints. A simula-

tion procedure was developed which includes surface continuity effects. This method corroborated with the linearized compliant assembly procedure.

8.3 Recommendations

This research has laid the groundwork for tolerance analysis of compliant assemblies. There are many research areas that could be examined further.

8.3.1 Experimental Verification

Research should be conducted to verify the assumptions of compliant tolerance analysis. This would require building and measuring test specimens and comparing the assembly results with compliant tolerance analysis results. A possible test assembly would be to build and test pairs of flanged plates as described in Chapter 7. Closure forces and displacements could be measured for a single assembly and compared to the linearized compliant tolerance FEA. By comparing the results of a random sample of assemblies with a Monte Carlo simulation of the same problem, it should be possible to validate the statistical compliant solution as well.

The verification would require the development of new load cells for measuring the internal assembly forces. New measuring technique for measuring internal displacements would also have to be developed.

8.3.2 Optimal Assembly Order

Preliminary results indicate that assembly order can affect the required assembly forces. It appears possible to minimize the assembly stresses by determining the optimal order of component assembly.

There are certain structures that will assemble easily in a specific order, but will not assemble at all if the order is changed. Current research indicates that this may be similar to assembling springs in parallel or in series (Liu et al. 1995). Structures that act like parallel springs will be stiffer and more difficult to assemble. Based on the compliant tolerance analysis techniques presented in this research, assembly order may be optimized to reduce residual stress and assembly force. From this optimization, methods could be developed for creating a rational process plan. This process plan would then have to be evaluated for efficiency and cost. It could also be used to verify process plans developed using traditional methods. Applying this methodology could help reduce tooling, redesign, labor costs as well as increasing part lifetimes.

8.3.3 Compliant Mechanisms

Mechanisms that use compliant joints are found in an increasing number of applications. They are of special interest in the development of Micro Electro-mechanical

Mechanisms (MEMS). The research developed in this dissertation could be used in the design and analysis of compliant mechanisms. It should be possible to determine the effects manufacturing variation will have on compliant mechanisms. This becomes especially interesting at microscopic scales. Process capabilities need to be evaluated and the effects of very small variations need to be considered. The assumptions of linearity need to be reconsidered at small scales. One challenge of this research is that compliant mechanisms typically exhibit large deformations. This would have to be considered in this research.

8.3.4 Propagation and Accumulation of Residual Stresses

As components are assembled, residual stresses develop at mating surfaces. Multiple components cause the residual stresses to accumulate and propagate through the assembly. This propagation and accumulation is similar to the geometric variation in rigid body assemblies which can only be transmitted through the joints where mating parts contact. The nature of the propagation depends on the joint type. Although residual stress decays with distance by St. Venant's principle, the average residual displacements can be transmitted through the assembly. It may be possible to develop a library of compliant joint definitions, similar to the kinematic joints in rigid body assemblies.

8.3.5 Gap Function Investigation

Different shaped gap functions should be evaluated for their effect on compliant tolerance analysis. This could be performed on a flanged plate model. The gap shapes could include tapered, sinusoidal (in phase and out of phase), and twisted out of plane. The results could then be compared with the experimental results.

8.3.6 Random Bezier Curves

There is much work that can still be done in this area of random Bézier curves. Some work has already been performed in examining 2-D variation normal to the curve rather than a circular tolerance zone on the control points. With normal variation, covariance occurs between the X and Y coordinates. Monte Carlo analysis can demonstrate this, but the underlying covariance relationship has not yet been studied.

The work that has been done on random Bézier curves could be expanded to define random Bézier surfaces. This could introduce new sources of covariance due to the increased degrees of freedom in a surface. The mathematical basis for random Bézier surfaces would need to be defined.

Random Bézier curves have applications outside of the area of tolerance analysis, such as the design of robust control systems, such as a robot path controller. It

should be possible to convert the control system into random Bézier curves and determine how variance in the system will impact the control system. Garloff (1993) has shown that Bernstein polynomials can be used in control system design. Including the effect of tolerances on the polynomials would allow random Bézier curves to be used as a tool to design robust control systems.

This research has examined only uniform tolerances where the tolerance is defined as plus or minus a single value. Non-uniform tolerances are not symmetric. They represent a plus tolerance at one value and a minus tolerance at another. This does not represent merely a mean shift of the Bézier curve since the offset of a Bézier curve is not another Bézier curve. It is unclear how this issue could be resolved.

8.3.7 Geometric Covariance

The effects of geometric covariance must be better understood. It is clear that certain applications exhibit geometric covariance, but it is unclear how to quantify this effect. It appears that surface waviness or spatial wavelength could have a pronounced effect. The work by Anderson (1997) could yield some insight into this problem. Design rules need to be determined to guide the selection of variation frequency in the geometric covariance term. The wavelength problem becomes more interesting and challenging when considering mating surfaces.

8.3.8 Residual Gaps

Compliant tolerance analysis, as presented in this dissertation, only examines the gaps at fastener locations. There may be residual gaps or interferences that occur in between the fasteners. Solving for the residual gaps requires an iterative procedure. A possible solution sequence for this problem follows.

1. Close fasteners via compliant tolerance analysis equations.
2. Find interference at intermediate nodes.
3. Reduce the interference to zero.
4. Iterate until there are no interferences along the original gap function.
5. Provide information about residual gaps and contact forces.

This could be important for applications involving gaskets, seals, aerodynamic surfaces, aesthetic appearance, etc.

8.3.9 Nonlinearities - Buckling, Yielding, Anisotropy

In some assemblies, joining processes may trap “bubbles” of material between fasteners. When a fastener is placed at the bubble location, the material may buckle in response to the load. Research could be conducted to determine if this

type of buckling load is within the bounds described by the statistical analysis. It may be possible to extract the critical buckling load from the component super-element stiffness matrices and compare this with the statistical assembly forces. This research would need to address the effects that buckling has on the residual stress in this non-linear problem.

The effects of material non-linearity is closely related to this problem. Non-linearities may arise from either material yielding or anisotropy. Methods should be developed for examining these problems.

8.3.10 Variable stiffness matrices

This dissertation assumed that small variations in geometry had little effect on the part stiffness. However, small variations in thickness can have a significant effect on shell type problems. Methods should be developed to include the effect of material and section properties on the stiffness matrix itself and their consequences on compliant assembly variations.

8.3.11 Effects of fixturing

Fixtures play an important role in the assembly process. The effects of fixtures could be included in the compliant tolerance analysis. The compliance of the fixture

and its interaction with a compliant assembly could be studied along with the effect of dimensional errors. This could lead to the design of fixtures that reduce the residual stress in a finished assembly.

Appendix A

A closed form random Bézier curve.

In Chapter 5, a definition of the random Bézier curve was developed. This appendix derives an alternate random Bézier curve. This method has a closed form solution for quadratic Bézier curves. It develops a family of Bézier curves with a proscribed standard deviation around a mean curve at a given value of t but at no other point on the curve.

This solution to equation 5.28 requires some examination of the fundamental properties of bounded Bézier curves. A common assumption of random polynomials is that all the random coefficients (or in this case control points) are independent. This would imply that $\nu_{ij} = 0$ for $i \neq j$ creating a diagonal covariance matrix. This assumption is not valid for all the covariance terms if the random polynomials are constrained to lie within a set of uniform bounds.

First, it should be noted that the end-points are independent of each other so that $\nu_{0n} = 0$. Moving one end-point does not constrain the allowable motion of the other end-point within the bounds.

There is non-zero covariance that exists between the other control points. This is demonstrated in figure A.1. The figure shows pairs of quadratic Bézier curves within linear bounds of $\pm$0.1. When the end-points are constrained at y = 0, the center control point $\vec{P}_1$ can vary between $y = \pm$0.2 and keep the curve within the $\pm$0.1 bounds. If the end-points are moved to the extreme limits, as in the right hand figure, the center control points can vary -0.3 $\leq y \leq$ 0.1 with the end-points at 0.1 or -0.1 $\leq y \leq$ 0.3 with the end-points at -0.1. It is interesting to note that in all cases, the total range of motion is 0.4. The allowable variation of the center control point P_1 depends on the location of the end-points. Thus, the covariance between end-points and the center control point is non-zero for a bounded random quadratic Bézier curve. Similar reasoning can be applied to higher order curves.

The values of the nu_{ij} terms are difficult to determine in general. However, for a quadratic curve the values may be determined by inspection. Equation 5.25 can be evaluated for n = 2 (a quadratic curve). Excluding the covariance term u_{02} for the endpoints, this expansion is

$$\nu_{x(t)} = \beta_0^2(t)^2\nu_{00} + \beta_1^2(t)^2\nu_{11} + \beta_2^2(t)^2\nu_{22} + 2\beta_0^2(t)\beta_1^2(t)\nu_{01} + 2\beta_1^2(t)\beta_2^2(t)\nu_{12}. \quad \text{(A.1)}$$

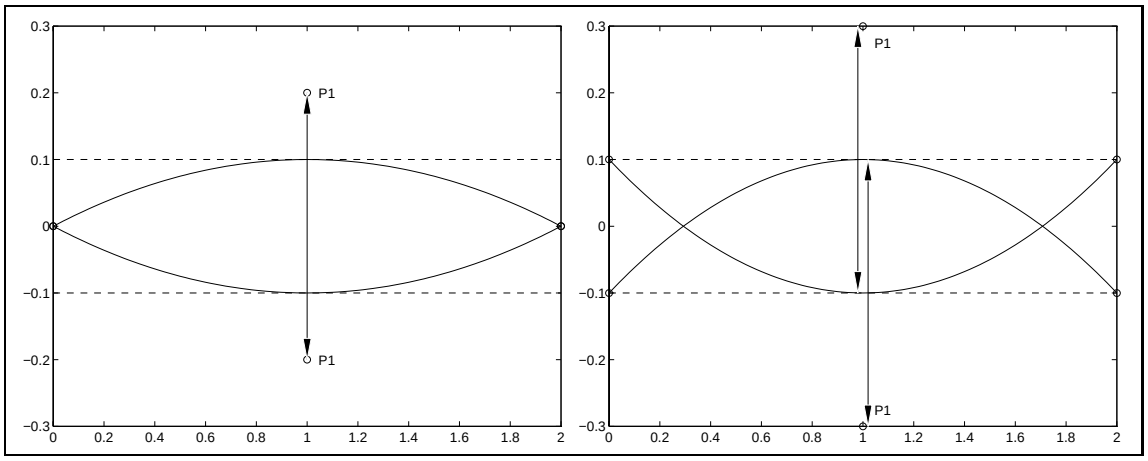

Figure A.1: Maximum variation of the center control point of a quadratic Bézier curve.

A constant bounding variance $\nu_{x(t)}$ may be found by letting the ν_{ii} terms equal the reciprocal of the coefficients times the variance in x and the ν_{ij} terms where $i \neq j$ equal the negative reciprocal of the coefficients times the variance in x so that

$$\nu_{00} = \frac{\nu_{x(t)}}{\beta_0^2(t)^2}, \tag{A.2}$$

$$\nu_{11} = \frac{\nu_{x(t)}}{\beta_1^2(t)^2}, \tag{A.3}$$

$$\nu_{22} = \frac{\nu_{x(t)}}{\beta_2^2(t)^2}, \tag{A.4}$$

$$\nu_{01} = -\frac{\nu_{x(t)}}{2\beta_0^2(t)\beta_1^2(t)}, \tag{A.5}$$

$$\nu_{12} = -\frac{\nu_{x(t)}}{2\beta_1^2(t)\beta_2^2(t)}. \tag{A.6}$$

These values are the second order reciprocal Bernstein Covariance functions.

Similar expressions can be written to describe variation the y and z.

Placing the reciprocal Bernstein Covariance functions into the covariance matrix gives

$$\mathbf{\Sigma}_{x(t)} = \begin{bmatrix} \frac{\nu_{x(t)}}{\beta_0^2(t)^2} & -\frac{1}{2}\frac{\nu_{x(t)}}{\beta_0^2(t)\,\beta_1^2(t)} & 0 \\ -\frac{1}{2}\frac{\nu_{x(t)}}{\beta_0^2(t)\,\beta_1^2(t)} & \frac{\nu_{x(t)}}{\beta_1^2(t)^2} & -\frac{1}{2}\frac{\nu_{x(t)}}{\beta_1^2(t)\,\beta_2^2(t)} \\ 0 & -\frac{1}{2}\frac{\nu_{x(t)}}{\beta_1^2(t)\,\beta_2^2(t)} & \frac{\nu_{x(t)}}{\beta_2^2(t)^2} \end{bmatrix}. \tag{A.7}$$

Substituting A.7 into equation 5.25 gives an expression of the curve variance in terms of the control point covariance:

$$\nu_{x(t)} = \begin{bmatrix} \beta_0^2(t) & \beta_1^2(t) & \beta_2^2(t) \end{bmatrix} \begin{bmatrix} \frac{\nu_{x(t)}}{\beta_0^2(t)^2} & -\frac{1}{2}\frac{\nu_{x(t)}}{\beta_0^2(t)\,\beta_1^2(t)} & 0 \\ -\frac{1}{2}\frac{\nu_{x(t)}}{\beta_0^2(t)\,\beta_1^2(t)} & \frac{\nu_{x(t)}}{\beta_1^2(t)^2} & -\frac{1}{2}\frac{\nu_{x(t)}}{\beta_1^2(t)\,\beta_2^2(t)} \\ 0 & -\frac{1}{2}\frac{\nu_{x(t)}}{\beta_1^2(t)\,\beta_2^2(t)} & \frac{\nu_{x(t)}}{\beta_2^2(t)^2} \end{bmatrix} \begin{bmatrix} \beta_0^2(t) \\ \beta_1^2(t) \\ \beta_2^2(t) \end{bmatrix}. \tag{A.8}$$

Thus, it is possible to find a set of covariance terms for the control points which describe a constant width tolerance zone for a Bézier curve.

Although equation A.8 provides a constant variance for any given t, it does not give a constant variance for all t simultaneously. The control point variances are functions of t; therefore, the bounds of the control points are not constant but must adjust for each value of t. A numerical example illustrates this problem.

If the covariance matrix in equation A.7 is evaluated at a point such as t=1/2, the result is

$$\mathbf{\Sigma}_{x(t)} = \begin{bmatrix} 16 & -4 & 0 \\ -4 & 4 & -4 \\ 0 & -4 & 16 \end{bmatrix}. \tag{A.9}$$

Substituting this covariance matrix into equation A.8 yields an expression for the curve variance in the x direction:

$$\nu_{x(t)} = 80t^4 - 160t^3 + 160t^2 - 80t + 16. \quad \text{(A.10)}$$

Equation A.10 indicates that although the variance is 1.0 at t=1/2, the variance of the end-points (t = 0 and t = 1) is 16. Similarly, if the coefficients of equation A.8 are calculated for any other value of t, the curve bounds are satisfied only at that value of t. Thus, this method does not create a constant relationship between the bounds on the curve and the control points.

Bibliography

Bibliography

Andersen, C. (1990, July). General system for least cost tolerance allocation in mechanical assemblies. Master's thesis, Brigham Young University.

Anderson, T. (1997, January). Surface variation and mating surface rotaional error in assemblies. Master's thesis, Brigham Young University.

Armenakas, A. (1991). *Modern Structural Analysis, the Matrix Method Approach*. New York: McGraw Hill.

ASME (1995). *ASME Y14.5M - 1994, Dimensioning and Tolerancing*. New York: ASME.

Bartels, R., J. Beatty, and B. Barsky (1987). *Introduction to Splines for use in Computer Graphics and Geometric Modeling*. Los Altos, CA: Morgan Kaufman.

Basilicas, A. (1992). Limit theorems for random polynomial forms. *Soviet Doklady Mathematics 44*(1), 1–3.

Bharucha-Reid, A. and M. Sambandham (1986). *Random Polynomials* (1st ed.). Orlando: Academic Press.

Billings, D. (1986). Tolerance analysis as an integral part of design optimization. Master's thesis, Brigham Young University.

Bjorke, O. (1978). *Computer-Aided Tolerancing*. Norway: Tapir Publishers.

Blum, H. (1967). A transformation for extracting new descriptors of shape. In *Models for the Perception of Speech and Visual Form*. MIT Press.

Brown, C. (1995). Statistical models for position and profile variation in mechanical assemblies. Master's thesis, Brigham Young University.

Carr, C. (1993). A comprehensive method for specifying tolerance requirements for assemblies. Master's thesis, Brigham Young University.

Chase, K. and W. Greenwood (1988, March). Design issues in mechanical tolerance analysis. *Manufacturing Review 1*(1), 50–59.

Chase, K., W. Greenwood, B. Loosli, and L. Hauglund (1990, March). Least cost tolerance allocation for mechanical assemblies with automated process selection. *Manufacturing Review 3*(1), 49–59.

Chase, K. W. and A. Parkinson (1991). A survey of research in the application of tolerance analysis to the design of mechanical assemblies. *Research in Engineering Design 3*(1), 23–27.

Cheney, D. (1994, December). A user interface specification for cad/cam application development. Master's thesis, Brigham Young University.

Choi, B. (1991). *Surface Modeling for CAD/CAM*. Amsterdam: Elsevier.

Chun, K. (1988). Development of two-dimensional tolerance modeling methods for cad systems. Master's thesis, Brigham Young University.

Cook, R. (1989). *Concepts and Applications of Finite Element Analysis* (3rd ed.). New York: John Wiley and Sons.

Crisfield, M. (1986). *Finite Elements and Solution Procedures for Structural Analysis*, Volume 1. Swansea, U.K.: Pineridge Press.

Emch, G. (1992, December). Robust optimization using worst case tolerances. Master's thesis, Brigham Young University.

Emch, G. and A. Parkinson (1993, September). Using engineering models to control variability: Feasibility robustness for worst-case tolerances. In *Proceedings of the 1993 ASME Design Automation Conf.*, Volume DE-65-1, pp. 411. ASME.

Emch, G. and A. Parkinson (1994, December). Robust optimal design for worst-case tolerances. *ASME Journal of Mechanical Design 116*, 1019.

Fang, Y. and F. Liou (1994). Geometric modeling and simulation of mechanical assemblies with elastic components. In *Advances in Design Automation*, pp. 45–53. ASME.

Farin, G. (1988a). *Curves and Surfaces for Computer Aided Geometric Design*. U.S.A.: Academic Press.

Farin, G. E. (1988b). *Curves and surfaces for computer aided geometric design : a practical guide*. Academic Press.

Farouki, R. and C. Neff (1990). Algebraic properties of plane offset curves. *Computer Aided Geometric Design 7*, 101–127.

Farouki, R. and T. Sakkis (1990). Pyathgorean hodographs. *IBM Journal of Research and Development 34*(5), 736–752.

Fortini, E. (1967). *Dimensioning for Interchangeable Manufacture*. Industrial Press Inc.

Francavilla, A. and O. Zienkiewicz (1975). A note on numerical computation of elastic contact problems:, surface contact and impact. *International Journal for Numerical Methods in Engineering 9*, 913–924.

Gao, J. (1993, August). *Nonlinear Tolerance Analysis of Mechanical Assemblies*. Ph. D. thesis, Brigham Young University, Provo, UT.

Garloff, J. (1993). The Bernstein Algorithm. *Interval Computations 2*, 154–168.

Gelston, S. and D. Dutta (1992). Boundary surface recovery from skeleton elements: Part I – Skeleton curves. In *Advances in Design Automation – Volume 2*, Dearborn, MI. ASME.

Glancy, C. (1994, December). A second-order method for assembly tolerance analysis. Master's thesis, Brigham Young University.

Goodrich, C. (1991). Representation and modeling of geometric form variations for 3-d tolerance analysis. Master's thesis, Brigham Young University.

Gordis, J. and W. Flannelly (1994, December). Analysis of stress due to fastener tolerance in assembled components. *AIAA Journal 32*(12), 2440–2446.

Greenwood, W. (1987, August). *A New Tolerance Analysis Method for Engineering Design and Manufacturing*. Ph. D. thesis, Brigham Young University, Provo, UT.

Greenwood, W. and K. Chase (1987, May). A new tolerance analysis method for designers and manufacturers. *Journal of Engineering for Industry 109*, 112–116.

Greenwood, W. and K. Chase (1988, August). Worst case tolerance analysis with nonlinear problems. *Journal of Engineering for Industry 110*, 232–235.

Greenwood, W. and K. Chase (1990, November). Root sum squares tolerance analysis with nonlinear problems. *Journal of Engineering for Industry 112*, 232–235.

Guilford, J. and J. Turner (1992). Representing geometric tolerance in solid models. In *Computers in Engineering*, Volume 1, pp. 319–327. ASME.

Haugland, L. (1987). Combining manufacturing process selection and optimum tolerance allocation in design automation. Master's thesis, Brigham Young University.

Hillyard, R. and I. Braid (1978, May). Analysis of dimensions and tolerances in computer-aided mechanical design. *Computer-Aided Design 10*(3), 161–166.

Huo, H. (1995, December). *New Tolerance Analysis Methods for Preliminary Design in Mechanical Assemblies*. Ph. D. thesis, Brigham Young University, Provo, UT.

Ibragimov, I. and S. Podkorytov (1995). Random real algebraic surfaces. *Doklady Mathematics 52*(1), 101–103.

Jackson, D. (1992, December). A standardized approach to developing application programs for geometric modelers. Master's thesis, Brigham Young Uni-

versity.

Jayaraman, R. and V. Srinivasan (1989, March). Geometric tolerancing: I. virtual boundary requirements. *IBM Journal of Research and Development 3*(2), 90–104.

Johnson, R. and D. Wichern (1988). *Applied Multivariate Statistical Analysis* (2nd ed.). Englewood Cliffs, NJ: Prentice Hall.

Klass, R. (1983, September). An offset spline approximation for plane cubic splines. *Computer-aided Design 15*(5), 297–299.

Larsen, D. (1989, April). An efficient method for iterative tolerance design using monte carlo simulation. Master's thesis, Brigham Young University.

Larsen, G. (1991). A generalized approach to kinematic modeling for tolerance analysis of mechanical assemblies. Master's thesis, Brigham Young University.

Law, M. J. (1996, April). Multivariate statistical analysis of assembly tolerance specifications. Master's thesis, Brigham Young University.

Lewis, L. (1993, January). A second order, non-normal statistical tolerance model for robust optimal design. Master's thesis, Brigham Young University.

Lewis, L., T. A., and A. Parkinson (1993, September). A general approach for robust optimal design applied to the design of a control system. *Advances in Theory and Application 59*, 291.

Lewis, L. and A. Parkinson (1994, December). Robust optimal design with a second order tolerance model. *Research in Engineering Design 6*, 25–37.

Light, R. and D. Gossard (1982, July). Modification of geometric models through variational geometry. *Computer-Aided Design 14*(4), 209–214.

Liu, S. and S. Hu (1995, *preprint*). Variation simulation for deformable sheet metal assemblies using finite element methods. *ASME Journal of Engineering for Industry*.

Liu, S., S. Hu, and T. Woo (1995, *preprint*). Tolerance analysis for sheet metal assemblies. *ASME Journal of Mechanical Design*.

Liu, S., H.-W. Lee, and S. Hu (1995, May). Variation simulation for deformable sheet metal assemblies using mechanistic models. *Transactions of the North American Manufacturing Research Institute of SME*.

Loosli, B. (1987). Manufacturing tolerance cost minimization using discrete optimization for alternate process selection. Master's thesis, Brigham Young University.

Marler, J. (1988). Nonlinear tolerance analysis using the Direct Linearization Method. Master's thesis, Brigham Young University.

Martinsen, K. (1993, September). Vectorial tolerancing for all types of surfaces. In *Proceedings of 19th Design Automation Conference*, Albuquerque, NM, pp. 187–198. ASME.

Merkley, K. and K. Chase (1997, April). Breakthroughs in tolerance analysis of compliant assemblies. In *Proceedings of the 1997 ADCATS Conference*, Provo, UT. Brigham Young University.

Merkley, K., K. Chase, and E. Perry (1996, June). An introduction to tolerance analysis of flexible assemblies. In *Proceedings of the 1996 MSC World Users Conference*, Newport Beach, CA. MacNeal-Schwendler Corp.

Mottershead, J. (1993, May). Finite element analysis of contact and friction: A survey. Technical report, NAFEMS, University College of Swansea, Swansea, Wales U.K.

Nielsen, D. (1989, April). The application of convolution methods to the statistical analysis of mating hole patterns. Master's thesis, Brigham Young University.

Ogot, M. and B. Gillmore (1994). A kinematic based analysis for tolerances within mechanical assemblies. In *Advances in Design Automation*, pp. 237–249. ASME.

Onicescu, O. and V. I. Istrătescu (1975). Approximation theorems for random functions. *Rendiconti di Matematica 8*(6), 65–81.

Parkinson, A. and L. Lewis (1993, January). A general approach for robust optimal design. In *Proceedings of the 1993 Design and Manufacturing Conf.*, Volume 1, pp. 659. NSF.

Peterson, D. (1990, August). A closed-form model for tolerance analysis of two-dimensional mating hole patterns. Master's thesis, Brigham Young University.

Reddy, J. (1993). *An Introduction to the Finite Element Method* (2nd ed.). New York: McGraw Hill.

Requicha, A. A. G. (1984). Representation of tolerance in solid modeling: Issues and alternative approaches. In J. Boyse and M. Pickett (Eds.), *Solid Modeling by Computers: from Theory to Application*, pp. 3–22. New York: Plenum Press.

Requicha, A. A. G. and S. C. Chan (1986, September). Representation of geometric features, tolerances, and attributes in solid modelers based on constructive geometry. *IEEE Journal of Robotics and Automation RA-2*(3), 156–166.

Rime, C. (1988, December). CICATS: CADAM interface to computer aided tolerance selection. Master's thesis, Brigham Young University.

Rivest, L., C. Fortin, and C. Morel (1993). Tolerancing a solid model with a kinematic formulation. In *Proceedings of 2nd ACM Solid Modeling*, Montreal, Canada, pp. 357–366. ACM.

Rizzo, A. (1991, June). FEA gap elements: Choosing the right stiffness. *Computers in Mechanical Engineering*, 57–59.

Robinson, R. (1989). A practical method for three-dimensional tolerance analysis using a solid modeler. Master's thesis, Brigham Young University.

Rossignac, J. and A. Requicha (1986). Offsetting operations in solid modeling. *Computer Aided Geometric Design 3*, 129–148.

Roy, U., C. Liu, and T. Woo (1991, September). Review of dimensioning and tolerancing: Representation and processing. *Computer Aided Design 23*(7), 466–483.

Rubinstein, R. (1981). *Simulation and the Monte Carlo Method* (1st ed.). New York: Wiley and Sons.

Sederberg, T. and R. Farouki (1992, September). Approximation by interval Bézier curves. *IEEE Computer Graphics and Applications 12*(5), 87–95.

Sederberg, T. W. and D. B. Buehler (1992). Offsets of polynomial Bézier curves: Hermite approximation with error bounds. In T. Lyche and L. L. Schumaker (Eds.), *Mathematical Methods in Computer Aided Geometric Design II*, pp. 549–558. Academic Press.

Simmons, A. (1990, August). Automated vector loop generation for kinematic models of mechanical assemblies. Master's thesis, Brigham Young University.

Spotts, M. (1959, November). An application of statistics to the dimensioning of machine parts. *Journal of Engineering for Industry 81*, 317–322.

Spotts, M. (1960, March 21,). A faster way to set statistical tolerances. *Product Engineering*, 55–57.

Srinivasan, V. and R. Jayaraman (1989, March). Geometric tolerancing: Ii. conditional tolerances. *IBM Journal of Research and Development 3*(2), 105–115.

Stoddard, J. (1995). Characterizing kinematic variation in assemblies from geometric constraints. Master's thesis, Brigham Young University.

Stout, J. and K. Chase (1997, April). Combining tolerance analysis with FEA - Prototype of a new tool. In *Proceedings of the 1997 ADCATS Conference*, Provo, UT. Brigham Young University.

Texas Instruments (1994). *TI/TOL 2D Multi-Dimensional Tolerance Management Tool User Reference Manual*. Plano, TX: Texas Instruments.

Trego, A. (1993). A comprehensive system for modeling variation in mechanical assemblies. Master's thesis, Brigham Young University.

Turner, J. (1989). Geos overview. Technical Report 89047, Rennsalaer Design Research Center, Troy, NY.

Turner, J. and M. Wozny (1990, Sept. 17-19,). The m-space theory of tolerances. In *Advances in Design Automation*, Chicago,, IL. ASME.

University of Utah (1988). *Alpha_1 User's Manual*. Salt Lake City, UT: University of Utah.

Voelker, H. B. (1993, June 17-19,). A current perspective on tolerancing and metrology. In V. Srinivasan and H. Voelker (Eds.), *Proceeding of the 1993 International Forum on Dimensional Tolerancing and Metrology*, Dearborn, MI. ASME.

Walker, R. and V. Srinivasan (1993, June 17-19,). Creation and evolution of the ASME y14.5.1m standard. In *1993 International Forum on Dimensional Tolerancing and Metrology*, New York. ASME.

Ward, K. (1993, August). Integrating geometric form variations into tolerance analysis of 3-d assemblies. Master's thesis, Brigham Young University.

Webb, S. (1994, April). The mathematical properties and efficient optimization of the linear variance function. Master's thesis, Brigham Young University.

Webb, S. and A. Parkinson (1995, September). The efficient optimization of the linear variance function. In *Proceedings of the 1995 ASME Design Automation Conf.*, pp. 407–414. ASME.

Weisberg, S. (1980). *Applied Linear Regression* (1st ed.). New York: Wiley and Sons.

Wilhelm, R. (1992). *Computer Methods for Tolerance Synthesis*. Ph. D. thesis, University of Illinois at Urbana-Champaign.

Wirtz, A. (1993, April 27–28,). Vectorial tolerancing: A basic element for quality control. In *3rd CIRP Seminars on Computer Aided Tolerancing*, Cachan,

France. CIRP.

Zhong, Z. and J. Mackerle (1994, February). Contact-impact problems: A review with bibliography. *Applied Mechanics Review 47*(2), 55–76.

Zienkiewicz, O. and R. Taylor (1988). *The Finite Element Method* (4th ed.). London: McGraw-Hill.